New phenomena in non-equilibrium quantum physics

Thesis advisor: Eugene Demler Takuya Kitagawa

New phenomena in non-equilibrium quantum physics

Abstract

From its beginning in the early 20th century, quantum theory has become progressively more important especially due to its contributions to the development of technologies. Quantum mechanics is crucial for current technology such as semiconductors, and also holds promise for future technologies such as superconductors and quantum computing. Despite of the success of quantum theory, its applications have been mostly limited to equilibrium or static systems due to 1. lack of experimental controllability of non-equilibrium quantum systems 2. lack of theoretical frameworks to understand non-equilibrium dynamics. Consequently, physicists have not yet discovered too many interesting phenomena in non-equilibrium quantum systems from both theoretical and experimental point of view and thus, non-equilibrium quantum physics did not attract too much attentions.

The situation has recently changed due to the rapid development of experimental techniques in condensed matter as well as cold atom systems, which now enables a better control of non-equilibrium quantum systems. Motivated by this experimental progress, we constructed theoretical frameworks to study three different

non-equilibrium regimes of transient dynamics, steady states and periodically drives. These frameworks provide new perspectives for dynamical quantum process, and help to discover new phenomena in these systems. In this thesis, we describe these frameworks through explicit examples and demonstrate their versatility. Some of these theoretical proposals have been realized in experiments, confirming the applicability of the theories to realistic experimental situations. These studies have led to not only the improved fundamental understanding of non-equilibrium processes in quantum systems, but also suggested entirely different venues for developing quantum technologies.

Your Pin Is: 142761 Your Password Is: XXAS

Contents

Listing of figures

Citations to previously published works

MOST OF THE WORK described in this thesis have appeared previously in print. Here, we list those works relevant to this thesis.

Study of dynamics in one-dimensional systems and prethermalization

- "Ramsey interference in one dimensional systems: The full distribution function of fringe contrast as a probe of many-body dynamics, " Takuya Kitagawa, Susanne Pielawa, Adilet Imambekov, Jorg Schmiedmayer, Vladimir Gritsev, Eugene Demler, Phys. Rev. Lett. **104**, 255302 (2010) ; arXiv:0912.4643

- "The dynamics and prethermalization of one dimensional quantum systems probed through the full distributions of quantum noise, " Takuya Kitagawa, Adilet Imambekov, J rg Schmiedmayer, Eugene Demler, New J. Phys. **13** 073018 (2011); arXiv:1104.5631

- "Relaxation Dynamics and Pre-thermalization in an Isolated Quantum System, " Maximilian Kuhnert, Remi Geiger, Tim Langen, Michael Gring, Bernhard Rauer, Takuya Kitagawa, Eugene Demler, David Adu Smith, J rg Schmiedmayer, Science **14** 337 1318 (2012); arXiv:1112.0013v1

- "Multimode dynamics and emergence of a characteristic length-scale in a one-dimensional quantum system, " Michael Gring, Maximilian Kuhnert, Tim Langen, Takuya Kitagawa, Bernhard Rauer, Matthias Schreitl, Igor Mazets, David A. Smith, Eugene Demler, J rg Schmiedmayer, arXiv:1211.5323

Study of topological phases in quantum walks

- "Exploring Topological Phases With Quantum Walks, " Takuya Kitagawa, Mark S. Rudner, Erez Berg, Eugene Demler, Phys. Rev. A **82**, 033429 (2010); arXiv:1003.1729

- "Observation of topologically protected bound states in a one dimensional photonic system, " Takuya Kitagawa, Matthew A. Broome, Alessandro Fedrizzi, Mark S. Rudner, Erez Berg, Ivan Kassal, Al n Aspuru-Guzik, Eugene Demler, Nature Communications, **3** 882 (2012) ; arXiv:1105.5334

Dynamical induction of topological properties in condensed matter and cold atom systems

- "Topological characterization of periodically driven systems , " Takuya Kitagawa, Erez Berg, Mark Rudner, Eugene Demler, Phys. Rev. B **82**, 235114 (2010) ; arXiv:1010.6126

- "Majorana Fermions in Equilibrium and Driven Cold Atom Quantum Wires, " Liang Jiang, Takuya Kitagawa, Jason Alicea, A. R. Akhmerov, David Pekker, Gil Refael, J. Ignacio Cirac, Eugene Demler, Mikhail D. Lukin, Peter Zoller, Phys. Rev. Lett. **106**, 220402 (2011) ; arXiv:1102.5367

- "Photo-induced quantum Hall insulators without Landau levels, " Takuya Kitagawa, Takashi Oka, Arne Brataas, Liang Fu, Eugene Demler, Phys. Rev. B **84**, 235108 (2011); ; arXiv:1104.4636

Dynamical control of transport properties

- "Photo control of transport properties in disorderd wire; average conductance, conductance statistics, and time-reversal symmetry , " Takuya Kitagawa, Takashi Oka, Eugene Demler , Ann. Phys. **10** 1016 (2012); arXiv:1201.0521

- "Photoinduced helical metal and magnetization in two-dimensional electron systems with spin-orbit coupling, " Teemu Ojanen, Takuya Kitagawa , Phys. Rev. B **85**, 161202 (R); arXiv:1201.5997v1

- "Conductance beyond the Landauer limit and charge pumping in quantum wires, " Jay D. Sau, Takuya Kitagawa, Bertrand I. Halperin, Phys. Rev. B **85** 155425(2012); arXiv:1202.6051

Novel phases in non-equilibrium steady states

- "Correlated phases of bosons in tilted, frustrated lattices, " Susanne Pielawa, Takuya Kitagawa, Erez Berg, Subir Sachdev, Phys. Rev. B **83**, 205135 (2011) ; arXiv:1101.2897v1

Quench dynamics from superfluid to Mott insulator

- "Signatures of the superfluid to Mott insulator transition in equilibrium and in dynamical ramps, " Susanne Pielawa, D. Pekker, B. Wunsch, T. Kitagawa, E. Manousakis, A. S. Sorensen, E. Demler, Phys. Rev. B **86**, 144527 (2012); arXiv:1206.1648

Cooling of quantum systems through driving

- "Cooling through optimal control of quantum evolution, " Armin Rahmani, Takuya Kitagawa, Eugene Demler, Claudio Chamon, arXiv:1210.5244

I dedicate this dissertation to my family. Particularly to my parents, Keiko and Takeo Kitagawa, who supported me for studying and carrying research in the country far from home. I also want to thank my sisters, Sayaka and Chihiro, who supported me in especially difficult times during graduate programs.

Acknowledgments

I WANT TO THANK all of the people who help me go through the graduate program and write this thesis. First of all, I would like to thank my fabulous adviser, Dr. Eugene Demler, for his encouragements, understandings and guidance in science. Not only have I obtained great inspirations of physics from him, I always have many things to learn from his broad perspectives of scientific as well as non-scientific disciplines. I also want to thank Dr. Markus Greiner, Dr. Subir Sachdev, Dr. Mihail Lukin, Dr. Bertrand Halperin, Dr. Joerg Schmiedmayer, Dr. Immanuel Bloch, Dr. Alain Aspect and Dr. Peter Zoller for their warm encouragements and exciting discussions for my ideas. I could never get so excited about physics without their lively discussions and insights, and my experience to collaborate with them is one of the most fun time during my graduate years. In addition, I wish to express my gratitude for many of my collaborators, Dr. Mark Rudner, Dr. Erez Berg, Dr. Jay D Sau, Dr. Takashi Oka, Dr. Liang Fu, Dr. Anatoli Polkovnikov, Dr. Liang Jiang, Dr. Teemu Ojanen, Dr. David Pekker, Dr. Adilet Imambekov, Dr. Dimitry Abanin, Dr. Anton R. Akhmerov, Dr. Belen Paredes, Dr. Ehud Altman, Dr. Gil Rafael, Dr. Vladimir Gritsev, Dr. Lucia Hackermuller, Dr. Ulrich Schneider, Dr. Maria Moreno-Cardoner, Dr. Armin Rahmani, Dr. Claudio Chamon, Dr. Susanne Pielawa, Dr. Michael Gring, Dr. Tim Langen, Dr. David A. Smith, Dr. Monika Aidelsburger, Dr. Matthew A. Broome, Dr. Alessandro Fedrizzi, Dr. Arne Brataas, Dr. Bernhard Wunsch and Dr. Yutaka Shikano who patiently taught and guided an immature physicist like me through collaborations and discussions. I learned tremendous amount of physics and being a physicist from all of them. Of course, I am

greatly indebted to many of my friends during the graduate program, and I would like to especially thank Yu Shoji, Yumiko Ito, Megumi Iso, Kaku Hiroki, Mariko Tani, Saki Mizuguchi, Yushiro Okamoto, Nao & Chihiro Ogi, Eli Visbal, Bryan gin-ge Chen, Mehtash Babadi, Dilani Kahawala, Ashwin Rastogi, Eunmi Che, Gaku Nagashima, Takuma Inoue, Albert Lee, Yuki Nakamura, Ruxuan Gao, Keiko Tsuruta and many others. I could not have accomplished what I have done without any of your support behind the scenes.

1

Overview

The study of non-equilibrium dynamics has made tremendous progress due to the recent development of artificial systems such as ions, photons and cold atom systems. While theoretical frameworks we constructed in our works are applicable to general quantum systems and thus are not limited to artificial systems, they are often motivated by the possibility of immediate experimental realizations in such artificial systems. In the first section of this chapter, we would like to give the overview of non-equilibrium physics in the context of experiments in cold atom systems. With this background, in the second section, we give the overview of our works from the perspective of three regimes of transient dynamics, periodical drives and steady states.

1.1 Overview of experimental works in artificial systems

In this section, we would like to summarize the experimental progress for studying non-equilibrium physics in cold atoms from the perspective of unique features of artificial systems. Artificial systems are advantageous compared to condensed matter materials when seen as a platform for investigating fundamental physics and as a testing bed for future quantum technologies. The advantages are contributing to the understandings of non-equilibrium physics in the following experiments;

1. Artificial systems are well-isolated and decoupled from environments, and thus coherent time is typically much longer than corresponding time of systems in the condensed matter environment. This feature of cold atom systems is demonstrated and taken advantage of in the following experiments;

   (a) Study of equilibration dynamics. While we have good understanding of equilibrated states through the framework of thermodynamics, the process of equilibration is yet ill-understood especially in quantum systems. This lack of understandings is partly due to the fast relaxation and equilibration time scale ($\approx 10^{-12}$s) in condensed mater systems, which requires special probes for its study. Moreover, the environment of electrons in solid states materials is not controlled or manipulated, and the detailed comparison between theories and experiments are challenging. Thus cold atom systems with long equilibration time scale with good controls of their environment provide ideal situations for investigating this important question of equilibration. For example,

Immanuel Bloch's group prepared a non-equilibrium initial state in a one dimensional lattice system, where every other site is occupied. They observed and studied the subsequent equilibration dynamics as this initial state freely evolves[158]. The same group also studied the dephasing dynamics in one dimensional bosonic systems with two-component spin, and showed that spin-echo type sequence does not rephase the spins in many-body dynamics[165]. On the other hand, the group led by Cheng Chin was interested in the equilibration process when the system is quenched across phase transitions. They observed the mass-redistributions in the process of equilibration by preparing superfluid states with bosonic particles in optical lattice and suddenly quenching into Mott-insulating state through the ramping up of the lattice[63]. Other groups have investigated the *lack of* equilibration when the system possesses certain special symmetries. For example, Kinoshita *et al* has observed the coherent dynamics of many-body one dimensional systems which stays out of equilibrium for exceedingly long time[83]. This experiment is a beautiful example of physics that became addressable for the first time due to cold atom systems that are well-isolated from environments. In more recent experiments by Joerg Schmiedmayer's group, a novel phenomenon called prethermalization is observed, where dynamics leads to a non-equilibrium steady state whose observables look like those of equilibrium states but their values correspond to temperature much lower than the true equilibrium temperature of the system[50, 97]. Such experiments demonstrate an intricate nature of equilibration which takes place not through monotonic

process but through several distinct stages.

(b) Study of coherent quantum dynamics. In condensed matter environments, it is often difficult to observe phase coherence, especially the revival of it. In the early time of cold atom experiments, Markus Greiner, Olaf Mandel, Theodor W. H nsch and Immanuel Bloch have demonstrated the possibility to observe the oscillations of phase coherence as the system is quenched from superfluid to Mott states by the ramping up of optical lattice[48]. The phase of the system revived in time inversely proportional to interaction strengths, in agreement with the theory of Bose-Hubbard model. In more recent years, the experiments become more sophisticated and the measurements of revival time become more precise. In such experimental systems, it now became possible to observe the effects of multi-body interactions through the deviations of the phase revival. S. Will *et al* measured the strength of multi-body interactions in this way[166]. Other examples of coherent dynamics is the study of Bloch oscillations. In the clean environment of cold atoms, M. B. Dahan *et al.* observed the Bloch oscillations and observed effective mass of particles in a lattice through the momentum distributions of Bloch states[14].

2. Cleanness of the system. Because artificial systems are something that experimentalists build, they understand well about the microscopic details of the systems. Thus, systems can be built clean without impurities, and ideal theoretical descriptions of the systems capture the physics of the experiments quite well. Such situations allow, for example, measurements of multi-body interactions in optical lattice[166]

as described above through the comparisons of experiments with theoretical descriptions. Such cleanness of cold atom systems can be used to check the validity of quantum theories, and it is now routine work to confirm the predictions of theories such as Bose-Hubbard model through the good agreements with experiments[6, 141, 165]. From reversed perspective, experimentalists can also introduce controlled impurities and study disordered systems. In this way, physicists deepened the understanding of Anderson localizations by realizing it in one [19, 132], as well as in three dimensions[76, 96].

3. Controllable microscopic parameters. Not only do artificial systems offer experimental systems described by ideal Hamiltonians, but also they allow experimentalists to tune the parameters of Hamiltonians at will. Such controllability allows the study of phase diagrams of static systems as demonstrated by the famous study of superfluid-Mott transitions by Greiner *et al.* [48]. For non-equilibrium systems, this means microscopic parameters can be changed in time in controllable fashions, and allow the study of;

   (a) Quench dynamics. For example, Chen *et al.*, Hung *et al.*, Tuchman *et al.* and Bakr *et al.* studied the dynamics of Bose-Hubbard model as the system is quenched from superfluid states to Mott-insulating states or vice versa[6, 28, 63, 159]. On the other hand, Sadler *et al.* studied the dynamics after quenching the system from paramagnetic phase to ferromagnetic phase in spinor condensates[138]. The controllability of parameters can also be used for the preparation of initial states. Schneider *et al.* has studied the transport property of Fermionic particles in Hubbard model by preparing the particles in

tightly confined potentials and observing the subsequent dynamics after the release[141].

(b) Periodical drives of the systems. Fast oscillations of parameters in the Hamiltonian leads to the the effective change of Hamiltonian for slow dynamics in Floquet picture. Experiments by Arimondo's group have successfully demonstrated such "photonics dressing" of particles[103, 171] and even have shown the phenomenon of dynamic localizations which makes the hopping amplitude to be zero through shaking[36]. Such shakings of optical lattice is proposed to allow the ingenious realizations of models such as XXZ spin models[30], and recently the phase diagrams of frustrated magnetism in triangular lattice have been experimentally studied through lattice modulation methods in Sengstock group[152].

4. Large length and time scale of the systems. Cold atom systems have different length scales compared to condensed matter materials. The typical length scale of cold atom is set by the wavelength of lasers making up the optical lattice. In the case of Rb^{87}, a typical choice of atoms in cold atom systems, the lattice constant of optical lattice is given by 532 nm. This number should be compared with the typical lattice constant of electronic systems, which is of the order of angstrom, or 0.1nm. Taking advantage of this fact that lattice length scale of cold atom is much bigger than that of electrons, the groups led by Markus Greiner successfully developed the imaging systems that allow the visualization of particle movements at single site level[7]. Other groups quickly followed, and realized a similar single-site microscope for cold atoms[162]. In addition to in-situ visualizations, the same technology allows the single-site

addressability, where particles at each site can be manipulated by the lasers. Such extraordinary ability for atomic controls is a big leap for the possibility to build quantum computers, which require coherent qubit preparations and controls. In addition to the large length scale, cold atom systems also have larger time scale compared to condensed matter materials. Time scale of systems is given by the inverse of energy scale. The typical energy scale of cold atoms is set by the confinement energy of atoms in the latice, which is given by the lattice recoil energy. In the case of Rb^{87}, then, this corresponds to milliseconds or 10^{-3}s time scale. For electronic systems, the typical energy scale is set by the electron electron interactions at the length scale of lattice constant, and given by pico to fempto second or $10^{-12} \approx 10^{-15}$s. Thus, any dynamics taking place in cold atom systems is much easier to follow through conventional technology, and therefore, the quantum dynamics is much easier to study in cold atom systems, as we described above in the study of equilibration dynamics.

5. New observables and probes. While many of the properties of cold atom systems can be made resemble those of electronic systems for condensed matter materials, some important differences remain. One of the largest difference between them is the absence of electromagnetic interactions in cold atoms, which implies that one cannot study the effect of "magnetic field" or "electronic" transport through the application of voltage as easily as one does for condensed matter materials. On the other hand, cold atoms come with its own unique probes that allow the observations of quantum states from much different point of view. Not only can non-equilibrium physics be studied with such novel probes, but non-equilibrium process provides such

new probes in the context of cold atoms. For example, the time of flight images is a standard technique in cold atom to measure the momentum distributions of the states[21]; the time of flight combined with interference experiments provide crucial insights about the coherence of the systems[61, 131]; modulations of lattice is now routinely used for spectroscopic measurements[168] or as a probe of excitation spectrum[144]; bloch oscillation is recently employed together with interference experiments for the measurements of topology in the band structures[5]; hydrodynamic expansions of cold atoms after the release from traps are used for the study of BEC-BSC crossovers[22].

All of the unique features described above contributes to the advancement of the fundamental understanding for quantum many-body dynamics. Questions that cold atom experiments addressed to help answer include those that have been previously asked but were never experimentally studied, such as the dynamics of mobile spin impurity[44] and spreading of correlations in quantum many-body systems[31]. Motivated by the experimental possibility, physicists also extended the previous influential ideas to new frontiers such as the study of Landau-Zener transitions in many-body physics[28] and doublon decays in Fermi Hubbard models [151]. Since the cold atom systems are controllable and its microscopic Hamiltonian is well-understood, we can also use cold atoms as quantum simulators of physics that we cannot analytically or numerically compute, such as the many-body relaxation dynamics in strongly correlated 1D gas[158].

We have summarized the study of non-equilibrium systems in cold atoms through the lens of experimental advantages in the hope of advocating new ideas in the field. The excitement of the field is now expanding due to the numerous experimental achievements that we

described in this section. While previous excitements mainly came from the possibility to study traditional, important questions in condensed matter physics but now physicists are looking toward achieving novel physics in cold atoms that would be difficult to realize in condensed matter materials. The hope is that such progress can then in turn give back novel ideas to condensed matter physics, which together create not only the fundamental understandings of non-equilibrium physics but also the advancement of quantum technologies. This is indeed what I tried to achieve in my works, and I now turn to describe them in details.

1.2 Overview of my works on non-equilibrium quantum dynamics

Non-equilibrium quantum systems include a wide range of situations since its name only indicates what it is *not* and does not really specify what it is. From the point of view of Hamiltonian $H(t)$, non-equilibrium systems are anything that is described by time-dependent Hamiltonian, and equilibrium system can be seen as the special case where Hamiltonian does not depend on time. Therefore, in order to study non-equilibrium quantum systems, we restrict ourselves to more specific situations and analyze their dynamics.

In this thesis, we focus on three different situations of non-equilibrium;

1. Periodic drives where Hamiltonian is changed in periodic fashion in time. For example, we have examined in the previous studies the application of light to graphene[91, 115] and to spin-orbit coupled semiconductors[114], as well as periodic change of laser intensity for optical lattices with cold atoms[86]. Another

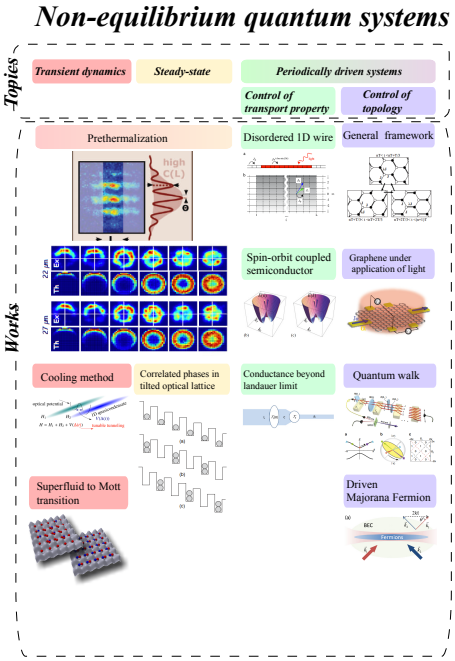

Figure 1.2.1: We have investigated three regimes of non-equilibrium through specific examples; transient dynamics, steady states and periodical drives.

important case of periodic drives includes the periodic applications of a set of quantum protocols to a single atom or a photon such as quantum walks [2, 81, 85, 89, 92].

2. Transient dynamics. Notable cases include quench dynamics where a parameter in the system (interaction strength, chemical potential, composition of particles, etc) is suddenly changed and subsequent dynamics is studied[6, 71]. In our works, we have demonstrated repeated quench operations can lead to the optimal cooling scheme for coupled one dimensional quasi-condensates[127].

3. Physics of steady-states. Non-equilibrium dynamic such as

quench dynamics and periodic drives sometimes leads to the states of systems that do not change in time, but are different from equilibrium states. Such steady states sometimes display response properties that are rarely observed in equilibrium states. We have demonstrated that intriguing correlated sates can exist as a steady-state in tilted optical lattice systems[123]. In addition, in one dimensional quasi-condensates, a quench of a parameter leads to prethermalization phenomena where the dynamics leads to a steady state whose observables look like those of equilibrium states but their values correspond to temperature much lower than the true equilibrium temperature of the system[50, 88, 90, 97].

In each of the situations, we find interesting phenomena that open new perspectives for the study of non-equilibrium systems. In the following, we briefly describe the main findings of each study to illustrate this point. For the summary figure of my works, see Fig. 1.2.1.

1.3 Periodically driven systems

One simple way to drive quantum systems out of equilibrium is to "shake" them in periodic fashions. For example, one can apply light or electromagnetic waves to condensed matter materials, or one can change the intensity of lasers for optical lattices of cold atom systems. A stationary state under such periodic drives is distinct from any equilibrium state of the system, and exhibit different physical properties in response functions. Thus, periodic drives can be employed, under certain circumstances, as a method to modify and control physical properties of materials. In my works, I have demonstrated 1. change of transport properties[91, 93, 114, 140] and 2. induction of topological properties through periodic drives

[85, 86, 89, 92]. In the followings, we describe this general ideas through explicit examples of such property controls.

1.3.1 Control of transport properties

Photo-induced insulator to conductor crossover in one dimensional disordered wire [93]

It is well-known from the study of disordered systems that dimensionality of the system dramatically change the transport properties of materials. In particular, for infinite systems, it has been argued that any one and two dimensional systems with disorders is an insulator, whereas there exists mobility edge energy above which particles can flow through the system in three dimensional system with disorder. For finite system, conductance shows analogous cross-over behaviors from insulator to conductor even in one or two dimensional systems, depending on the ratio of localization lengths ξ and system size L; for $\xi/L \ll 1$, the average conductance is exponentially suppressed and the system is insulator and for $\xi/L \gg 1$, the system behaves as a conductor.

The major insight into the control of transport properties in disordered systems with light comes from the possibility to effectively change the dimensionality of the system with periodic drives. This can be seen quite easily as follows. For Hamiltonians which change periodically in time with period T, Schrodinger equations can be cast into time-independent form as follows;

$$i\frac{\partial}{\partial t}|\psi(t)\rangle = H(t)|\psi(t)\rangle \tag{1.1}$$

$$\rightarrow \quad (E + m\Omega)|\psi_E(m)\rangle = \sum_k H(m-k)|\psi_E(k)\rangle \tag{1.2}$$

where the state $|\psi(t)\rangle$ and $H(t)$ is expanded in the Fourier transform

as $|\psi(t)\rangle = \sum_m \int_{-\Omega/2}^{\Omega/2} dE e^{-it(E+m\Omega)} |\psi_E(m)\rangle$ and $H(t) = \sum_m H(m) e^{-im\Omega t}$ with $\Omega = 2\pi/T$. This way of expanding periodically driven systems is known as Floquet formalism. Intuitively, Eq. (1.2) shows that in periodically driven systems, a state can absorb or emit energies in units of Ω, where magnitude of absorbing k units of energy is given by $H(k)$. Thus, periodic drives add one more index to the state of the system where the additional index label the "energy layer" of the system that indicate how many units of energy it has absorbed/emitted. In this perspective, $H(m-k)$ in Eq. (1.2) is a hopping term from kth layer to mth layer, and $m\Omega$ on the left side of Eq. (1.2) is a linear potential in the direction of energy layers. If the original problem involves n dimensional tight-binding models, then periodically driven systems correspond to $n+1$ dimensional static systems with linear potential.

Motivated by these observations, I have numerically calculated conductance distributions for disordered 1D wire under the application of light by extending the transfer matrix method to periodically driven systems. For intermediate disorder regime, conductance distributions are log-normal distributions for weak intensity of light, indicating insulating behaviors. On the other hand, when the intensity of light is strengthened, the conductance distributions qualitatively change its shape to normal distributions, indicating conducting behaviors (see Fig. 1.3.1).

Conductance beyond Landauer limit under the application of light [140]

The insight of dimensional increase obtained in Eq. (1.2) leads to yet another physical consequence, which is the possibility to reach conductance beyond Landauer limit in periodically driven systems. For one dimensional wire with a single channel, unitarity of scattering

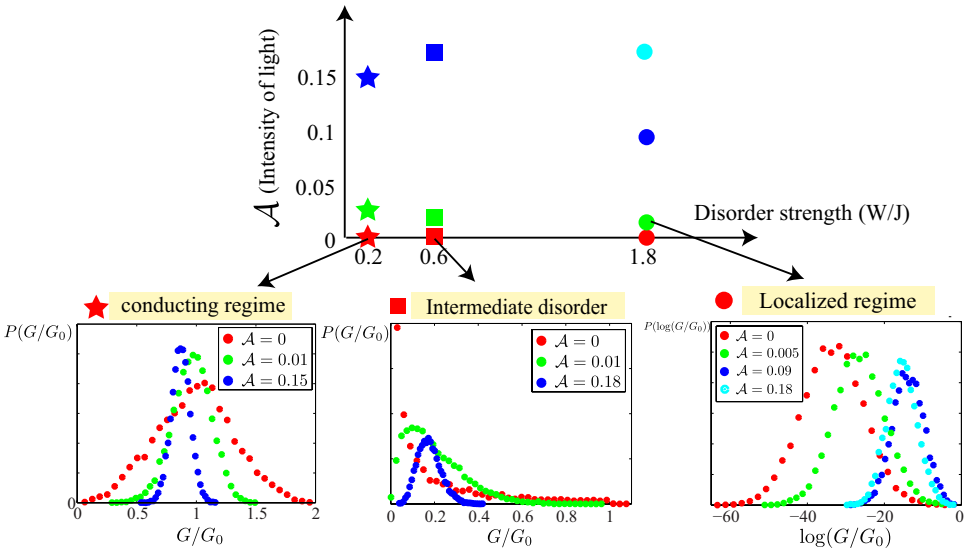

Figure 1.3.1: Conductance distributions for one dimensional disordered wire under the applications of light for various disorder strength and intensity of light. For strong disorder, the system is insulator with log-normal conductance distributions, and for weak disorder, it is conductor with normal conductance distributions. In the intermediate disorder regime, the distributions display cross-over behaviors from insulator (log-normal distributions) to conductors (normal distributions) as the intensity of light is increased.

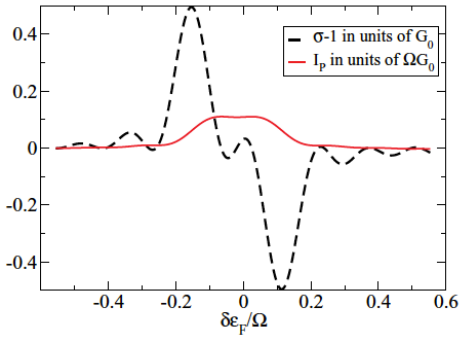

Figure 1.3.2: The conductance beyond Landauer limit of unit quantum conductance ($2e^2/h$ for spin 1/2 electrons) for the system considered in Ref. [140].

matrix dictates that the conductance cannot exceed $2e^2/h$ for an electron with spin $1/2$. However in the periodically driven systems, the number of channels are effectively increased by the absorption/emission of photons, enabling the conductance to exceed this Landauer limit. In the work *Conductance beyond the Landauer limit and charge pumping in quantum wires*, we have proposed a concrete, physically sensible scheme with a simple quantum point contact where such conductance can be attained, and theoretically calculated the expected conductance (Fig. 1.3.2). The demonstration of such conductance will be the explicit evidence of additional Floquet channels, and thus provide important experimental verifications of Floquet theory in realistic systems.

1.3.2 Control of topological properties[86]

Topological property of a physical system refers to a property that is robust against small changes of microscopic parameters of the system, where its property is protected by the underlying topology of the state. Most well-known example of a topological property is integer

quantum Hall effect[58, 94, 100], where Hall conductance takes the quantized value of integers times e^2/h. This quantized Hall conductance is robust against small changes of magnetic fields, sample shapes and sizes, or introductions of small disorders. In this case, the topological origin of the effect comes from the direct relation between Hall conductance and Chern number of ground states through so-called TKNN formula[156], where Hall conductance is simply given by Chern number times e^2/h. Here, Chern number is an example of topological invariant, and it is an integer value characterizing the topology of the ground state of the system. Topological invariants take only integer values, and thus cannot change its value under continuous deformations of the ground state in accordance with the property of topology. Thus, small change of microscopic parameters in the system does not change topological invariants, and so according to TKNN formula, Hall conductance does not change either.

Therefore, topological properties are unique characteristics of the ground state of a Hamiltonian, and thus of a Hamiltonian itself. Conventionally, such topological characterizations are often studied with static Hamiltonians, a simple extension of the idea can be applied also to periodically driven systems.

A conceptually simple idea is to reduce a time-dependent Hamiltonian to a static Hamiltonian. For periodic Hamiltonian with period T, the system evolves, after one period of time, through the unitary evolution operator

$$U_T = \mathcal{T} e^{-i \int_0^T H(t) dt}, \tag{1.3}$$

If we define the effective Hamiltonian H_{eff} as

$$U_T \equiv e^{-iH_{\text{eff}}T}. \tag{1.4}$$

then the evolution under H_{eff} coincides with the evolution under periodic drives $H(t)$ after integer multiple time of T. Thus, long-time evolution of the system is described by H_{eff}. By turning it around, you could say that $H(t)$ is a stroboscopic realizations of H_{eff}. In this way, by controlling the drives, one could design $H(t)$ such that H_{eff} possesses non-trivial topological properties.

Such topology of periodically driven systems associated with H_{eff} is analogous to the topological property of static systems. On the other hand, it is also possible that the evolution operator U_T itself possesses unique topology, which is not associated with any topology of H_{eff}. This particular topology is related to the periodicity of energy for H_{eff}. The definition of H_{eff} in Eq. (1.4) reveals that H_{eff} is only defined up to $2\pi/T$, and thus 0 and $2\pi/T$ energies are equivalent in this definition. Because of this, the system can possess "windings" in energy direction, which creates additional topological invariant for the system.

In my works, we demonstrated these general ideas through explicit examples, which we now describe in turn.

Discrete quantum walks [85, 89, 92]

Discrete quantum walk, in its simplest form, is a dynamical protocol for controlling a single spin $1/2$ particle in one dimensional lattice (see Fig. 2.1.1). It consists of two operations; 1. rotation around y axis by angle θ, whose operator is given by $R_y(\theta) = e^{-i\theta\sigma_y/2}$; 2. spin-dependent translation T where spin up particle is move to the right by one lattice site and spin down particle is moved to the left by one lattice site. One step of the quantum walk is given by $U = TR_y(\theta)$ The evolution of quantum walk results from the repeated applications of these two operations in alternate fashion. Such repeated protocols applied to particles is an example of periodic drives.

A crucial insight into the topological descriptions of quantum walks

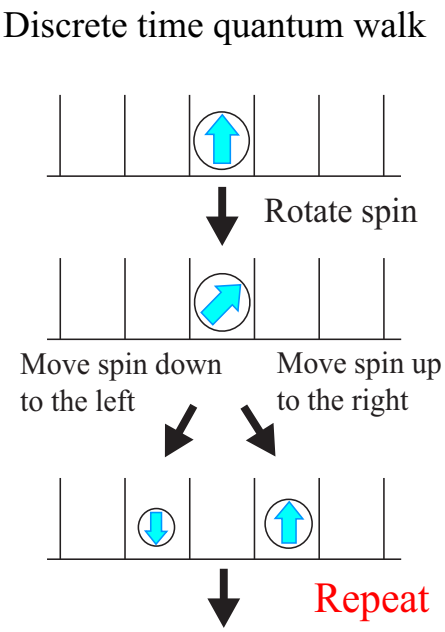

Figure 1.3.3: The protocol of a conventional discrete quantum walk. A conventional quantum walk is a dynamical protocol for controlling a spin $1/2$ quantum particle in one dimensional lattice. It consists of two operations; 1. rotation around y axis by angle θ, whose operator is given by $R_y(\theta) = e^{-i\theta\sigma_y/2}$; 2. spin-dependent translation T where spin up particle is move to the right by one lattice site and spin down particle is moved to the left by one lattice site. One step of the quantum walk is given by $U = TR_y(\theta)$ and the evolution of the particle after many steps are studied.

is the description from effective Hamiltonians given by $U \equiv e^{-iH_{\rm eff}T}$. As is described in detail later in this thesis, the study of $H_{\rm eff}$ reveals non-trivial topology, whose topological class is the same as the well-known model of polyacetylene called Su-Schrieffer-Heeger model. This topological class results from the characteristic symmetry of $H_{\rm eff}$ called chiral or sub-lattice symmetry, which is given by the existence of unitary operator Γ which anti-commutes with the Hamiltonian, *i.e.* $\Gamma H_{\rm eff} = -H_{\rm eff}\Gamma$.

The physical manifestations of non-trivial topology of quantum

walks is the existence of zero energy bound state at the boundary between two distinct topological phases. We have proposed concrete experimental protocols to detect such topologically protected bound states, and in collaboration with Andrew White's group in University of Queensland, we explicitly observed this zero-energy state for the first time[92].

This example with quantum walks shows the possibility to generate interesting topological phenomena *by design* of protocols. Motivated by this perspective, we have further explored if other topological phases classified for static Hamiltonians with certain symmetries can be realized with extensions of quantum walk protocols[89]. Through a simple modification, we have shown that any of known topological classes in one and two dimensions can indeed be realized with quantum walks (see Fig. 1.3.4).

The study of quantum walks not only demonstrates the rich possibility to realize known topological classes, but also revealed the existence of unique topological phenomena to periodically driven systems; the existence of topologically protected π energy state.

A single zero-energy state in quantum walks was special because chiral (sub-lattice) symmetry dictates that any state $|\psi\rangle$ with eigenenergy E comes with another state $\Gamma|\psi\rangle$ with energy $-E$. Thus, for static systems, $E = 0$ state is the only state that could exist singly without a paired state. If a system possesses a single zero energy state and moreover there is no other states near zero energy, then this zero energy state cannot be removed with a small modifications of Hamiltonian due to chiral (sub-lattice) symmetry.

In the case of periodically driven systems, $E = \pi$ state is yet another special state. As is noted below Eq. (1.4), H_{eff} is defined only up to $2\pi/T$. Thus $E = \pi/T$ is the same as $E = -\pi/T$ and such state can exist, just as $E = 0$ state, without a paired state. (Here, the driving

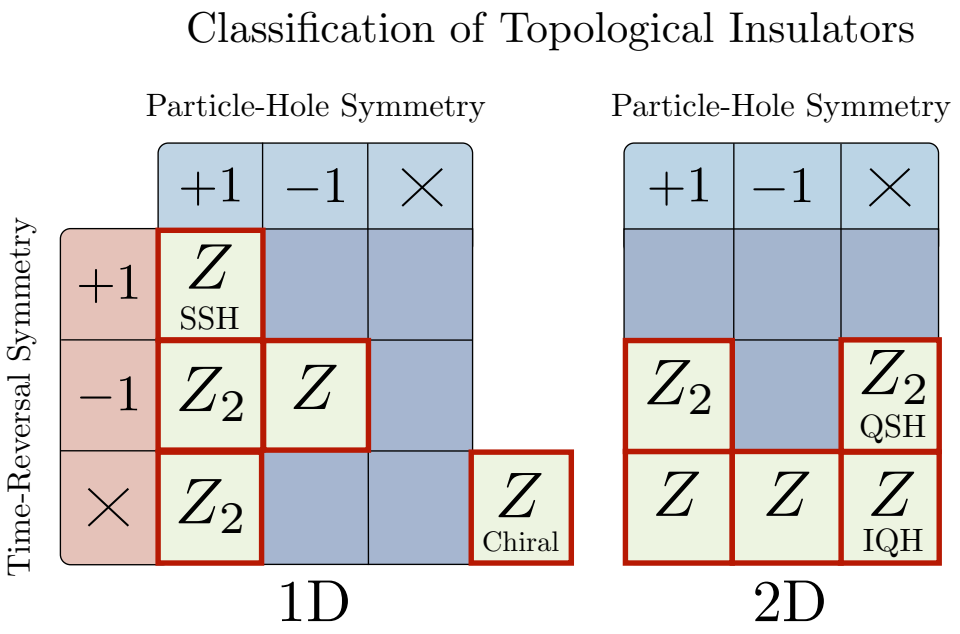

Figure 1.3.4: Classification of topological phases by symmetry for one (1D) and two (2D) dimensions, adapted from Ref.[84, 142]. Discrete time quantum walks can naturally realize all ten classes of nontrivial topological phases in 1D and 2D. Time reversal symmetry (TRS) and particle-hole symmetry (PHS) are defined by the existence of antiunitary operators $\mathcal{T}$ and $\mathcal{P}$ satisfying $\mathcal{T}H\mathcal{T}^{-1} = H$ and $\mathcal{P}H\mathcal{P}^{-1} = -H$, and may be absent, or present with $\mathcal{T}^2 = \pm 1$ ($\mathcal{P}^2 = \pm 1$). In the absence of both TRS and PHS, a distinct "chiral" symmetry with a unitary Γ satisfying $\mathcal{C}H\mathcal{C}^{-1} = -H$ may be found. In each case, the symmetry-allowed phases are classified by an integer (Z) or binary (Z_2) topological invariant. Classes containing the Su-Schrieffer-Heeger model (SSH)[153], integer quantized Hall (IQH)[58, 94, 100], and quantum spin-Hall (QSH)[16, 41, 62, 79, 98] phases are indicated.

period T in the quantum walk protocol is arbitrary, so we set $T = 1$) The existence of such $E = \pi$ in addition to $E = 0$ bound states was theoretically predicted and observed in the experiment by Andrew White's group[92].

Graphene under the application of light [91]

Quantum walk example provides proof of principle demonstrations of the versatility of periodically driven systems for studying topological phenomena. For more practical and natural example, we studied graphene under the application of light. As we will explain below, graphene is theoretically shown to display integer quantum Hall effect under the application of circularly polarized light *without* magnetic fields. In effect, the system realizes so-called Haldane model[57] in a dynamical fashion.

Generally speaking, the application of light on electron systems has two important physical effects; 1. photon-dressing of band structures through the mixing of different bands 2. redistribution of electron occupation numbers through the absorptions/emissions of photons leading to non-equilibrium distributions. First, we discuss the first part of effective dressing of band structures with light, and later come back to discuss the second part.

Photon-dressing of band structures can be most easily understood for the light with off-resonant frequency. In this case, the modifications from the static Hamiltonian can be captured in perturbation theory. Intuitively, an absorption (emission) of a single photon takes an electron out of the energy bands, and thus an electron can only virtually make such a transition. Thus the second process of an emission (absorption) of a photon has to follow. Since such process is suppressed by the energy of the photon, which here is assumed to be large, this second order processes are the main

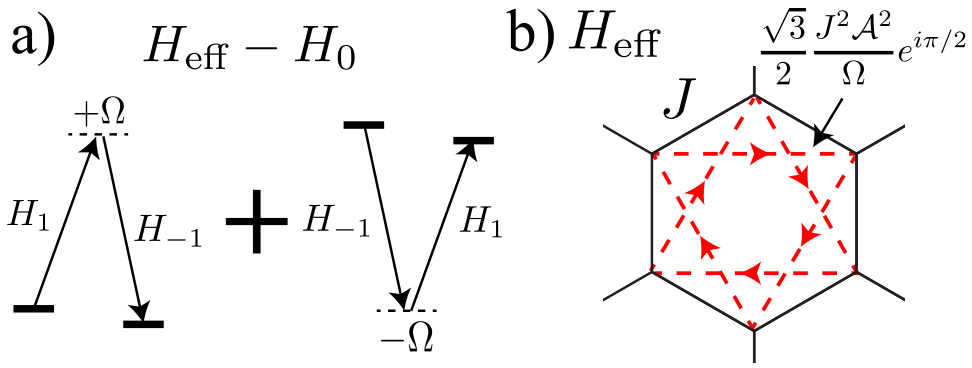

Figure 1.3.5: a) The modification of the Hamiltonian due to the virtual photon process can be intuitively understood as the sum of two second order processes where electrons absorbs and then emits a photon, and electrons first emit and absorb a photon. b) The illustration of the structure of H_{eff} in real space for graphene under the application of right circularly polarized light in Eq. (1.6). The commutator $[H_1, H_1]$ is the second neighbor hopping with phase $\phi = \pi/2$. Thus, the tight-binding model under the application of light realizes Haldane model proposed in Ref. [[57]].

contributions to the photon-dressings.

Including the light effect, Hamiltonian of the system becomes periodic in time (with one period T). If we consider Fourier components of Hamiltonian

$$H(m) = \int_0^T dt H(t) e^{im\Omega t} \tag{1.5}$$

then $H(m)$ represents the absorptions/emissions of m photons. Here $\Omega = 2\pi/T$ is the frequency of the drive.

There are two processes that contribute as illustrated in Fig. 1.3.5 a); one where electron absorbs a photon and then emits a photon $H_1 \frac{1}{\omega-(\omega+\Omega)} H_{-1}$ where ω is the energy of the original electron; another where electrons first emits a photon and then absorbs a photon, which leads to $H_{-1}\frac{1}{\omega-(\omega-\Omega)}H_1$. By summing these two contributions, we

obtain the correction due to the second order process, leading to the effective Hamiltonian,

$$H_{\text{eff}} \approx H_0 + \frac{[H_{-1}, H_1]}{\Omega} \tag{1.6}$$

When this formalism is applied to graphene under the application of circularly polarized light as described later in the thesis, the second term in Eq. (1.6) corresponds to the second order hopping with imaginary amplitude, as illustrated in Fig. 1.3.5 b). Such a model is nothing but the one described earlier by Haldane[57], and its band structure leads to integer quantum Hall effects without magnetic field! In this case, however, such second order hopping is generated in a dynamical fashion, in contrast to artificial constructions of the model by Haldane.

The considerations above only take into account the photon-dressings of band structures, and ignore the issue of electron occupations in driven environments. Topological properties only appear when certain bands are fully filled, and it is not clear how this band occupation can be achieved and topological properties survive when the system is strongly driven out of equilibrium by the application of light.

In order to answer these questions, we studied the physical consequence of the application of light through DC many-terminal transport measurements as in Fig. 1.3.6. The coupling of the driven systems with leads, that are in return coupled with equilibrium reservoirs, plays the crucial role to determine the occupations of electrons. Using the formalism for transport properties in periodically driven systems developed by various groups[75, 95, 112], we explicitly demonstrate that for *off-resonant* light where electrons cannot directly absorb photons, the transport properties of the non-equilibrium

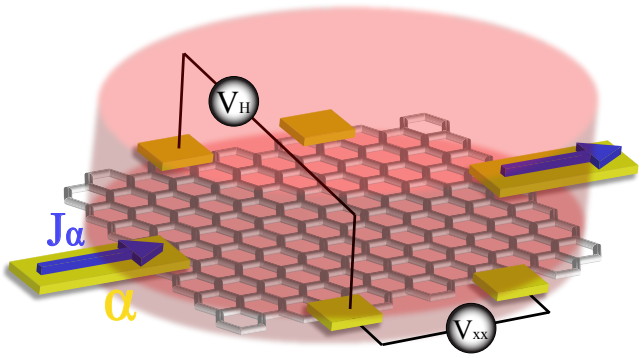

Figure 1.3.6: The many-terminal measurements of DC current for graphene under the application of light. Graphene is attached to multiple leads labeled by $\{a\}$, and the leads are connected to reservoirs at chemical potentials, $\{\mu_a\}$. Off-resonant, circularly polarized light is applied to the graphene. In the absence of impurities and interactions, electrons coming from leads coherently propagate under the application of light, asborb or emit photons, and leak out into leads. Current measurements between each leads determine longitudinal and Hall conductances.

systems attached to the leads are well approximated by the transport properties of the system described by the *static* effective Hamiltonian that incorporates the virtual photon absorption processes [91]. In particular, the occupations of the electrons under this situation are close to the filling of the photon-dressed bands. This study constitutes the first direct approach to investigate the topological transport property in periodically driven systems, and can provide the starting point for more in-depth analysis of the difficult problems that include relaxation processes and on-resonant light applications.

Realizations of Majorana Fermions in static and driven cold atomic systems [77]

Thanks to recent development of technology, cold atom systems allow versatile controls of their parameters and thus provide an ideal

platform for realizing periodically driven systems. In this paper, we proposed long-sought realizations of Majorana Fermions, using two hyperfine states of Fermions with multiple lasers.

The ideas to realize Majorana Fermions in this system are motivated by recent proposals to realize it in one dimensional spin-orbit coupled semiconductors in proximity with s-wave superconductors in the presence of transverse magnetic field[104, 118]. In order to provide all the necessary ingredients in the Hamiltonian, we consider the application of the following 2 lasers.

1. We realize "superconducting pairing" term Δ in cold atoms as "molecule pairing," by applying the laser which associate/de-associate Fermion particles in two hyperfine states into a molecule and vice versa. Note that since this laser creates Fermions from molecules, it acts as a chemical potential term μ as well when the laser is detuned in frequency.

2. We effectively realize both "spin-orbit coupling" term u and "transverse magnetic field" B by applying a laser which induces the transition between two hyperfine states of Fermions, while giving the particle a momentum kick by transferring the photon momentum.

In the static case, this system realizes topological phases when the intensity of second laser which realizes "transverse magnetic field" B becomes sufficiently stronger than the intensity of the first laser which induces "superconducting pairing" Δ amplitudes.

We also consider periodically driving this system by, for example, periodically changing the chemical potentials of Fermions through periodical change of detuning frequency of the first laser. Then it is possible to induce topologically non-trivial phase even when Δ and B correspond to values for topologically trivial phase in the static system. Moreover, just in the case of π energy state of discrete

quantum walks, this periodically driven systems allows the realization of two flavors of Majorana Fermions at 0 and π energy, which could never happen in static systems. Thus, this example gives yet another demonstration that periodically driven systems provide rich platform for studying topological phenomena.

1.4 Transient Dynamics

There could also be a number of interesting physics in the transient dynamics of non-equilibrium quantum systems. However, descriptions and calculations of quantum dynamics for many-body systems are typically very hard and can be solved under only a special circumstances. During previous studies, we have analyzed two types of tractable systems 1. one dimensional Bostonic systems where systems whose low-energy dynamics is described by Tomonaga-Luttinger theory[88, 90] 2. Superfluid and Mott insulating states of three dimensional Bosonic systems, where mean-field theory provides a good starting point for understanding the systems[122]. These systems provide examples of unique dynamics and demonstrate ideas as a proof-of-principle. In the following, we describe examples of the dynamics with one-dimensional quasi-condensates.

Cooling of a quantum many-body system [127]

While thermodynamics of classical systems are well-understood and such understandings are applied for the heating and cooling of systems, a similar idea is absent for quantum systems. Traditionally, quantum systems are hard to control, and thus, any disturbances you introduce to quantum systems are thought to lead to heating of the system in experiments. Recent advances of quantum technologies now allow much more intricate controls of quantum systems, and as a consequence *coherent* driving of the system became possible.

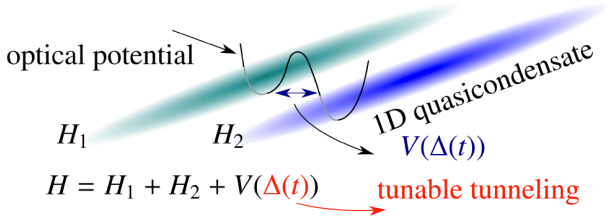

Figure 1.4.1: Two coupled one-dimensional condensates. The tunneling amplitude $\Delta(t)$ can be tuned by raising or lowering the potential barrier.

Motivated by the extraordinary experimental progress in cold atom systems, here we sought to find cooling protocols of quantum, many-body cold atom systems. Lowering of the temperature for cold atom systems is crucial for the study of many interesting physics including the study of Fermionic Hubbard model with repulsive interactions. Study of high-temperature superconductivity indicates that this system leads to d-wave pairings of superconductivity, but yet, this expectation has never been directly confirmed in experiments and remains to be controversial. Due to the small energy scale of cold atom systems, observations of d-wave superconductivity requires an order of magnitude smaller temperature than the one achieved with the current state of art cooling methods (sub-nano Kelvin regime).

In order to study whether cooling of quantum systems is possible through coherent dynamics, we studied the systems of one dimensional Bosonic quasi-condensate on an atomchip, where current on the atom chip creates a potential barrier in the middle of the one dimensional condensate so that it splits the quasi-condensate into two(see Fig. 1.4.1).

In this paper, we considered dynamically changing the barrier between the two one dimensional quasi-condensates. Our aim is to find the optimal dynamics for the barrier so that one of the

quasi-condensate has the lowest energy possible at the end of the dynamics.

The study of this system, two coupled one dimensional quasi-condensates, reduces to the study of multi-mode harmonic oscillators in the low energy descriptions of Tomonaga-Luttinger theory. Such optimization problems can be solved through well-established classical optimization theory. Applying so-called Pontryagin's maximum principle, we found that the optimal protocols of barrier dynamics are given by "bang-bang" protocols, where, at a given time of the dynamics, the height of the barriers is set to either at its maximum value or minimum value. Through such protocols, cooling of the one of the quasi-condensate by the factor of 5 is possible under reasonable experimental settings.

Prethermalization phenomena probed through the distribution functions of interference patterns [50, 90, 97]

In this work, we studied the similar system as the previous study of "cooling of quantum many-body systems" but asked conceptually different questions. Here we start from a one-dimensional quasi-condensate, and suddenly split it into two. The subsequent dynamics is studied through Tomonaga-Luttinger formalism. This is an example of quench dynamics, where a parameter in the system is suddenly changed and subsequent dynamics is evolved under a constant Hamiltonian. Here, one of the main questions we are interested in is whether the split condensates equilibrate after sufficient amount of time.

One of the challenges to answer this question is the characterizations of dynamical states through observables. Unlike equilibrium states where states are determined by thermodynamical variables such as temperature and volume, dynamical states are

characterized by larger set of variables and thus, richer observables are required to more holistically capture their states.

Previous studies of equilibrium one dimensional quasi-condensates employed studied interference patterns after the release of two quasi-condensates[61, 69, 124]. Average amplitude of interference patterns, for example, successfully captures the strength of fluctuations in the condensates. In order to capture quantum nature of the systems, they also studied quantum fluctuations of interference patterns. In fact, by repeated observations of interference patterns, experiments successfully constructed the full distributions of interference patterns. For equilibrium systems, Imambekov *et al* theoretically calculated the distributions, and the theory agrees very well with experimental results[61, 69].

Motivated by these studies, we extended the calculations of full distribution functions of interference patterns to this dynamical systems, and we have analytically calculated the time evolution of the distributions of interference patterns after the quench (splitting). The resulting distribution functions are visualized as a two-dimensional heat map, where radius corresponds to the interference amplitudes and angle corresponds to (average) phase difference between the two quasi-condensates(see Fig. 1.4.2).

Using this theoretical framework, it is possible to observe long-time limit of the dynamics in the low energy sectors. One crucial insight is that in the low energy sectors, modes with different momenta do not mix, and thus can never truly equilibrate. A true equilibration takes place only when high order terms contribute to the dynamics, which usually takes much longer time than the typical time scale of the dynamics for interference patterns governed by low energy sectors. Yet, it is possible to show that interference patterns becomes indistinguishable from those interference patterns between two

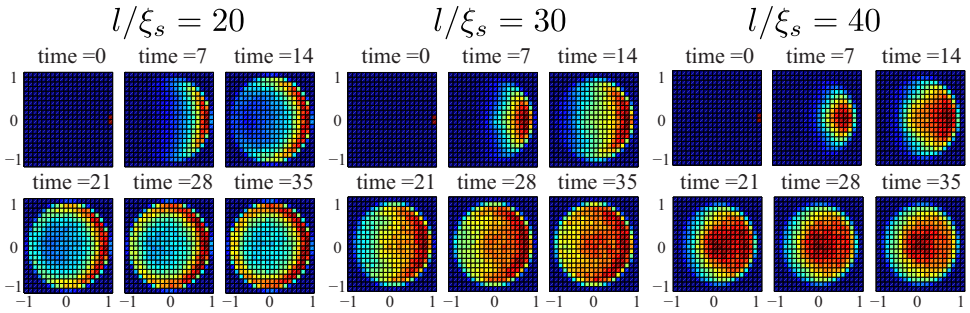

Figure 1.4.2: Time evolution of the joint distribution function $P^{x,y}(\alpha, \beta)$ for the system size $L/\xi_s = 200$, the spin Luttinger parameter $K_s = 20$ and various integration lengths $l/\xi_s = 20$(left),30(middle), and 40(right). Time is measured in units of ξ_s/c_s where c_s is the spin sound wave velocity. Here axes are scaled such that the maximum value of α and β are 1. For for short integration length $l/\xi_s = 20$, the dynamics leads to the distribution with the "ring"-like structure, showing that the magnitude of spins does not decay much (spin diffusion regime). On the other hand, for longer integration lengths, the magnitude of spins decays quickly and the distribution forms a "disk"-like structure(spin decay regime).

equilibrium quasi-condensates after relatively short time within the theory of low energy sectors(See Fig. 1.4.3).

This phenomena, that display observables corresponding to equilibrium states when the state is far from equilibrium, are known as *prethermalizations*. Prethermalizations are first proposed to explain the observed phenomenon in ion collisions where equilibrium equations of states seem to be satisfied way before true equilibration is expected to establish[15]. Our calculations show that one dimensional quantum system is yet another example of the system where prethermalizations can be observed.

Following our theoretical calculations and proposals, Schmiedmayer's group in Vienna has carried out the proposed experiments[50, 97]. Indeed, the prethermalization phenomenon has been confirmed as expected from the theory. They have demonstrated

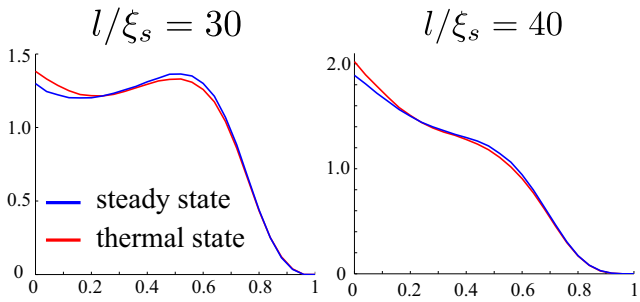

Figure 1.4.3: The distributions of interference contrast for steady states of split quasi-condensates and two thermal quasi-condensates. Here x axis is scaled such that the maximum value of interference contrast is 1. For the split condensates, we plot the distribution at time $t = 60\xi_s/c_s$ for Luttinger parameter $K_s = 20$, system size $L = 400\xi_s$ and two different integration length $l/\xi_s = 30, 40$. The thermal quasi-condensates are for temperature $\frac{\pi c_s}{2\xi_s}$ for the same integration length corresponding to the effective temperature obtained in Eq. (3.52).

that the distribution of interference patterns observed in the experiments agree well with the one predicted in theory. This implies, in return, that this distributions of interference patterns closely resembles those obtained from equilibrium condensates. Thus one can define so-called effective temperature T_{eff} which is nominal temperature of quasi-condensates observed from the interference patterns between the steady state after the quench dynamics. The existence of such effective temperature is one signature of prethermalization. Moreover in their experiments, they have confirmed the correctness of the theory by further studying the following dependence of effective temperature on the parameters of the experiments;

1. Independence of the effective temperature on the initial temperature of quasi-condensate, see Fig. 1.4.4 B. Since this effective temperature is entirely determined by quench dynamics in the theory, it should be independent of the initial

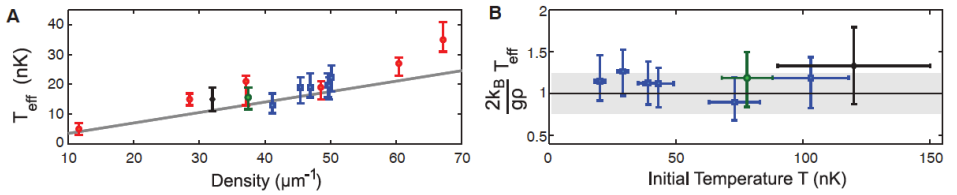

Fig. 4. **(A)** Dependence of T_{eff} on ρ and **(B)** independence of T_{eff} from the initial temperature T of the system before splitting, corrected for the scaling of T_{eff} with density. The colors encode different data sets. The (black) solid line corresponds to the theoretical prediction $k_B T_{eff} = g\rho/2$. In (A) and (B), the black data point corresponds to the data set presented in Fig. 3, and the green data point corresponds to the data set presented in Fig. 2.

Figure 1.4.4: (A) Dependence of T_{eff} on ρ and (B) independence of T_{eff} from the initial temperature T of the system before splitting, corrected for the scaling of T_{eff} with density. The colors encode different data sets. The (black) solid line corresponds to the theoretical prediction $k_B T_{\text{eff}} = g\rho/2$.

temperature of the quasi-condensate. On the other hand, the true equilibrium temperature of the system crucially depends on the initial temperature of the system. In fact, the observed effective temperature is $\approx 14nK$ whereas the initial quasi-condensate temperature is as large as $100nK < T$. Thus, this result unambiguously demonstrate that the resulting steady state is distinct from true equilibrium states, despite of the nominal effective temperature of interference patterns.

2. Linear dependence of the effective temperature on the density of particles, see Fig. 1.4.4 A. In the experiment, the density of particles can be changed by loading fewer number of particles at the beginning. Then, the effective temperature of the interference patterns is measured after steady states are reached.

These results convincingly show that the observed phenomenon is prethermalization.

1.5 Steady states

When one hears the word "non-equilibrium quantum systems," one typically thinks about dynamical processes. However, even when the system is not evolving, non-equilibrium systems could produce interesting physics. An example comes from the study of steady states. There are a few different scenarios where steady states that are distinct from equilibrium states are created;

1. Steady states as a result of competitions between drivings and dissipations. Drivings are constantly disturbing systems to bring them out of equilibrium, and dissipations are pushing them toward equilibration. After sufficient amount of time, this competition can lead to steady states that are not equilibrium states. One interesting result of such dynamics is the preparation of dark states, where dissipations put systems into states that are not affected by the drivings. A group of Peter Zoller has proposed that intricate correlated states including topological phases can be realized through this method[34].

2. Existence of (approximate) conserved quantities prevents true equilibration to take place for a long time, and thus leads to the generation of steady states distinct from equilibrium states. Prethermalization we discussed above is one example of phenomena that result from this mechanism.

3. Separation of energy scales sometimes leads to the equilibration of states within restricted energy range.

The possibility to produce steady states that are distinct from equilibrium states implies that such physics could lead to novel physics that could never be possible in equilibrium systems. In the following, we describe our previous work where this third example,

generations of steady states due to separation of energy scales, produced strongly correlated states that are otherwise very difficult to create in realistic situations for static systems.

Correlated phases in tilted optical lattices [123]

The original idea of this work comes from the work by Subir Sachdev and company[137], where he demonstrated that tilting the (one-dimensional) Mott insulating states created with cold atoms and optical lattices leads to the effective Hamiltonian for Ising ferromagnet in a transverse field and zero longitudinal field.

The description of this physics is simple. Consider one dimensional Mott insulating state, with, for simplicity, tunneling strength t set to zero, see Fig. 1.5.1, a). We tilt the optical lattice by applying a linear potential with strength E which corresponds to the potential difference between the neighboring sites. If we increase E, then there would be a transition point at $E = U$ where U is the interaction strength of the particles. When $E < U$, the system with one particle per site is the lowest energy state. On the other hand, when $E > U$, lowest energy states are states with alternate occupations of 0 and 2. There are two states with this property as described in Fig. 1.5.1, b) and c). Thus the ground state is doubly degenerate, which can be interpreted as two degenerate ferromagnetic phases. With this interpretation in mind, it is possible to more formally map this model to Ising ferromagnetic Hamiltonian with a transverse magnetic field.

Notice that as soon as $E > 0$, true ground state of the system is no longer Mott insulating state with one particle per site, but sliding states where all the particles are piled up at the bottom of the ladder. When tunneling strength t is non-zero, the state follows this ground state if we increase E sufficiently slowly due to the adiabatic theory. However, if E is initially increased rapidly, then in the subsequent

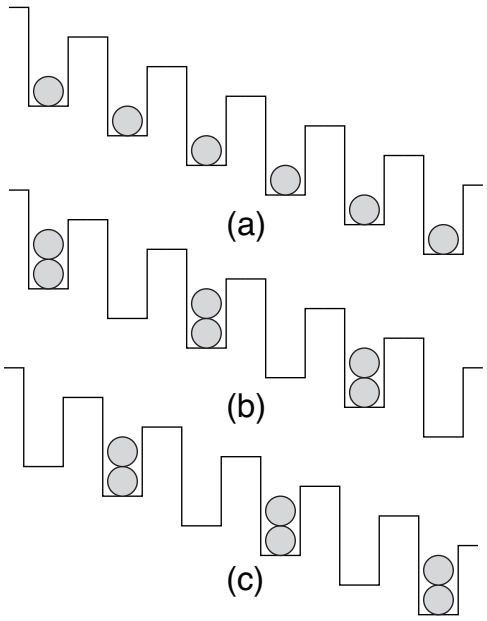

Figure 1.5.1: a) ground Mott insulator when $E < U$. b), c) states with Ising order when $U > E$.

time, sliding down of particles are suppressed due to the energy gap for hopping a particle to next site, given by $\Delta = U - E$. In other words, the energy sector of the state with one particle per site is separated from the energy sector of ground state as E takes a finite value. Due to this separation of energy, one particle per site state remains a stable steady state. Within this energy sector, the system can be studied as effective transverse Ising model.

Now my idea was to extend this simple magnetic model to richer models that possess interesting correlated physics. By applying this tilting ideas to lattices in larger dimensions, I noticed it is possible to introduce the physics of geometrical frustrations, that are known to lead to correlated phases[110, 133]. The simplest example comes from tilting the Kagome lattice. When $E > U$, all the particles try to slide down to lower energy site to create $0 - 2$ pair. However, due to the

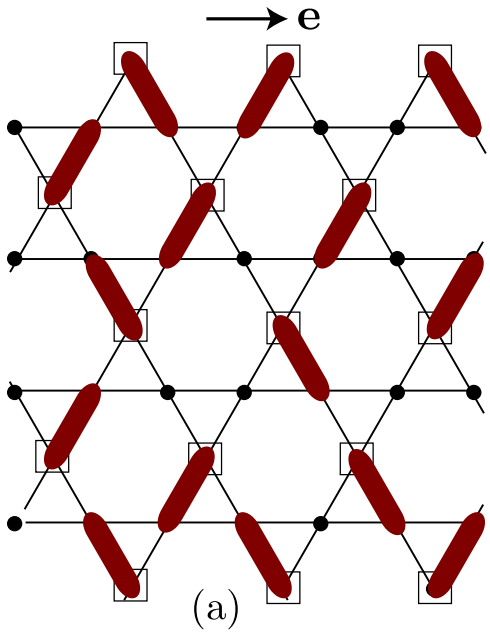

Figure 1.5.2: An example of steady states prepared when $E > U$ for geometrically frustrated lattice. Here, we assume that three particle interaction U_3 is positive and non-zero.

geometrical frustration, it is not possible for all the particles to slide down, but only 1 in 3 particles can slide down, as illustrated in Fig. 1.5.2.

Such geometrical frustration generates exponentially large number of degenerate ground states when the tunneling strength is zero. When the tunneling strength is non-zero, corrections to the effective Hamiltonian generate lead to "order by disorder" mechanism, where quantum fluctuations lift the degeneracy and pick out a few ground state. In the case of tilted Kagome lattice, I have proven that the ground state is unique and is equal superposition of all the degenerate states when $t = 0$. Such a state, which lacks any magnetic order in the ground state, is known as quantum liquid phase[8]. Such lack of

magnetic order at temperature much lower than the typical energy scale of magnetic interaction strength is surprising, and has attracted tremendous attentions in recent years in condense matter communities. Our example here provides the first realistic systems where such quantum liquid states can be realized as *non-equilibrium, many-body states*.

1.6 Summary of overview

Previous sections give overviews of my works on the rich physics that can be found in non-equilibrium quantum systems, in three large topics of 1. periodically driven systems 2. transient dynamics and 3. steady states.

In the rest of the thesis, we focus on the following two topics and describe their physics in detail.

1. Topological phenomena in discrete quantum walks

2. Prethermalization in one dimensional quasi-condensates

These topics are representatives of physics described in this overview. Both of these theoretical frameworks led to concrete experimental proposals and predictions that are realized and confirmed by Andrew White's group in Queensland, Australia and Joerg Schmiedmayer's group in Vienna, Austria, respectively. These ideas, together with other topics introduced in this overview, can be extended to provide further novel phenomena and examples, which not only lead to fundamental understandings of non-equilibrium quantum systems, but also possibly to advancement of quantum technologies.

2

Topological phenomena in quantum walks

Discrete quantum walks are dynamical protocols for controlling a single quantum particle. Despite of its simplicity, quantum walks display rich topological phenomena and provide one of the simplest systems to study and understand topological phases. In this chapter, we review the physics of discrete quantum walks in one and two dimensions in light of topological phenomena and provide elementary explanations of topological phases and their physical consequence, namely the existence of boundary states. We demonstrate that quantum walks are versatile systems that simulate many topological phases whose classifications are known for static Hamiltonians.

Furthermore, topological phenomena appearing in quantum walks go beyond what has been known in static systems; there are phenomena unique to quantum walks, being an example of periodically driven systems, that do not exist in static systems. Thus the quantum walks not only provide a powerful tool as a quantum simulator for static topological phases but also give unique opportunity to study topological phenomena in driven systems.

2.1 Introduction

Discrete quantum walk, in its simplest form, is a dynamical protocol for controlling a single spin $1/2$ particle in one dimensional lattice (see Fig. 2.1.1). It consists of two operations given by a spin rotation and spin-dependent translation. The evolution of quantum walk results from the repeated applications of these two operations in alternate fashion. From the first introduction of the concept of quantum walks by Aharonov[2], quantum walks attracted tremendous attentions due to their implications in quantum information science[81]. One of the attractive features of quantum walks is its simplicity which allows any student of physics who has a basic understanding of quantum mechanics to grasp its definition. Yet, the consequence of quantum walks is profound; on one hand, it provides a powerful tool for quantum algorithms[37, 81] and on the other, it displays rich topological phenomena revealing the deep relation between physics and the abstract field of mathematics[87]. In this article, we review the topological phenomena appearing in discrete quantum walks. While the concept of topological phases is often challenging to understand because it tends to be intimately intertwined with the physics of solid state materials, discrete quantum walks provide a rare opportunity to explain the idea of topological phases in the most

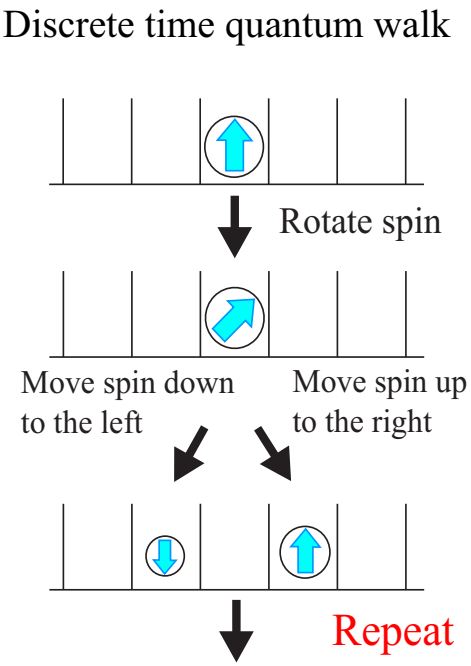

Figure 2.1.1: The protocol of a conventional discrete quantum walk. A conventional quantum walk is a dynamical protocol for controlling a spin $1/2$ quantum particle in one dimensional lattice. It consists of two operations; 1. rotation around y axis by angle θ, whose operator is given by $R_y(\theta) = e^{-i\theta\sigma_y/2}$; 2. spin-dependent translation T where spin up particle is move to the right by one lattice site and spin down particle is moved to the left by one lattice site. One step of the quantum walk is given by $U = TR_y(\theta)$ and the evolution of the particle after many steps are studied.

elementary form due to its simplicity.

This chapter is organized as follows. In Section 2.2, we study the physics of a one dimensional quantum walk. First, in Section 2.2.1, we define the simplest one dimensional quantum walk and give the description of quantum walks through so-called effective Hamiltonians. This quantum walk possesses a symmetry that is not apparent at a first sight but plays a crucial role for its topological properties, and we describe this symmetry in Section 2.2.2. The effective Hamiltonian approach to quantum walks gives an intuition behind the behavior of quantum walks, which we use to derive the analytic expression for their asymptotic distribution in Section 2.2.3. This conventional quantum walk and slight variations of it has been realized in a numerous experiments with different physical settings, and we explain some of their realizations with cold atoms, photons and ions in Section 2.2.4.

In Section 2.3, we first briefly review the main ideas of topological phases that will be relevant to the study of quantum walks.

Starting from Section 2.4, we investigate the topological nature of the quantum walks. In Section 2.4.1, we describe the concept of topological invariants in the context of quantum walks. In order to fully explore the topological phases in quantum walks, we extend the conventional quantum walks to so-called split-step quantum walk in Section 2.4.2, which displays multiple topological phases in its phase diagram. Using split-step quantum walks, we argue in Section 2.4.3 that physical manifestations of topological nature of quantum walks are the appearance of bound states across distinct topological phases. We demonstrate the existence of such bound states in two physically distinct situations; one is inhomogeneous quantum walks where rotation angles are varied in space (Section 2.4.3) and the other is the quantum walks with reflecting boundary (Section 2.4.4). The unique nature of these bound states lies in the robustness of their existence

against small perturbations. We provide additional understandings of this robustness in Section 2.4.5, which is based on the spectrum and topological invariants associated with the bound states. These bound states in the quantum walk have the same topological origin as the bound states predicted to arise in polyacetylene described by the Su-Schrieffer-Heeger model and Jackiw-Rebbi model in high energy physics.

Remarkably, there are also phenomena in quantum walks that have not been predicted before in static systems; the existence of two flavors of bound states at quasi-energy $E = 0$ and $E = \pi$. This phenomenon is unique to periodically driven systems, and we illustrate the physics in Section 2.4.8. These one dimensional topological phenomena in quantum walks have been experimentally verified in [92].

From Section 2.5, we extend the idea of quantum walks to two dimension and study their topological properties. In Section 2.5.1, we define the two dimensional quantum walks that display non-zero Chern numbers, which is the topological invariant responsible for integer quantum Hall effects. We explain in detail how Chern number arises in quantum walks in this section and demonstrate that non-trivial topology in this class results in unidirectionally propagating modes at the edge of the systems. As is the case for one dimensional quantum walks, two dimensional quantum walks display topological phenomena unique to periodically driven systems. In Section 2.5.2, we describe a simple quantum walk which possesses unidirectionally propagating modes as a result of topological invariants unique to driven systems, namely the non-trivial winding number in energy direction. Due to its simplicity, this quantum walk has the advantage of being easier to implement in experiments compared to the quantum walk introduced in Section 2.5.1.

In Section 2.6, we briefly discuss the realization of other topological

phases, using quantum walks. In Section 2.7, we conclude with possible extensions of ideas reviewed in this article.

2.2 One dimensional quantum walk : general property

2.2.1 Effective Hamiltonian description of quantum walk

The simplest form of discrete quantum walks[1] is defined as a protocol acting on a single particle in one dimensional lattice with two internal degrees of freedom. Here and throughout the paper, we consider the infinite one dimensional lattice, where the lattice site ranges from $j = -\infty$ to $j = \infty$. In an analogy with spin $1/2$ particle, we refer to the internal degrees of freedom as as "spin up" and "spin down." This quantum walk, which we call as a conventional quantum walk in this article, consists of two operations(see Fig. 2.1.1);

1. rotation of the spin around y axis by angle θ, corresponding to the operation $R_y(\theta) = e^{-i\theta\sigma_y/2}$ where σ_y is a Pauli operator. The operator on the spatial degrees of freedom is identity, and we suppress this in the following.

2. spin-dependent translation T of the particle, where spin up particle is move to the right by one lattice site and spin down particle is moved to the left by one lattice site. Explicitly, $T = \sum_{j=-\infty}^{\infty} |j+1\rangle\langle j| \otimes |\uparrow\rangle\langle\uparrow| + |j-1\rangle\langle j| \otimes |\downarrow\rangle\langle\downarrow|$.

These two operations make up one step $U = TR_y(\theta)$ of the quantum walk, and the evolution of the particle after many steps of the walk is studied. It is possible to define more general quantum walks by

[1]Throughout the paper, we consider discrete quantum walks, so we interchangeably use the word "discrete quantum walk" and "quantum walk" when confusion does not arise.

replacing the first operation by any unitary operation $R(\theta, \phi)$, which can be written as the product of the rotation of the spin around some axis $\mathbf{n}$ by angle θ and the phase accumulation ϕ *i.e.* $R(\theta, \phi) = e^{-i\theta \mathbf{n}\cdot\boldsymbol{\sigma}/2} e^{-i\phi}$. However, many central concepts of topological phases in quantum walks can be illustrated with the simple quantum walk defined above, so we focus on the conventional quantum walk in this paper. The extensions to more general case is straightforward. Discrete quantum walks have been realized in variety of experiments with ions, cold atoms and photons [23, 80, 145, 170]. In Section 2.2.4, we describe experimental realizations of quantum walks in some of these systems in details.

Many properties of quantum walks, such as the distribution of the particle after many steps, have been extensively studied from mathematical physics point of view[18, 49]. In this paper, we take the intuitive picture in which quantum walk is considered as a stroboscopic realization of static effective Hamiltonian, defined through the evolution operator of one step quantum walk protocol $U = TR_y(\theta)$;

$$U = TR_y(\theta) \tag{2.1}$$
$$\equiv e^{-iH_{\text{eff}}\Delta T} \tag{2.2}$$

Here, ΔT is the time it takes to carry out one step of the quantum walk. Because n steps of quantum walk correspond to the evolution $U^n = e^{-iH_{\text{eff}}nT}$, the evolution under the quantum walk coincides with the evolution under the effective Hamiltonian $U = TR_y(\theta)$ at integer multiple times of T. From this perspective, quantum walk provides a unique quantum simulator for the static effective Hamiltonian H_{eff} through periodic drive of a quantum particle. In the following, we set $\Delta T = 1$. While the effective Hamiltonian H_{eff} represents a static Hamiltonian, there is one important difference from the truly static

Hamiltonian; the energy is only defined up to $2\pi/\Delta T$, as is clear from the definition Eq. (2.2). This periodic structure of the eigenvalues of effective Hamiltonian, called quasi-energy, is the result of discrete time-translational symmetry of the system. Just as momentum becomes quasi-momentum with periodic structure when the system possesses only discrete spatial translational symmetry, energy also becomes quasi-energy with periodic structure in this case. This distinction between energy and quasi-energy plays an important role in understanding the topological phenomena unique to quantum walks, or periodically driven systems, as we explain later.

For the quantum walk defined above, the evolution operator of one step $U = TR_y(\theta)$ possesses spatial translational symmetry, and thus the evolution operator becomes diagonal in quasi-momentum space. In particular, spin-dependent translation T can be written as

$$T = \sum_{j=-\infty}^{\infty} |j+1\rangle\langle j| \otimes |\uparrow\rangle\langle\uparrow| + |j-1\rangle\langle j| \otimes |\downarrow\rangle\langle\downarrow| \tag{2.3}$$

$$= \int_{-\pi}^{\pi} dk \;\; e^{ik\sigma_z} \otimes |k\rangle\langle k| \tag{2.4}$$

In this expression, we see that the spin-dependent translation mixes the orbital degrees of freedom represented by quasi-momentum k and spin encoded in σ_z. The presence of such spin-orbit coupling is a key to realizing topological phases. We note that the continuous quantum walk does not have such spin-orbit coupling and thus is distinct from discrete quantum walks in the topological properties[81]

Now in quasi-momentum space, the effective Hamiltonian for the conventional quantum walk takes the form

$$H_{\text{eff}} = \int_{-\pi}^{\pi} dk \, [E(k)\, \mathbf{n}(k) \cdot \boldsymbol{\sigma}] \otimes |k\rangle\langle k|, \tag{2.5}$$

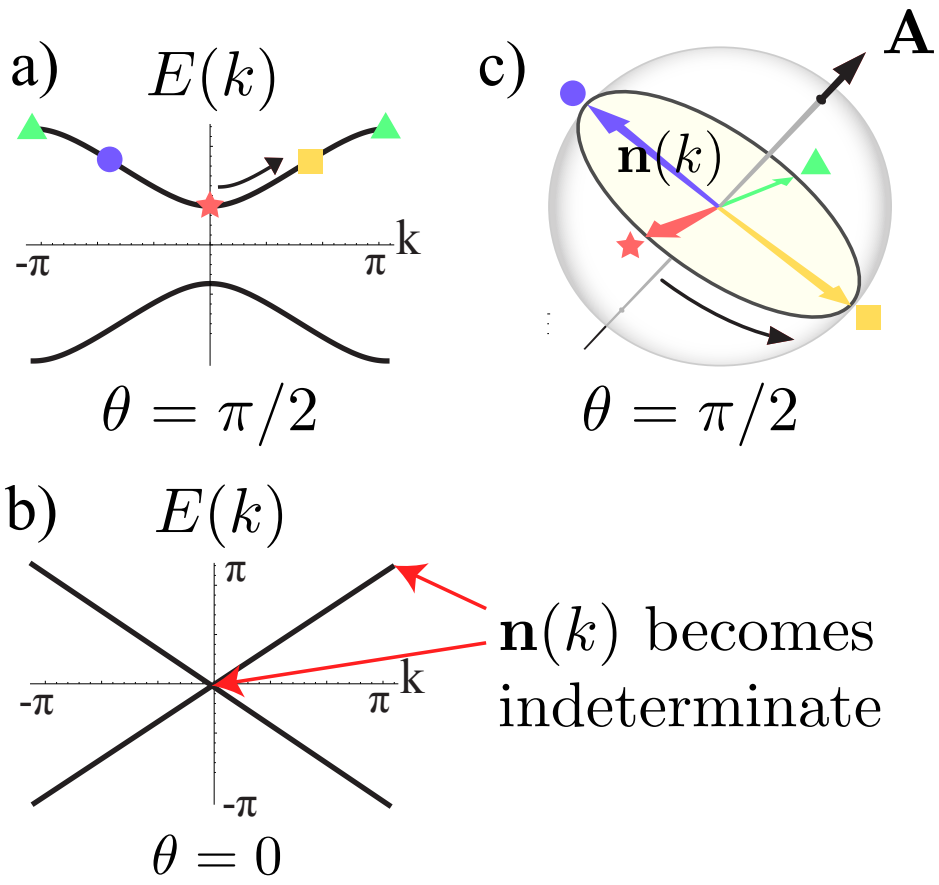

Figure 2.2.1: a), b) quasi-energy spectrum of the effective Hamiltonian Eq. (2.5) for conventional quantum walks with rotation angle $\theta = \pi/2$ and $\theta = 0$. The spectrum consists of two bands coming from two internal degrees of freedom, and there is a finite gap between the two bands for general value of θ except for $\theta \neq 0, 2\pi$. For $\theta = 0, 2\pi$, the spectrum closes the gap as is observed in b). Note that the gap is closing in this case at quasi-energy $E = 0$ as well as at $E = \pi$. c) The behavior of the eigenstates $\mathbf{n}(k)$ in Eq. (2.7) represented on a Bloch sphere. For a given quasi-momentum k, the eigenstate is the superposition of spin up and down, and therefore, can be represented as a point on a Bloch sphere given by $\mathbf{n}(k)$. For a conventional quantum walk, $\mathbf{n}(k)$ traces a circle around the origin as k goes from $-\pi$ to π. Note that $\mathbf{n}(k)$ is perpendicular to a vector $\mathbf{A} = (\cos(\theta/2), 0, \sin(\theta/2))$ for all k in our quantum walk. For gapless quantum walk with $\theta = 0, 2\pi$, $\mathbf{n}(k)$ becomes ill-defined at those k corresponding to the gap closing point.

where $\boldsymbol{\sigma} = (\sigma_x, \sigma_y, \sigma_z)$ is the vector of Pauli matrices and the unit vector $\mathbf{n}(k) = (n_x, n_y, n_z)$ defines the quantization axis for the spinor eigenstates at each momentum k. For $\theta \neq 0$ or 2π, explicit expressions for $E(k)$ is given by

$$\cos E(k) = \cos(\theta/2)\ \cos k \tag{2.6}$$

Typical band structure of quasi-energies $E(k)$ is plotted in Fig. 2.2.1a) for $\theta = \pi/2$. There are two bands because the system has two internal degrees of freedom, and for generic values of θ, the two bands are separated by a band gap.

On the other hand, at $\theta = 0$, $R_y(\theta) = I$, and therefore the effective Hamiltonian is $H_{\text{eff}} = k\sigma_z$. Thus the quasi-energy bands close the gap at quasi-momentum $k = 0$ at quasi-energy $E = 0$. Moreover, due to the periodicity of energy, the spectrum also closes the gap at quasi-momentum $k = \pi$ at quasi-energy $E = \pi$. The spectrum for $\theta = 0$ is illustrated in Fig. 2.2.1b). Similar situation occurs at $\theta = 2\pi$.

Interesting structure appears in $\mathbf{n}(k)$ of Eq. (2.5). For $\theta \neq 0, 2\pi$, $\mathbf{n}(k)$ is given by

$$\mathbf{n}(k) = \frac{(\sin(\theta/2)\sin k,\ \sin(\theta/2)\cos k,\ -\cos(\theta/2)\sin k)}{\sin E(k)}. \tag{2.7}$$

Note that the eigenstates of the effective Hamiltonian $H_{\text{eff}}(\theta)$ are the superposition of spin up and spin down, and therefore can be represented as a point on a Bloch sphere. The unit vector $\mathbf{n}(k)$ is nothing but the unit vector that determines the direction of this point. The behavior of $\mathbf{n}(k)$ on a Bloch sphere for $\theta = \pi/2$ as k goes from $-\pi$ to π is plotted in Fig. 2.2.1c). We see that $\mathbf{n}(k)$ "winds" around the equator of the Bloch sphere. This peculiar feature is in fact the origin of topological nature of quantum walks, as we see in Section 2.4.

Note that at $\theta = 0, 2\pi$, the states at quasi-momentum $k = 0$ and π become degenerate and thus any superposition of spin up and down becomes the eigenstates of the Hamiltonian at these quasi-momentum. Thus, eigenvector $\mathbf{n}(k)$ becomes indeterminate at these points.

2.2.2 Hidden symmetry of quantum walks

The effective Hamiltonian of the quantum walk H_{eff} as given in Eq. (2.5) has an interesting symmetry. First, we note that $\mathbf{n}(k)$ is perpendicular to the vector $\mathbf{A} = (\cos(\theta/2), 0, \sin(\theta/2))$ as is easy to check from Eq. (2.7). The symmetry of the system is then given by the rotation around the axis $\mathbf{A}$ by angle π which takes H_{eff} to $-H_{\text{eff}}$, or

$$\Gamma^{-1} H_{\text{eff}} \Gamma = -H_{\text{eff}} \qquad \Gamma = e^{-i\pi \mathbf{A}\cdot\sigma/2} \tag{2.8}$$

Indeed, as is clear from the picture of Fig. 2.2.1, such rotation takes $\mathbf{n}(k)$ to $-\mathbf{n}(k)$ for each k, and thus takes $H_{\text{eff}} = \int dk E(k)\mathbf{n}(k)\cdot\sigma \otimes |k\rangle\langle k|$ to minus itself. This symmetry given by a unitary operator is called sublattice or chiral symmetry[2].

One interesting feature of quantum walks which results from the sublattice (chiral) symmetry is the symmetric spectrum; states with energy E and $-E$ always appear in pairs. This is easy to demonstrate. Given a state $|\psi\rangle$ with eigenvalue E, one can check that the state $\Gamma|\psi\rangle$

[2]These two words are used interchangeably in the literature. The word, "sublattice symmetry" is intuitive. When one has a Hamiltonian, for example, with sublattice structure with sublattice A and B such that the Hamiltonian is only hopping from sites of A to sites of B, then Hamiltonian can be made minus of itself by multiplying all the creation and annihilation operators of sublattice A. This operation is unitary, and thus, the Hamiltonian possesses sublattice symmetry. The word, "chiral symmetry," originates from the high energy physics, where it relates the two handedness of Dirac fields. Because the word "chiral" has the meaning of "handedness," the word "chiral symmetry" is also used in solid state physics for some crystal symmetries, and care has to be taken to use the word.

is an eigenstate of the Hamiltonian with energy $-E$;

$$\begin{aligned} & H_{\text{eff}}|\psi\rangle = E|\psi\rangle \\ \rightarrow \quad & H_{\text{eff}}\left(\Gamma|\psi\rangle\right) = -E\left(\Gamma|\psi\rangle\right) \end{aligned}$$

There are exceptions to this pairing of states. When E satisfies $E = -E$, the states $|\psi\rangle$ and $\Gamma|\psi\rangle$ can represent the same state. Due to the periodicity of quasi-energy, quantum walk has two special energies that satisfies the condition $E = -E$, given by $E = 0$ and $E = \pi$. We will later see that this property of $E = 0$ and $E = \pi$ leads to the topological protection of $E = 0$ and $E = \pi$ states. The existence of a single $E = 0$ state is known in the non-driven systems with sublattice (chiral) symmetry [136], but $E = \pi$ energy state is the novel feature of periodically driven systems.

2.2.3 Asymptotic distribution; ballistic propagation

In this section, we provide an intuition behind the propagation of a particle under quantum walks by considering their asymptotic distributions. Quantum walk was originally conceived as quantum analogue of random walk[2]. In fact, it is easy to check that if one carries out a measurement of the particle after each step, quantum walk reduces to a biased random walk. Thus, by varying the amount of decoherence in the system, one can smoothly go from a quantum walk to classical a random walk[23]. However, the behavior of a random walk is quite different from that of a quantum walk in the absence of decoherence. We remind the reader that a (non-biased) random walk asymptotically approaches the Gaussian distribution with the peak centered around the origin where the mean squared travel distance is given by $\langle x^2 \rangle = Na^2$ where a is the step size of one step. Thus, the particle propagates in a diffusive fashion under a classical random walk.

On the other hand, a particle under quantum walks propagates in a ballistic fashion[18, 49]. This fact almost trivially results from the understanding of quantum walks as simulations of static effective Hamiltonian of non-interacting particle as given by Eq. (2.2) and Eq. (2.5). If one prepares a particle in a state such that its quasi-momentum is narrowly concentrated around k, then it is intuitively clear that the particle ballistically propagates with the group velocity given by $v_k = \frac{\partial E(k)}{\partial k}$ where $E(k)$ is the quasi-energy given in Eq. (2.6).

This intuition can be made rigorous by deriving the asymptotic distribution of quantum walks. The argument above shows that the distribution of the variable $X = x/N$ in the asymptotic limit converges to a finite form. Here we consider the quantum walk of a particle initially localized at the origin $x = 0$ with spin state given by $|s\rangle$. In Appendix 2.8.1, we show that the distribution function of X takes the following form

$$\begin{aligned} P(X) &= \int_{-\pi}^{\pi} \frac{dk}{2\pi} \frac{1}{2} \left(1 + \langle \mathbf{n}(k) \cdot \sigma \rangle\right) \delta(v_k - X) \\ &\quad + \frac{1}{2} \left(1 - \langle \mathbf{n}(k) \cdot \sigma \rangle\right) \delta(v_k + X) \end{aligned} \tag{2.9}$$

where $\langle \mathbf{n}(k) \cdot \sigma \rangle = \langle s | \mathbf{n}(k) \cdot \sigma | s \rangle$, and $v_k = \frac{\partial E(k)}{\partial k}$. This result is quite intuitive; each momentum state k propagates with velocity $\pm v_k$ where $+$ sign is for spin parallel to $\mathbf{n}(k)$ and $-$ sign is for spin anti-parallel to $\mathbf{n}(k)$. Because the initial state is localized at a single site, it is the superposition of all quasi-momentum state k, and thus, the asymptotic distribution is given by the sum of the contributions for each k.

The form of asymptotic distribution written above immediately leads to various results known in quantum walks [18, 49]. For example, symmetry of the asymptotic distribution $x \leftrightarrow -x$ exists whenever $\langle \mathbf{n}(k) \cdot \sigma \rangle$ is an even function of k, which is the case when the

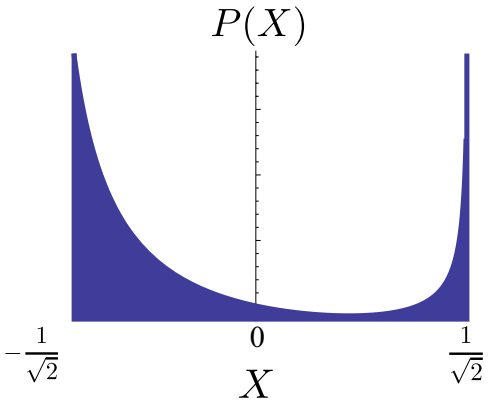

Figure 2.2.2: The asymptotic distribution of a conventional quantum walk with $\theta = \pi/2$, whose analytical solution is obtained in Eq. (2.9) and Eq. (2.10). The result is expressed for rescaled coordinate $X = x/N$ where N is the total number of quantum walk steps. X takes a finite value for $N \to \infty$ limit because a particle propagates in a ballistic fashion.

initial spin state is pointing in y direction. Otherwise, the distribution is generically not symmetric around the origin. Numerical evaluation of asymptotic distribution is always possible, and in certain cases, the analytic result can be expressed in a compact form. For example, for the asymptotic distribution of $\theta = \pi/2$ quantum walk with initial spin state pointing in z direction, the asymptotic distribution is given by

$$P(X) = \frac{1}{\pi}\frac{1}{1+X}\frac{1}{\sqrt{1-X^2}} \qquad -\frac{1}{\sqrt{2}} \leq X \leq \frac{1}{\sqrt{2}} \tag{2.10}$$

The distribution is plotted in Fig. 2.2.2. The derivation given here and Appendix 2.8.1 can be easily extended to more general quantum walks with different unitary operations or even to higher dimensions.

2.2.4 Experimental realizations of quantum walks

One dimensional quantum walks described in previous sections have been realized in experiments. Since quantum walk is a general

concept applicable to many different physical systems, there are realizations with cold atoms, ions, and photons[23, 80, 145, 170]. Such realizations in different physical settings allow different controls of the systems, such as the ability to choose the rotation operations, to introduce known amount of dephasing[23], or to create spatial boundary between regions with different rotation operations[92]. Thus, study of quantum walks in experimental settings is versatile and is not usually restricted by the technology of a specific field.

The realization of quantum walks takes a widely different forms for different systems. The realization with cold atom[80] is probably the simplest and most straightforward. In this experiment, Karsi *et al.* realized the quantum walk, using the cesium atoms (Cs). Here, two hyperfine states of cesium (Cs) atoms are used as spin degrees of freedom. The spin rotation is implemented through the application of resonant microwave radiation between these two hyperfine states. The spin-dependent translation, on the other hand, is implemented by the adiabatic translation of spin dependent optical lattices. This experiment implemented quantum walks up to 10 steps, and observed the distributions of the particle. The experiment shows a good agreement, but quantum walks were dephased after 10 or so steps.

On the other hand, in the case of photonic realization by Broome *et al.*[23], the vertical and horizontal polarization of a photon is used as spin degrees of freedom. The rotation operation is implemented through half wave plates, where the polarization of a photon is rotated as a photon goes through the plate. The polarization-dependent translation is implemented by birefringent calcite beam displacer. The optical axis of the calcite prism was cut in such way to displace horizontally polarized light to the perpendicular direction to the propagation direction and transmit the vertical polarized light without displacement. Now these optical components are put in series in, say, z direction, so that the photon goes through

them one by one as it propagates in z direction. Thus, z direction plays the role of time direction, and the photon is evolved according to the quantum walk as it propagates through these optical components. This experiment implemented 6 steps. In the subsequent experiments, this experiment was extended to create the boundary between regions with different rotation angles, which was used to investigate the topological nature of quantum walks[92]. Yet another implementations of quantum walks with photonic architecture is demonstrated in [145], using a fiber network loop.

Lastly, we describe the quantum walk implemented with ions. In [170], Zhringer *et al.* realized quantum walks in a phase space with ion $^{40}Ca^{+}$ They used the internal states $|S_{1/2}, m = 1/2\rangle$ and $|D_{5/2}, m = 3/2\rangle$ as spin degrees of freedom. For spatial degrees of freedom, they used the excitation of the ions in the harmonic traps, where the superposition of raising and lowering operators are identified as the coordinate operator $\hat{x} = a^{\dagger} + a$ and momentum operator $\hat{p} = \frac{a^{\dagger}+a}{2}$. In this space, they implemented the spin dependent translation by applying a bichromatic light that is resonant with both the blue and red axial sideband. This shows the interesting fact that quantum walks can be encoded in abstract space. The experiment demonstrates that the quantum walk in this space can maintain the coherence up to even 23 steps.

While they are not an experimental demonstrations, there are two interesting possible realizations of quantum walks proposed in natural systems.

Oka *et al.* proposes in [116] that the evolution of electrons on a ring under the application of DC electric field can be understood as quantum walks in energy level space. When the electric field is understood as the time-dependent vector potential, the problem represents a time-dependent problem, where the Landau-Zener transitions of electrons among different levels can be mapped to

quantum walks. In this work, they proposed the existence of a localized state near the ground state of the system, which is a manifestation of the topological nature of quantum walks explained in this article[87] (see Section 2.4.4).

Another proposal by Rudner and Levitov[135] concerns an extension of quantum walk to include the decaying sites at every other lattice sites, which can arise in the problem of coupled electron and nuclear spins in quantum dots in the presence of competing spin-orbit and hyperfine interactions. This quantum walk, intriguingly, displays topological phenomena as well, where the mean walking distance of a particle before it decays at one of the sites is quantized to be an integer.

2.3 Brief introduction to topological phases

Quantum walks described in Section 2.2 display rich topological phenomena. In this section, we review the ideas of topological phases, and provide the background for understanding the topological phenomena in quantum walks.

The relation between quantum phases of matter and topology was first discovered through the study of integer quantum Hall effect, which revealed the quantization of Hall conductance for two dimensional electron gas in the presence of a strong magnetic field[94, 105]. The quantization of Hall conductance is very precise, and moreover is robust against perturbations such as the impurity of the materials. The fundamental origin for such robustness is the topological nature of ground state wavefunction. Ground state wavefunction of integer quantum Hall systems is associated with a topological number. A topological number is a global property of the shape of wavefunction, like "winding," and thus cannot be changed by a continuous change. Because Hall conductance is directly given by

this topological number[156], its value does not change under the small change of Hamiltonian or its ground state wavefunction.

In addition to the quantized Hall conductance, yet another direct physical consequence of non-trivial topology of wavefunction is the existence of unidirectional edge states at the boundary of the sample[58]. The two phenomena, the quantized Hall conductance and unidirectional edge states, are closely related where the current for the quantized Hall conductance is carried by the edge states. From this point of view, the robustness of the Hall conductance against impurities results from the robustness of unidirectional edge propagation against impurity scatterings. As we explain in this article, while quantized Hall conductance is a unique phenomenon to the topological class of integer quantum Hall systems, the existence of robust edge states is generic feature of any topological class.

Because topology is a general property of ground state wavefunction, such idea is extendable to other systems in other dimensions[59, 125]. In one dimension, Su Schrieffer and Heeger gave a simple model of conducting polyacetylene and found the existence of topological solitons at edges[153]. This so-called Su-Schrieffer-Heeger model of polyacetylene is an example of one dimensional topological phase with sublattice (or chiral) symmetry. Independently, physics in the same topological class was also studied in the context of high energy physics by Jackiw and Rebbi[72, 73]. In recent years, band insulators with time-reversal symmetry are predicted to possess topological properties called quantum spin Hall effect[16, 78], and these so-called topological insulators were soon realized in experiments with HgTe[98]. One important conceptual advance of these topological phases compared to integer quantum Hall phase is that these are new topological phases appearing in the presence of symmetries such as sublattice and time-reversal symmetry, whereas the integer quantum Hall effect originally discovered in the presence

of strong magnetic field and disorders is the phenomena that appear in the absence of these symmetries. The idea has been further extended to three dimensional systems in the presence of time-reversal symmetry[29, 42, 169].

Motivated by these findings, a several groups independently classified the non-interacting systems in the presence of particle-hole, time-reversal, or sublattice (chiral) symmetry, giving the "periodic table" of topological phases[84, 126, 142]. While the possible existence of topological classes are known for the symmetry class within these categories, their realizations are not easy in condensed mater materials and consequently, some table entries have not yet found physical realizations. Moreover, even when such topological phases are proposed to be realized in condensed matter materials, it is usually hard to directly image the wavefunction of, say, topologically protected bound states with current technology. Due to the outstanding controllability, artificial systems are promising alternative candidates for studying these novel phases, and there is a number of theoretical and experimental studies of topological phenomena using cold atoms and photons [74, 77, 86, 92, 120, 148, 161, 172]. Among them, quantum walks provide unique platform where any topological phase classified in one and two dimensions is realizable with simple modifications of their protocols, as we will explain in this paper[87]. In fact, one dimensional topological class predicted to arise in Su-Schrieffer-Heeger model and Jackiw-Rebbi model has been already realized in the photonic architecture[92]. The key ingredient in the versatility of quantum walks is the controllability of the protocols. Because protocols are something experimentalists choose to implement, it is possible to design the protocols in such a way to preserve or break certain kind of symmetries. From the following section, we study how such topological structure appears in discrete quantum walks.

2.4 Topological phenomena in quantum walks

2.4.1 Topological characterization of quantum walks

In Section 2.2.1, we have seen that the eigenvectors of quantum walks $\mathbf{n}(k)$ illustrated in Fig. 2.2.1 have non-zero winding as k goes from $-\pi$ to π. Such winding gives a topological characterization of quantum walks in the presence of sublattice (chiral) symmetry.

As we noted in Section 2.2.1, the effective Hamiltonian of the quantum walk possesses the sublattice (chiral) symmetry, which constrains the eigenvector of Hamiltonian for each quasi-momentum $\mathbf{n}(k)$ to lie on the plane perpendicular to the vector $\mathbf{A}$. Under this sublattice (chiral) symmetry, $\mathbf{n}(k)$ represents a map from the first Brillouin zone, which is a circle, to the equator of Bloch sphere, which is also a circle. Then quantum walk described by Eq. (2.5) possesses non-trivial winding of this map, where $\mathbf{n}(k)$ goes around once the equator of Bloch sphere as k goes from $-\pi$ to π. In the presence of the symmetry, the winding observed in Fig. 2.2.1 c) is robust against small perturbations; one cannot change the winding number by small change of the Hamiltonian H_{eff} which preserves the sublattice (chiral) symmetry. One can intuitively check this robustness by trying to change the winding through the continuous deformations of $\mathbf{n}(k)$. We call this winding number as topological number due to their robustness against perturbations, and the topological number associated with H_{eff} is 1 whenever $\theta \neq 0, 2\pi$[3] for our quantum walks. More generally, the winding of $\mathbf{n}(k)$ around the equator can take any integer value, and different topological phases in this topological class are associated with different integers (winding numbers), and thus the topological classification is given by $\mathbf{Z}$ (a set of integers).

It is important to note that this winding number is not topological

[3] More concretely, the two bands of quantum walks both possess winding number 1.

in the absence of any symmetry constraint, in the sense that the winding number can be made zero by continuous change of $\mathbf{n}(k)$. For example, one can shrink the loop of $\mathbf{n}(k)$ into a point on a Bloch sphere.

More generally, the concept of topological numbers (or topological invariants) are defined for a collection of Hamiltonian that represent band insulators with certain symmetries. A topological invariant is assigned to each band, and its value cannot change under the continuous deformations of Hamiltonian which preserve the symmetry. There is one exception to this statement; when two bands mix with each other, the topological invariants can be changed in these two bands. We can flip this argument and say that topological numbers can change their values only if two bands close their band gaps in the process. We argue in Section 2.4.3 that this property of topological numbers results in the creation of topologically protected bound states in the spatial boundary between regions that belong to two distinct topological phases.

In the conventional quantum walk, the winding number associated with the effective Hamiltonian is always 1, and no other topological phase exist in this family of quantum walks. In the next section, Section 2.4.2, we give yet another family of quantum walks that display two distinct topological phases with winding number 0 and 1 in the presence of sublattice (chiral) symmetry. We illustrate how topological numbers can change as Hamiltonian is changed in this example.

2.4.2 Split step quantum walks

In this section, we extend the conventional quantum walk by modifying the protocols and define so-called split-step quantum walks. This example illustrates how one can engineer topological phases in

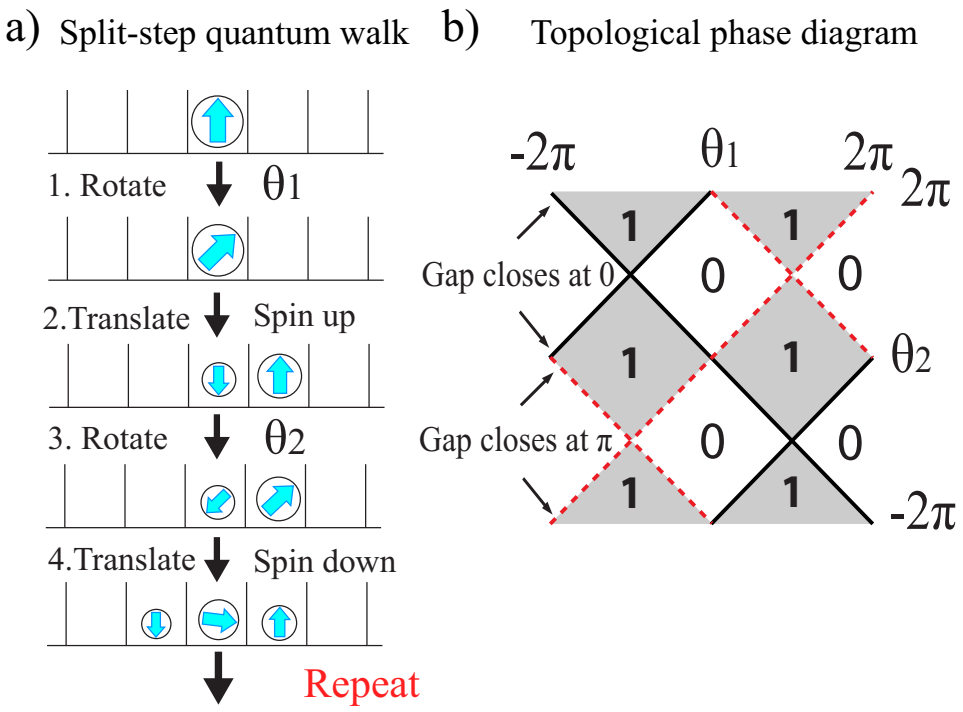

Figure 2.4.1: a) Protocol for a split-step quantum walk. Split-step quantum walk is defined for spin $1/2$ particle in one dimensional lattice, and consists of four operations; 1. spin rotation around y axis by angle θ_1, given by $R_y(\theta_1)$; 2. Translation of spin up to the right by one lattice, $T_\uparrow$; 3. spin rotation around y axis by angle θ_2, given by $R_y(\theta_2)$; 4. Translation of spin down to the left by one lattice, $T_\downarrow$. The evolution operator of one step is given by $U = T_\downarrow R_y(\theta_2) T_\uparrow R_y(\theta_1)$. b) The topological phase diagram of split-step quantum walk for various rotation angles θ_1 and θ_2. The phase is characterized by the winding number W, and split-step quantum walks realize either $W = 0$ or $W = 1$. Since winding number is a topological number, it can change its value only when the band gap closes, and these gapless phases are denoted by solid black line (band gap closes at quasi-energy $E = 0$) and by red dotted line (band gap closes at quasi-energy $E = \pi$).

quantum walks through the active design of the protocols.

Split-step quantum walks is a simple extension of conventional quantum walks which have one additional rotation and translation process(see Fig. 2.4.1 a)). The complete protocol is as follows;

1. Rotation of the spin around y axis by angle θ_1, corresponding to the operation $R_y(\theta_1) = e^{-i\theta_1\sigma_y/2}$.

2. Translation of spin up particle to the right, given by $T_\uparrow = \sum_j |j+1\rangle\langle j| \otimes |\uparrow\rangle\langle\uparrow| + 1 \otimes |\downarrow\rangle\langle\downarrow|$. Spin down particle stays in the original position.

3. Second rotation of the spin around y axis by angle θ_2, corresponding to the operation $R_y(\theta_2) = e^{-i\theta_1\sigma_y/2}$.

4. Translation of spin down particle to the left, given by $T_\downarrow = \sum_j |j-1\rangle\langle j| \otimes |\downarrow\rangle\langle\downarrow| + 1 \otimes |\uparrow\rangle\langle\uparrow|$. Spin up particle stays in the original position.

Thus, the evolution operator of one step is given by $U(\theta_1, \theta_2) = T_\downarrow R_y(\theta_2) T_\uparrow R_y(\theta_1)$. This split-step quantum walk is reduced to the conventional quantum walk defined in Section 2.2.1 with $\theta_2 = 0$. As before, we can find the effective Hamiltonian through $U \equiv e^{-iH_{\text{eff}}}$. The effective Hamiltonian again takes the form Eq. (2.5) where the quasi-energy is

$$\cos E(k) = \cos(\theta_2/2)\cos(\theta_1/2)\cos k - \sin(\theta_1/2)\sin(\theta_2/2), \qquad (2.11)$$

and the eigenvector $\mathbf{n}(k)$ is

$$\begin{aligned} n_x(k) &= \frac{\cos(\theta_2/2)\sin(\theta_1/2)\sin k}{\sin E(k)} \\ n_y(k) &= \frac{\sin(\theta_2/2)\cos(\theta_1/2)+\cos(\theta_2/2)\sin(\theta_1/2)\cos k}{\sin E(k)} \\ n_z(k) &= \frac{-\cos(\theta_2/2)\cos(\theta_1/2)\sin k}{\sin E(k)}. \end{aligned}$$

It is straightforward to check that $\mathbf{A}(\theta_1) = (\cos(\theta_1/2), 0, \sin(\theta_1/2))$ is perpendicular to $\mathbf{n}(k)$ for all k. Therefore, the system possesses sublattice (chiral) symmetry with the symmetry operator $\Gamma(\theta_1) = e^{-i\pi\mathbf{A}(\theta_1)\cdot\sigma/2}$. Notice that this symmetry operation only depends on the first rotation angle θ_1.

The existence of sublattice (chiral) symmetry allows us to characterize the split-step quantum walk by the winding number, denoted by W, of $\mathbf{n}(k)$ around the equator of Bloch sphere. Using the explicit expression for $\mathbf{n}(k)$ in Eq. (2.12), we find $W = 1$ if $|\tan(\theta_2/2)/\tan(\theta_1/2)| < 1$, and $W = 0$ if $|\tan(\theta_2/2)/\tan(\theta_1/2)| > 1$. Thus the split-step quantum walk can realize different winding number for different rotation angles θ_1 and θ_2. We plot the phase diagram of split-step quantum walk in Fig. 2.4.1 b).

For a given θ_1, a set of Hamiltonian for varying values of second rotation θ_2 has the same sublattice (chiral) symmetry, and thus $\{H_{\theta_1}(\theta_2)\}$ defines quantum walks in the same topological class. Because the dependence of $H_{\theta_1}(\theta_2)$ on θ_2 is continuous, topological nature of the winding number implies that the winding number is the same for wide range of the rotation angle θ_2 as phase diagram Fig. 2.4.1 b) shows.

However, the winding number can change its value when the two bands close their gap. Such gapless points are given by the points $|\tan(\theta_2/2)/\tan(\theta_1/2)| = 1$, or $\theta_2 = \pm\theta_1, 2\pi \pm \theta_1$ denoted by solid and

dotted lines in Fig. 2.4.1 b). The mechanism behind the change of winding numbers is the following. At the value of θ_2 where two bands close the gap, for example, $\theta_2 = \theta_1$, eigenvector $\mathbf{n}(k)$ in Eq. (2.12) becomes ill-defined at the quasi-momentum k corresponding to the degenerate points, because any superposition of spin up and down is the eigenstate of the Hamiltonian at that points. At this $\theta_2 = \theta_1$, the winding number cannot be defined, and winding numbers of bands at $H_{\theta_1}(\theta_1 - \varepsilon)$ and $H_{\theta_1}(\theta_1 + \varepsilon)$ do not have to be the same.

Note that this argument can be used to find the phase diagram in Fig. 2.4.1 b) without calculating the winding number at each point of the phase diagram. Since the winding number can change only when the bands close their gap, the phase transition between two topological phases is always gapless. Thus, in order to draw the phase diagram, it is only necessary to identify the gap closing points in the parameter space, and find the winding number of the region bounded by the gapless phase lines. In quantum walks, the periodicity of quasi-energy allows the closing of the gap at either quasi-energy $E = 0$ and $E = \pi$ as we saw in Fig. 2.2.1 b). These gap closing lines at quasi-energy $E = 0$ and $E = \pi$ are denoted in Fig. 2.4.1 b) as solid and dotted lines, respectively.

The topological structure of split-step quantum walk described above has a strong asymmetry between θ_1 and θ_2, but this asymmetry is an artifact. One can shift the starting time of the quantum walk by unitary transformation and define an equivalent dynamics through $U' = T_\uparrow R_y(\theta_1) T_\downarrow R_y(\theta_2)$. It is straightforward to show that this quantum walk has sublattice (chiral) symmetry given by $\Gamma(\theta_2) = e^{-i\pi \mathbf{A}(\theta_2)\cdot\sigma/2}$ with $\mathbf{A}(\theta_1) = (\cos(\theta_1/2), 0, \sin(\theta_1/2))$. In this case, the quantum walks with constant θ_2 correspond to the Hamiltonians in the same topological classes.

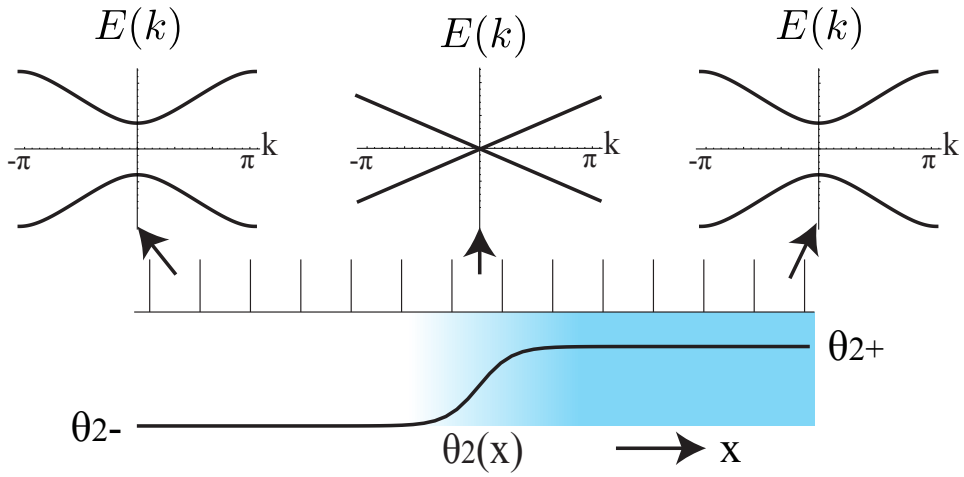

Figure 2.4.2: Illustration of the existence of bound states across the boundary of regions that belong to distinct topological phases. Here, we consider the inhomogeneous split-step quantum walk where the second rotation $\theta_2(x)$ changes in space, and the winding number associated with the phase $\theta_{2-} = \theta_2(x \to -\infty)$ is different from the winding number associated with the phase $\theta_{2+} = \theta_2(x \to \infty)$. In both limit of $x \to -\infty$ and $x \to \infty$, the bands are gapped. However, the winding number cannot change its value unless band gap closes, and thus it is expected that the band gap closes in the middle near the origin. States at $E = 0$ that exist near $x = 0$ must be localized since there is no state at this energy far into the left or into the right of the system.

2.4.3 Physical manifestations of topological band structure

The non-trivial winding, or topological number, of the bands in quantum walks gives rise to a robust bound states at the boundary between two phases with different topological numbers. In the following, we first give an intuition behind the existence of such robust edge states.

Here we consider the split-step quantum walks with inhomogeneous rotations in space, in order to create a boundary between quantum walks with different winding numbers. Here we take the first rotation

θ_1 to be homogeneous in space and make the second rotation θ_2 space dependent, see Fig. 2.4.2. The effective Hamiltonian of this inhomogeneous quantum walk, having the homogeneous first rotation θ_1, possesses the sublatice (chiral) symmetry given by $\Gamma(\theta_1) = e^{-i\pi \mathbf{A}(\theta_1)\cdot\sigma/2}$. While this statement is intuitively clear, it is instructive to explicitly show the existence of sublattice (chiral) symmetry, and we provide the proof in the Appendix 2.8.2.

We take the second rotation angle to approach θ_{2-} for $x \to -\infty$ and θ_{2+} for $x \to \infty$. We take the region in which the rotation angle changes from θ_{2-} to θ_{2+} to be finite region around $x = 0$. Now we take θ_{2-}, θ_{2+} to be such that winding number is 0 for the split-step quantum walk with the rotation angle θ_1, θ_{2-} and winding number is 1 for the walk with the rotation angle θ_1, θ_{2+}. Then the region near the origin represents the phase boundary between two distinct topological phases.

In Fig. 2.4.2, we illustrate the local band structures in this inhomogeneous quantum walk. Strictly speaking, the system is spatially inhomogeneous, so quasi-momentum is no longer a good quantum number, and band structures cannot be drawn. Yet, it is helpful to visualize band structures to understand what happens at the boundary. If the variation of rotation angle θ_2 is slow, then one can visualize the band structures at point x_0 to be the band structures of homogeneous quantum walk with rotation angles θ_1 and $\theta_2(x_0)$. Such description is certainly applicable in the limit $x \to -\infty$ and $x \to \infty$.

The band structures of both $x \to -\infty$ and $x \to \infty$ represent band insulators where two bands are separated by a band gap. By definition, the two bands are characterized by winding number $W = 0$ in $x \to -\infty$ and $W = 1$ in $x \to \infty$. However, since the sublattice

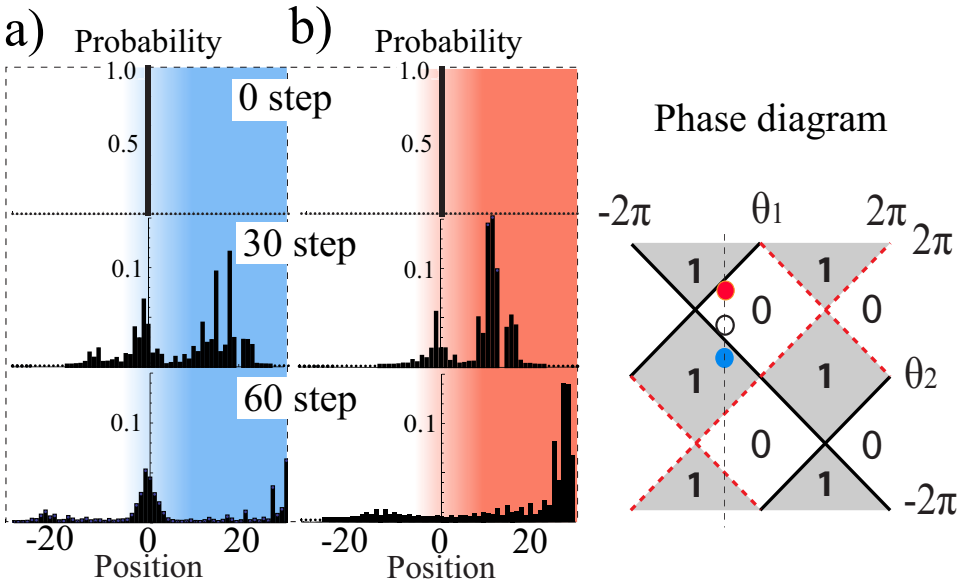

Figure 2.4.3: Evolution of the spatially inhomogeneous split-step quantum walk. The initial spin of the particle is spin up, and particle is initialized at $x = 0$. a) The rotation angles of quantum walk are chosen such that the quantum walk corresponds to trivial topological phase with winding number $W = 0$ as $x \to -\infty$ indicated as a white dot in the phase diagram and non-trivial topological phase with $W = 1$ as $x \to \infty$ indicated as a blue dot. Here we took the uniform first rotation $\theta_1 = -\pi/2$ and second rotation $\theta_{2-} = 3\pi/4$ and $\theta_{2+} = \pi/4$ with $\theta_2(x) = \frac{1}{2}(\theta_{2-} + \theta_{2+}) + \frac{1}{2}(\theta_{2+} - \theta_{2-}) \tanh(x/3)$. After many steps of quantum walks, a large probability of finding a particle near the origin remains, indicating the presence of bound states. b) In this quantum walk, the phase of the two sides of the origin has the same winding number. The phase as $x \to -\infty$ is indicated by the white dot in the phase diagram and phase as $x \to \infty$ is indicated by the red dot. Here we took $\theta_1 = -\pi/2$ and $\theta_{2-} = 3\pi/4$ as before and $\theta_{2+} = 11\pi/8$. In this case, the probability to find the walker near $x = 0$ after many steps decays to 0, indicating the absence of a localized state at the boundary.

(chiral) symmetry exists throughout the space, the winding numbers can only change by closing the gap across the boundary near $x = 0$. Therefore, the gap must close near $x = 0$, as illustrated in Fig. 2.4.2.

This argument shows that there must be states in the gap (near $E = 0$) around the origin. Now because there is no state near $E = 0$ in the limit $x \to \infty$ and $x \to -\infty$ (this energy is in the gap of the bands), we can conclude these states near $E = 0$ around the origin must be confined around the origin. Thus there is generically a bound state near $E = 0$ at the boundary between two different topological phases.

This prediction can be confirmed by running a simple simulations of inhomogeneous quantum walks. The presence or absence of bound states can be confirmed by initializing the particle near the origin and running the quantum walk protocols. If there are bound states near the origin, there is generically an overlap between the initial state and the bound state, and even after many steps of quantum walk, there remains a non-zero probability to find the particle near the origin. On the other hand, if there is no bound state, the particle quickly propagates away from the origin due to the ballistic propagation of quantum walks as described in Section 2.2.3.

In Fig. 2.4.3, we present the result of two inhomogeneous quantum walks. In Fig. 2.4.3 a), the boundary between two topologically distinct phases is created near the origin with winding number $W = 0$ as $x \to -\infty$ and $W = 1$ as $x \to \infty$. Specifically, the uniform first rotation is $\theta_1 = -\pi/2$ and second rotation $\theta_{2-} = 3\pi/4$ and $\theta_{2+} = \pi/4$. Here we considered a smooth variation of the second rotation given by $\theta_2(x) = \frac{1}{2}(\theta_{2-} + \theta_{2+}) + \frac{1}{2}(\theta_{2+} - \theta_{2-}) \tanh(x/3)$, where the second rotation changes from θ_{2-} to θ_{2+} with the length scale of ~ 6 sites. The phases of quantum walks in the limit $x \to -\infty$ and $x \to \infty$ are indicated on the phase diagram as the white and blue dot, respectively. In the simulation, the initial spin of the particle is spin up, and particle starts at $x = 0$. As we expect, a peak in the

probability distribution appears even after 60 steps of the simulation, indicating the existence of topological bound states.

On the other hand, we studied the quantum walk in Fig. 2.4.3 b), where the system is characterized by $W = 0$ throughout the space. Here we took $\theta_1 = -\pi/2$, $\theta_{2-} = 3\pi/4$ and $\theta_{2+} = 11\pi/8$ again with the same functional dependence on x, $\theta_2(x) = \frac{1}{2}(\theta_{2-} + \theta_{2+}) + \frac{1}{2}(\theta_{2+} - \theta_{2-})\tanh(x/3)$. The phases of quantum walks in the limit $x \to -\infty$ and $x \to \infty$ are indicated on the phase diagram as the white and red dot, respectively. With the same initial state of spin up, we implemented the quantum walk simulation, and the resulting probability distribution shows a fast decay of probability near the origin. After 60 steps, the probability near the origin decays close to zero, indicating the absence of bound states.

For further details of the simulation, the interactive demonstration of inhomogeneous quantum walks is available on the Mathematica demonstration website[1][4], where one can change the values of θ_1 and θ_2 and run the quantum walks.

The topological class realized by the conventional quantum walk and by the split-step quantum walk is the same topological class as is proposed in Su-Schrieffer-Heeger model of polyacetylene and Jackiw-Rebbi model. This is the topological class in one dimension with sublattice (chiral) symmetry. In this respect, quantum walk acts as a quantum simulator of the topological phase. Since quantum walks are realizable with many different systems such as ions, photons and cold atoms, they allow the study of topological phases in a manner that is not possible in traditional condensed matter materials. The proposal to study topological phases and topologically protected bound states in split-step quantum walk was first proposed in [87],

[4]In the demonstration, the rotation angle θ_2 is constant and the first rotation angle θ_1 is varied in space. As we have explained at the end of Section 2.4.2, such quantum walk also possess sublattice (chiral) symmetry and thus the essential physics remains the same.

and later realized in experiments with photonic architecture[92]. The controllability of the experimental apparatus not only allow the direct imaging of the wavefunctions of topological bound states, but also allow to confirm the robustness of the bound states with parameter changes, the signature of topological origin for the bound states. This topological bound state in one dimensional system has not been directly observed in materials such as polyacetylene, and this photonic architecture provided the first experimental imaging of the bound states with topological origin in one dimension.

2.4.4 Quantum walks with a reflecting boundary

A special case of Hamiltonian with trivial topology is the vacuum, where the topological number associated with the system is zero. Thus, we can make a phase boundary by simply terminating the quantum walk with winding number $W = 1$. In this setup, the boundary exists at the edge of the quantum walk, and it is expected that a bound state exists at this edge according to the general argument in Section 2.4.3.

As we briefly mentioned in Section 2.2.4, such a setup is not unphysical, and intriguing realization of quantum walks with a reflecting edge has been suggested in [116] through the understanding of a particle under the electric field in discrete energy level structure as a quantum walk. The transition between different levels occurs as Landau-Zener process in this system, which corresponds to the translation operation in quantum walks. Thus, the ground state of the system acts as the reflecting boundary. They predicted the existence of a bound state near the ground state, which we can now understand as a topological bound state as a result of non-trivial topological number of quantum walks.

Here we consider the conventional quantum walk described by

$U = TR_y(\theta)$ which extends from $x = -\infty$ up to $x = 0$. The quantum walk is terminated at $x = 0$. In order to conserve the particle number, we require the operation at the boundary to be unitary, *i.e.* the spin $\uparrow$ particle needs to be reflected at the edge $x = 0$. Here we take the following operation at the edge $x = 0$;

1. Rotation of the spin around y axis by angle θ, as in other sites, given by $R_y(\theta) = e^{-i\theta\sigma_y/2}$.

2. Translation of the spin $\downarrow$ to site $x = -1$. Spin $\uparrow$ stays at $x = 0$ and its spin is flipped to spin $\downarrow$ with phase accumulation $e^{i\phi}$

Explicitly, the operation at $x = 0$ is

$$\begin{aligned} U(x = 0) &= T_{\text{edge}} R_y(\theta) \\ T_{\text{edge}} &= |-1\rangle\langle 0| \otimes |\downarrow\rangle\langle\downarrow| + e^{i\phi}|0\rangle\langle 0| \otimes |\downarrow\rangle\langle\uparrow| \end{aligned}$$

In order to have a quantum walk in a topological class, it is crucial to have the sublattice (chiral) symmetry of the whole system. In particular, the sublattice (chiral) symmetry needs to be present for the evolution operator including the edge. If we denote the total evolution of the system with an edge as $U_{x\leq 0}$, then we require

$$\Gamma^{-1} U_{x\leq 0} \Gamma = U_{x\leq 0}^{\dagger} \tag{2.12}$$

where $\Gamma = e^{-i\pi \mathbf{A}\cdot\boldsymbol{\sigma}/2}$ with $\mathbf{A} = [\cos(\theta/2), 0, \sin(\theta/2)]$. This is a simple extension of the definition of sublattice (chiral) symmetry in Eq. (2.8) to evolution operator. It is straightforward to check that the necessary and sufficient condition for the existence of sublattice (chiral) symmetry in $U_{x\leq 0}$ is $\phi = 0, \pi$ for the phase accumulated at the reflecting boundary.

According to the general argument in Section 2.4.3, bound states exist near the boundary of $x = 0$. For this simple quantum walk, it is

not very difficult to obtain the analytical solution of the bound state. The details of the derivation is given in the Appendix 2.8.3. We note that a straightforward extension of the derivation given in the Appendix should allow similar analytical solutions of bound states for the inhomogeneous split-step quantum walks.

Here we describe the solution for the boundary condition of $\phi = 0$ and rotation angle $\theta = \pi/2$. The analytical solution shows that the bound state is at quasi-energy $E = \pi$ and the wavefunction takes the form

$$\begin{aligned} |\psi_b^{E=0}(-j)\rangle &= \frac{1}{\mathcal{N}}(-1)^j e^{-j/\lambda} \otimes \begin{pmatrix} 1-\sqrt{2} \\ 1 \end{pmatrix} \quad 0 \leq j \\ \lambda &= -\frac{1}{\log(\sqrt{2}-1)} \end{aligned} \tag{2.13}$$

where $\mathcal{N}$ is the normalization factor. Since the localization length $\lambda \approx 1.1$ is small, this bound state is tightly localized around $x = 0$.

For the same boundary condition $\phi = 0$ but different rotation angle $\theta = 5\pi/2$, the evolution operator $U = TR_y(\theta)$ is different from the one with the rotation angle $\theta = \pi/2$ by only a minus sign, *i.e.* $TR_y(\theta = 5\pi/2) = -TR_y(\theta = \pi/2)$. Thus, the same wavefunction in Eq. (2.13) is the bound state for this case as well, but now the quasi-energy of the bound state is $E = 0$ due to the extra minus sign.

On the other hand, for the reflecting boundary condition with phase accumulation $\phi = \pi$ with $\theta = \pi/2$, the bound state exists at quasi-energy $E = 0$ and wavefunction is

$$\begin{aligned} |\psi_b^{E=\pi}(-j)\rangle &= \frac{1}{\mathcal{N}} e^{-j/\lambda} \otimes \begin{pmatrix} 1-\sqrt{2} \\ 1 \end{pmatrix} \quad 0 \leq j \\ \lambda &= -\frac{1}{\log(\sqrt{2}-1)} \end{aligned}$$

Generally, the quasi-energy of bound states for quantum walks with sublattice (chiral) symmetry is at $E = 0$ or $E = \pi$. We will see in the next section, Section 2.4.5, that these energies represent special points where sublattice (chiral) symmetry provides the topological protection of the states at these energies.

For the special rotation angles of $\theta = \pi$, it is possible to obtain the bound state solution by following the quantum walk for a few steps. Since this calculation is elementary, the existence of a bound state can be easily understood. This rotation angle corresponds to the rotation operation

$$\begin{aligned} R_y(\theta = \pi) &= -i\sigma_y \\ &= \begin{pmatrix} 0 & -1 \\ 1 & 0 \end{pmatrix} \end{aligned}$$

Thus, the rotation turns $|\uparrow\rangle \to |\downarrow\rangle$ and $|\downarrow\rangle \to -|\uparrow\rangle$. Let us take the phase accumulation upon reflection to be $\phi = 0$. If we initialize the particle at $x = 0$ with spin down, the quantum walk follows the following evolution.

$$|0\rangle \otimes |\downarrow\rangle \xrightarrow{R} |0\rangle \otimes (-|\uparrow\rangle) \xrightarrow{T} |0\rangle \otimes (-|\downarrow\rangle)$$

Thus in this special case, $|0\rangle \otimes |\downarrow\rangle$ is an eigenstate of quantum walk operator localized at the edge. Since the state gains a minus sign after one step of the quantum walk, the quasi-energy of the bound state is π, in accordance with the result obtained in the general analytical solution.

2.4.5 Topological protection of the bound states: topological invariants

The bound states resulting from topology studied in Section 2.4.3 and Section 2.4.4 are protected in a sense that they are robust against small changes in the quantum walk protocols or the introduction of small static disorder potentials. The logic is the following; since the bound states are the result of topological winding numbers, and topological winding numbers cannot change their values unless the bands close their gaps, the bound states cannot disappear for a small change of rotation angles unless they are changed by a large amount such that the gap of the corresponding effective Hamiltonian closes.

There is a more direct way to confirm such robustness by simply looking at the spectrum. In Section 2.4.4, we found that the energies of the topological bound states is always either $E = \mathsf{o}$ or $E = \pi$. Because the spectrum of the bulk (or the spectrum of the system without boundaries) is gapped, the total spectrum of the system studied in the previous section look as in Fig. 2.4.4 a) and b), where a single localized state sits at $E = \mathsf{o}$ or $E = \pi$ and the bands of states away from $E = \mathsf{o}$ or $E = \pi$ correspond to extended states in the bulk.

Now we argue that the energy of the bound state sitting at the energy $E = \mathsf{o}$ or $E = \pi$ cannot be changed by a continuous change of Hamiltonian which preserves the sublattice (chiral) symmetry. First of all, the presence of sublattice (chiral) symmetry implies that the states with energy E and $-E$ have to come in pairs. In order to shift the energy of the bound state at $E = \mathsf{o}$ by a small amount ε, then, it is necessary to create two states at energy $\pm\varepsilon$. However, since a single state cannot be split into two, this is impossible, and the energy of the single state initially at $E = \mathsf{o}(\pi)$ is pinned at $E = \mathsf{o}(\pi)$. According to this argument, the only way to remove such a zero (or π) energy bound state is to change the Hamiltonian until the bulk energy bands

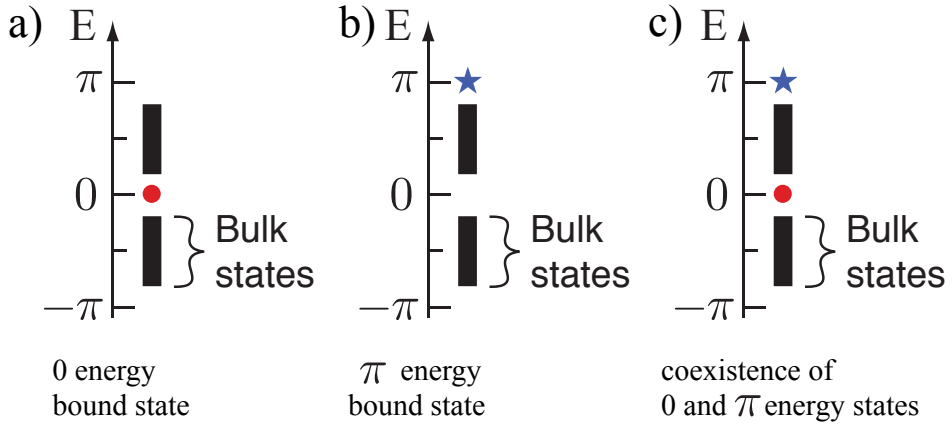

Figure 2.4.4: General spectrum structure for inhomogeneous quantum walks with bound states. a), b) in Section 2.4.4, we analytically showed that there is a 0 or π energy bound state at the boundary of a conventional quantum walk. In a similar fashion, these bound states also appear in the inhomogeneous split-step quantum walks. These bound states energy are well separated from the extended, bulk states. Sublattice (chiral) symmetry requires that states with energy E and $-E$ appear in pairs, and thus, a single 0 and π energy bound state cannot disappear unless bulk energy gap closes at 0 or π. c) Inhomogeneous conventional quantum walks can possess 0 and π energy bound states, even though the winding numbers associated with the both sides of the boundary are zero. Such existence of two flavors of topologically protected bound states is a unique feature of periodically driven systems and quantum walks. As is shown in Section 2.4.5, each bound state at 0 or π energy is associated with a topological number ± 1. For a given system, a sum of these topological numbers Q^0 for $E = 0$ and Q^π for $E = \pi$ is a conserved quantity that cannot change its value unless the gap of the system closes.

close the gap so that bulk states mix with the the boundary state.

The structure of the spectrum illustrated in Fig. 2.4.4 a) and b) is generic. All the topological bound states exist at $E = 0$ or $E = \pi$. It is possible to assign topological numbers to these bound states, which give yet another understanding of the topological protection of the bound states. These topological numbers are different from the winding numbers we assigned to the quantum walk band structures. These topological numbers are now assigned to the bound states themselves. The following consideration shows that the topological classification of the quantum walks with sublattice (chiral) symmetry is $Z \times Z$, which means any integer numbers of $E = 0$ and $E = \pi$ energy states are topologically protected.

In the following, we consider general one dimensional systems with sublattice (chiral) symmetry, as in the case of quantum walks. Here we consider the bound states at energy 0. Analogous arguments can be applied to the bound states at π. Suppose that there is N_0 number of degenerate bound states with energy 0. We label these states by $|\phi^0_{a'}\rangle$ with $a' = 1 \cdots N_0$. Let the sublattice (chiral) symmetry operator be given by Γ. Sublattice (chiral) symmetry implies that we have the anti-commutation relation between Γ and Hamiltonian, H, such that $\{\Gamma, H\} = 0$. As a consequence, Γ^2 commutes with H. When there is no conserved quantity associated with Γ^2, it is possible to choose the phase of Γ such that $\Gamma^2 = 1$. For example, in the case of quantum walks, we choose $\Gamma = ie^{i\mathbf{A}\cdot\boldsymbol{\sigma}\pi/2}$. Because of the sublattice (chiral) symmetry, we know that $\Gamma|\phi^0_{a'}\rangle$ is also an eigenstate of H with $E = 0$, so Γ represents a rotation within the subspace of zero energy states, $\{|\phi^0_{a'}\rangle\}$. Then we can choose the basis of zero energy states such that they become eigenstates of Γ. We denote the zero energy states in this basis as $\{|\psi^0_a\rangle\}$ and their eigenvalues under Γ as $\{Q^0_a\}$. Since $\Gamma^2 = 1$, Q^0_a is either ± 1.

We now show that the sum of eigenvalues, $Q^0 \equiv \sum_a Q^0_a$, represents

the topological invariant associated with zero energy bound states. We define the integer number Q^0 for zero energy bound states and Q^π for π energy bound states constructed in an analogous fashion, as

$$Q^0 = \sum_a \langle \psi_a^0 | \Gamma | \psi_a^0 \rangle \tag{2.14}$$

$$Q^\pi = \sum_a \langle \psi_a^\pi | \Gamma | \psi_a^\pi \rangle \tag{2.15}$$

where $\{|\psi_a^\pi\rangle\}$ are the π energy bound states.

In order to show that these quantities are indeed topological invariants, we show that perturbations of the Hamiltonian which preserves the sublattice (chiral) symmetry cannot mix two states both at the zero (π) energy with the same eigenvalues of Γ. This implies that such perturbations do not lift the energies of these states away from 0 or π. Thus, Q^0 (Q^π) number of bound states at energy $E = 0 (E = \pi)$ cannot change under small deformations of the Hamiltonian.

Let H' be a perturbation to the system such that $\{\Gamma, H'\} = 0$. Now we evaluate the matrix element of $\{\Gamma, H'\} = 0$ in the $0(\pi)$ energy states. The result is

$$\begin{aligned} 0 &= \langle \psi_a^0 | \{\Gamma, H'\} | \psi_\beta^0 \rangle \\ &= \begin{cases} 2\langle \psi_a^0 | H' | \psi_\beta^0 \rangle & \text{for} \quad Q_a^0 = Q_\beta^0 \\ \langle \psi_a^0 | H' | \psi_\beta^0 \rangle - \langle \psi_a^0 | H' | \psi_\beta^0 \rangle = 0 & \text{for} \quad Q_a^0 \neq Q_\beta^0 \end{cases} \end{aligned}$$

This calculation shows that bound states with the same eigenvalues Q_a^0 cannot mix. On the other hand, the same calculation does not give any constraint on the mixing of states with different eigenvalues Q_a^0. Because one can break up any finite change of the Hamiltonian into successive changes of small perturbations, one can repeat this argument and show that the values Q^0 and Q^π cannot change unless

the bound states at 0 and π energies mix with the bulk states.

2.4.6 Temporal disorder

While we argued the robustness of bound states against spatial disorders through the general argument in the previous section, the bound state is not robust against temporal disorders[92, 113]. One way to understand this is to consider the wave functions of bound states in each one step operations. As long as the effective Hamiltonian of each one step operation is topologically non-trivial, the bound state exists at the boundary at each step. However, if one step operation changes due to the temporal change of operations, the bound state wave function changes after each step. Thus, after each step, small portion of the bound state wave function in the previous step becomes extended states and escape from the boundary. After sufficiently long evolution of the quantum walks, a bound state eventually decays to zero. In a similar fashion, the bound state is not robust against decoherence. Such effect of decoherence on the bound state has been experimentally studied in Ref[92].

2.4.7 Breaking of sublattice (chiral) symmetry

Here we briefly comment on the perturbations of the Hamiltonian that breaks sublattice (chiral) symmetry. In the previous section, we give the argument that zero or π energy bound states are protected as long as the bands in the spectrum do not close the gap. Now one can ask what happens if we consider the perturbations of Hamiltonians that break sublattice (chiral) symmetry. Since no topological structure can be defined in the absence of sublattice (chiral) symmetry, there is no longer topological protection of the bound states. Yet, the statement that bound states cannot disappear until they mix with the bulk states remains true. Therefore, if we perturb the system that

possesses topological bound states by adding small perturbations that break sublattice (chiral) symmetry, the existence of the bound states is still protected by the existence of the gap. However, the bulk gap does not have to close to remove such a bound state; now the energy of the bound state can take any value in the absence of sublattice (chiral) symmetry and the state can be lifted away from 0 or π energy.

2.4.8 0 AND π ENERGY BOUND STATES ; TOPOLOGICAL PHENOMENA UNIQUE TO PERIODICALLY DRIVEN SYSTEMS

Zero-energy bound state in one dimensional system with sublattice (chiral) symmetry has been known for almost 30 years, and their existence was first predicted by Su-Schrieffer-Heeger model of polyacetylene and Jackiw-Rebbi model[72, 73, 153]. On the other hand, we saw in previous sections that quantum walks have two topologically protected bound states; 0 and π energy states. The appearance of π energy states is the result of the periodicity of quasi-energy. In return, quasi-energy is a property of periodically driven systems, and thus such appearance of two flavors of topologically protected bound states is a unique phenomenon to driven systems, which cannot occur in non-driven systems.

In previous examples, only one of these states, 0 and π energy bound states, appears in a single system. From the argument given in Section 2.4.3, which of $E = 0$ and $E = \pi$ bound states appears across the boundary of two topological phases is determined by whether the band gap closes at quasi-energy $E = 0$ or $E = \pi$. For example, consider the creation of a boundary between two different topological phases in the inhomogeneous split-step quantum walk, as we considered in Section 2.4.3. By choosing θ_{2-} and θ_{2+} appropriately, one can either make the boundary between the two phases to be gapless at either $E = 0$ or $E = \pi$, as one can see from the phase diagram in Fig. 2.4.1.

When the boundary closes the gap at $E = 0(\pi)$, the bound state appears at $E = 0(\pi)$ as is depicted in Fig. 2.4.4 a) and b).

Now consider the creation of the boundary between the phases with *the same winding numbers* by setting $\theta_1 = 0$. This quantum walk whose evolution operator is given by $U = T_\downarrow R_y(\theta_2) T_\uparrow$ is nothing but the conventional quantum walk described in Section 2.2.1 with initial time shifted. This time-shifted quantum walk realizes only a single phase with $W = 0$[5]. If we set θ_{2-} to be $-2\pi < \theta_{2-} < 0$ and θ_{2+} to be $0 < \theta_{2+} < 2\pi$, then the two phases corresponding to $x \to -\infty$ and $x \to$ both have $W = 0$. From the point of view of the winding topological number defined on the band structures, one expects no topologically protected bound states to be present. However, this inhomogeneous quantum walk possesses two topological bound states at quasi-energies $E = 0$ and $E = \pi$.

The existence of two bound states near the origin can be easily confirmed for the simple case of $\theta_{2-} = -\pi$ and $\theta_{2+} = \pi$ where the rotation θ_{2-} is applied to all the sites $x \leq 0$ and the rotation θ_{2+} is applied to sites $0 < x$. These rotations act on the spins as

$$\begin{aligned} \theta_{2-} = -\pi \quad &: \quad |\uparrow\rangle \to -|\downarrow\rangle, |\downarrow\rangle \to |\uparrow\rangle \\ \theta_{2+} = \pi \quad &: \quad |\uparrow\rangle \to |\downarrow\rangle, |\downarrow\rangle \to -|\uparrow\rangle \end{aligned}$$

Now we consider the evolution of the particle after one step for a

[5]The conventional quantum walk described in Section 2.2.1 realized a single phase with $W = 1$. The difference in the winding number of two quantum walks related by unitary transformation arises because these two walks are described by different sublattice (chiral) symmetry. The sublattice (chiral) symmetry of split-step quantum walks with $\theta_1 = 0$ is given by the rotation of spin by π around the axis $\mathbf{B} = (1, 0, 0)$, which is *independent* of the rotation angle θ_2. On the other hand, the winding number of the conventional quantum walks in Section 2.2.1 is given in terms of the rotation of spin by π around the axis $\mathbf{A} = (\cos(\theta/2), 0, \sin(\theta/2))$. Topology of the system crucially depends on the symmetry, and thus, winding numbers do not have to be identical when symmetry operators are different.

particle at site $x = 1$ with spin either up or down. This state evolves as

$$|0\rangle \otimes |\uparrow\rangle \xrightarrow{T_\uparrow} |1\rangle \otimes |\uparrow\rangle \xrightarrow{R} |1\rangle \otimes |\downarrow\rangle \xrightarrow{T_\downarrow} |0\rangle \otimes |\downarrow\rangle$$
$$|0\rangle \otimes |\downarrow\rangle \xrightarrow{T_\uparrow} |0\rangle \otimes |\downarrow\rangle \xrightarrow{R} |0\rangle \otimes |\uparrow\rangle \xrightarrow{T_\downarrow} |0\rangle \otimes |\uparrow\rangle$$

Thus it is clear that $|\psi_{E=0}\rangle = |0\rangle \otimes \frac{1}{\sqrt{2}}(|\uparrow\rangle + |\downarrow\rangle)$ is an eigenstate of the one-step evolution operator with quasi-energy 0 and $|\psi_{E=\pi}\rangle = |0\rangle \otimes \frac{1}{\sqrt{2}}(|\uparrow\rangle - |\downarrow\rangle)$ has quasi-energy π. It is straightforward to check that any other states in this system has energy $E = \pm\pi/2$. Because this system possesses a single bound state at energy $E = 0$ and $E = \pi$, these states cannot be removed from these states until the gap of the bulk states closes, and thus these states must be present for any parameter values $-2\pi < \theta_{2-} < 0$ and $0 < \theta_{2+} < 2\pi$. The general spectrum of such inhomogeneous quantum walks is illustrated in Fig. 2.4.4 c). As we noted in Section 2.4.5, these bound states are associated with topological numbers. In this walk, since $\theta_1 = 0$, the sublattice (chiral) symmetry is given by the operator $\Gamma = \sigma_x$. Then the topological number associated with the bound state $|\psi_{E=0}\rangle$ is nothing but the eigenvalue of Γ, so $|\psi_{E=0}\rangle$ has $Q^0 = 1$ and $|\psi_{E=\pi}\rangle$ has $Q^\pi = -1$.

Such coexistence of 0 and π energy bound state can also be observed in inhomogeneous split-step quantum walks, where the two phases on the left and on the right are separated by two gapless phases where one closes the gap at $E = 0$ and the other at $E = \pi$.

The winding number is the comprehensive topological description of static Hamiltonians, but quantum walks are periodically driven systems. More completely, periodically driven systems should be described by the evolution operator over one period, and the topological numbers for such systems should be written in terms of the evolution operator and not in terms of the static effective Hamiltonian. Thus the topological classification of quantum walks is not given by $\mathbf{Z}$ as for the winding numbers, but in fact given by $\mathbf{Z} \times \mathbf{Z}$

as we have seen in the topological invariants of bound states in Section 2.4.5. More detailed analysis of the difference of topological classification between static systems and periodically driven systems is given in [86].

2.5 Quantum walks in two dimension

2.5.1 effective Hamiltonian and Chern number

In the previous sections, we illustrated the ideas of quantum walks and topological phases realized in these systems in the simplest setting, one dimensional quantum walks with two internal degrees of freedom. However, the idea of topological phases is much more general, and it is possible to extend the quantum walk protocols to study different topological phases in different dimensions. In this section, we illustrate the idea by describing the two dimensional quantum walks and demonstrating that this quantum walk realizes topological phases with Chern numbers, the phases that are responsible for integer quantum Hall effects that we explained in Section 2.3.

We consider the quantum walk of spin $1/2$ particle on a square lattice. In the literature, quantum walks in dimensions larger than 1 are defined for larger number of internal degrees of freedom, but the quantum walk defined here is simpler and easier to realize in experiments. The quantum walk consists of three rotations and three translations, implemented in alternative fashion (see Fig. 2.4.5);

1. Rotation of the spin around y axis by angle θ_1, given by $R_y(\theta_1) = e^{-i\theta_1\sigma_y/2}$.

2. Translation of the spin $\uparrow$ one lattice to the right and up, and translation of the spin $\downarrow$ one lattice to the left and down.

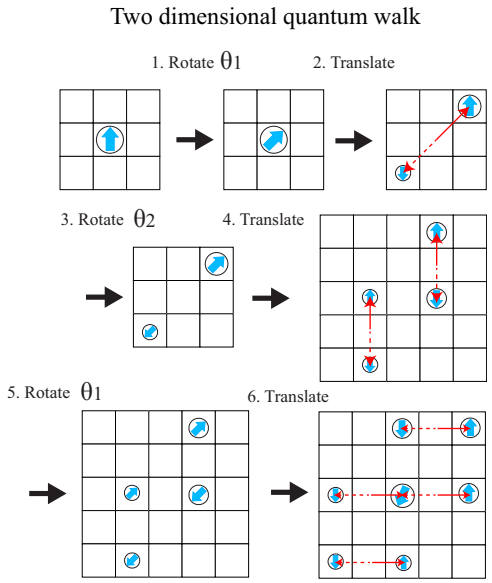

Figure 2.4.5: Protocol of two dimensional quantum walk considered in Section 2.5.1. The quantum walk is defined for a single spin $1/2$ particle in two dimensional lattice. The protocol consists of 6 operations. In the figure, the spin-dependent translation is denoted by red arrows, where solid arrow is the movement for spin up and dotted arrow is for spin down. The protocols are 1. spin rotation around y axis by angle θ_1; 2. spin-dependent translation where spin up is move to right and up by one lattice site, and spin down is moved to left and down; 3. spin rotation around y axis by angle θ_2; 4. spin-dependent translation where spin up is moved to up, and spin down to down; 5. spin rotation around y axis by the same rotation angle as the first rotation θ_1; 6. spin-dependent translation where spin up is move to right and down to left. Each step of quantum walk takes a particle from even (odd) coordinate to even (odd) coordinate, so the lattice constant of the effective Hamiltonian is 2. Thus, the first Brillouin zone is $-\pi/2 \leq k_x \leq \pi/2$ and $-\pi/2 \leq k_y \leq \pi/2$.

Explicitly,
$T_1 = \sum_{x,y} |x+1, y+1\rangle\langle x, y| \otimes |\uparrow\rangle\langle\uparrow| + |x-1, y-1\rangle\langle x, y| \otimes |\downarrow\rangle\langle\downarrow|$.

3. Rotation of the spin around y axis by angle θ_2, given by $R_y(\theta_2) = e^{-i\theta_2\sigma_y/2}$.

4. Translation of the spin $\uparrow$ by one lattice to up, and translation of the spin $\downarrow$ by one lattice to down. Explicitly,
$T_2 = \sum_{x,y} |x, y+1\rangle\langle x, y| \otimes |\uparrow\rangle\langle\uparrow| + |x, y-1\rangle\langle x, y| \otimes |\downarrow\rangle\langle\downarrow|$.

5. Rotation of the spin around y axis by the same angle as the first rotation θ_1, given by $R_y(\theta_1) = e^{-i\theta_1\sigma_y/2}$.

6. Translation of the spin $\uparrow$ by one lattice to right, and translation of the spin $\downarrow$ by one lattice to left. Explicitly,
$T_3 = \sum_{x,y} |x+1, y\rangle\langle x, y| \otimes |\uparrow\rangle\langle\uparrow| + |x-1, y\rangle\langle x, y| \otimes |\downarrow\rangle\langle\downarrow|$.

Note that in this quantum walk, the particle after one step of quantum walk moves from even (odd) coordinate sites to even (odd) coordinate sites as one can see from Fig. 2.4.5. Thus the effective Hamiltonian of the quantum walk has the lattice constant equal to 2. Therefore, for translationally invariant quantum walks, the first Brillouin zone is given by $-\pi/2 \leq k_x \leq \pi/2$ and $-\pi/2 \leq k_y \leq \pi/2$. The evolution of the particle distribution in this walk can be studied in a similar fashion as the one dimensional analogue, and in particular, the asymptotic distribution is obtained through the formalism developed in Section 2.2.3.

In order to study the topological properties of this quantum walk, we consider the effective Hamiltonian of the quantum walk. As we

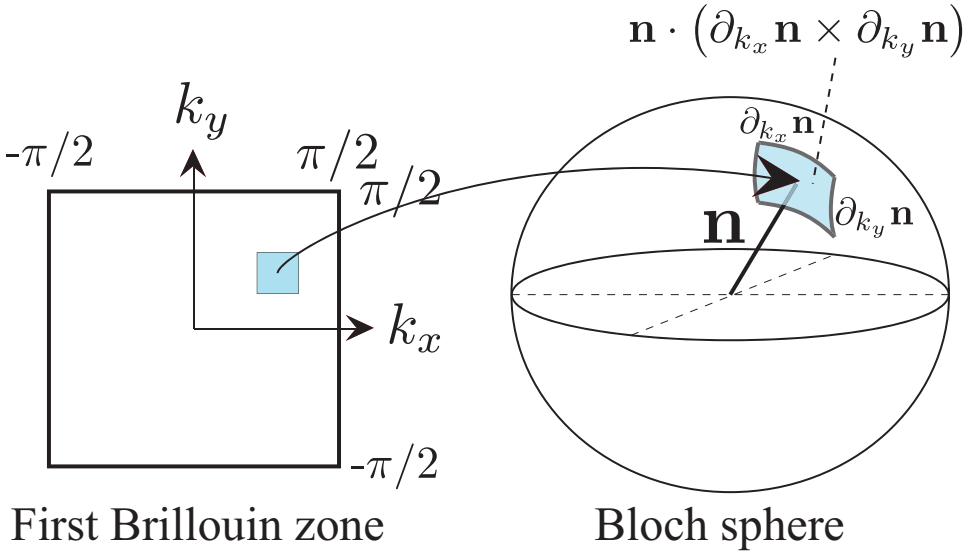

Figure 2.5.1: Illustration of Chern number of two dimensional systems with two bands. The eigenstate for each quasi-momentum $\mathbf{k}$ is a superposition of spin up and down, and can be represented as a point on Bloch sphere, given by $\mathbf{n}(\mathbf{k})$. Thus $\mathbf{n}(\mathbf{k})$ represents a map from the first Brillouin zone to Bloch sphere. In order to obtain a topological number for this system, we consider the area mapped by $\mathbf{n}(\mathbf{k})$ from the first Brillouin zone to Bloch sphere. Due to the periodic boundary condition of the first Brillouin zone, which is a torus, such map has to wrap around the Bloch sphere by integer number of times. This integer is what is called a Chern number, and represents the topological number associated with the system. The formal expression of the Chern number is then obtained by calculating the area covered by the map $\mathbf{n}(\mathbf{k})$, which can be calculated in the way illustrated in this picture and results in the expression Eq. (2.18)

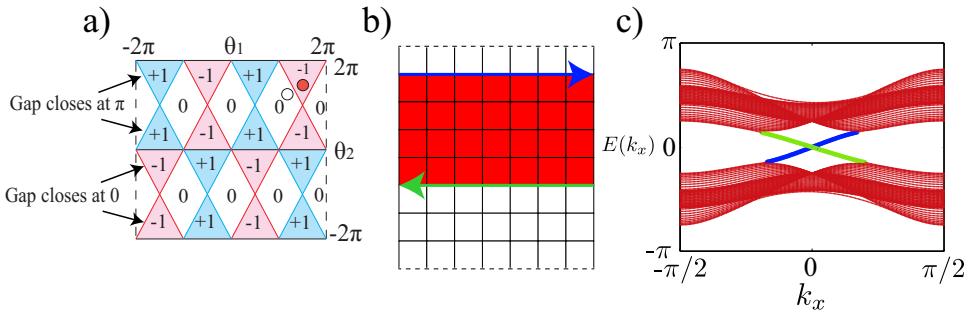

Figure 2.5.2: a) Phase diagram of the two dimensional quantum walk. Each phase is characterized by a Chern number of a lower band with quasi-energy $-E(\mathbf{k})$, which can take values $0, \pm 1$ in this quantum walk. The Chern number can change only when the system crosses gapless phases, and the lines of gapless phases are indicated by the red and blue line in the diagram. b) physical manifestation of Chern numbers appears at the boundary between regions that belong to phases with different Chern numbers. Here we illustrate the inhomogeneous quantum walk, where the quantum walk in the central region (colored as red) corresponds to $\theta_{1+} = 7\pi/6$ and $\theta_{2+} = 7\pi/6$ (red dot in a)), whereas in the other half (colored as white), the quantum walk corresponds to $\theta_{1-} = 3\pi/2$ and $\theta_{2-} = 3\pi/2$ (white dot in a)). In the simulation, we took the periodic boundary condition for both x and y direction, and the system size is 100×100. c) Quasi-energy spectrum of the inhomogeneous quantum walks illustrated in b). The states colored as red are bulk states, and the states that go from the lower band to the upper band are the unidirectionally propagating edge states that are localized near the boundary of the two phases. States colored as blue are the states that run along the upper edge and those colored as green are the states that run along the lower edge, as illustrated in b).

detail in Appendix 2.8.4, the effective Hamiltonian takes the form

$$H_{\text{eff}} = \sum_{\mathbf{k}} E(\mathbf{k})\mathbf{n}(\mathbf{k}) \cdot \sigma \otimes |\mathbf{k}\rangle\langle\mathbf{k}| \tag{2.16}$$

The spectrum $E(\mathbf{k})\mathbf{n}(\mathbf{k})$ is determined by the equation

$$\begin{aligned} \cos\left(E(\mathbf{k})\right) &= \cos(k_x)\cos(k_x + 2k_y)\cos(\theta_1)\cos(\theta_2/2) \\ &\quad - \sin(k_x)\sin(k_x + 2k_y)\cos(\theta_2/2) \\ &\quad - \cos^2(k_x)\sin(\theta_1)\sin(\theta_2/2) \end{aligned} \tag{2.17}$$

The topological structure of two dimensional system appears in $\mathbf{n}(\mathbf{k})$ as in the case of one dimensional quantum walk. Since now we have two dimensional Brillouin zone, the function $\mathbf{n}(\mathbf{k})$ is a map from two dimensional torus to Bloch sphere, see Fig. 2.5.1. A small area on the torus is mapped to the small area on the Bloch sphere. If one maps the total area of the torus onto the Bloch sphere, the map necessarily wraps around the sphere an integer number of times due to the periodic boundary condition of the torus. Thus, if one calculates the total area covered by the map $\mathbf{n}(\mathbf{k})$, the value is $4\pi n$ where n is an integer. This integer is so-called Chern number, which is responsible for integer quantum Hall effect in two dimensional electron gas. Explicitly, the Chern number can be expressed in terms of $\mathbf{n}(\mathbf{k})$ as

$$C = \frac{1}{4\pi}\int_{\text{FBZ}} d\mathbf{k}\ \mathbf{n}\cdot\left(\partial_{k_x}\mathbf{n}\times\partial_{k_y}\mathbf{n}\right) \tag{2.18}$$

As opposed to the winding number of one dimensional quantum walk, this topological number does not rely on any symmetry of the system, and thus can exist in the absence of any symmetry.

Conventionally, Chern number is associated with each band of Hamiltonian. The definition of Chern number above gives the Chern number of "lower" band with quasi-energy of $-E(\mathbf{k})$ in Eq. (2.17), and

the Chern number of upper band is given by simply $-C$ so that the Chern numbers of all the bands sum to zero. More generally, if the wavefunction of a band at a given quasi-momentum $\mathbf{k}$ is given by $|\psi(\mathbf{k})\rangle = e^{i\mathbf{r}\cdot\mathbf{k}}|\phi(\mathbf{k})\rangle$, where $|\phi(\mathbf{k})\rangle$ is the periodic part of the Bloch wave function, then the Chern number associated with the band is given by the famous TKNN formula[156];

$$\begin{aligned} C &= \frac{1}{2\pi}\int_{\mathrm{FBZ}} d\mathbf{k}\left[\partial_{k_x}A_{k_y} - \partial_{k_y}A_{k_x}\right] \\ (A_{k_x}, A_{k_y}) &= (i\langle\phi(\mathbf{k})|\partial_{k_x}|\phi(\mathbf{k})\rangle, i\langle\phi(\mathbf{k})|\partial_{k_y}|\phi(\mathbf{k})\rangle) \end{aligned} \tag{2.19}$$

This TKNN formula calculates the Berry phase of an electron as it goes around the first Brillouin zone. This expression of Chern number reduces to Eq. (2.18) in the case of systems with two bands.

One can calculate the Chern numbers for the two dimensional quantum walk described above for various values of θ_1 and θ_2. The phase diagram is plotted in Fig. 2.5.2 a). A convenient way to obtain such phase diagram is to first obtain the lines of gapless phases. Since the topological number can only change its value across gapless phase, it is only necessary to compute the Chern number at a single point of the gapped region and any gapped phase that is continuously connected with that point without crossing gapless phase must have the same topological number as that point. We detail the calculation to identify gapless phases for this two dimensional quantum walk in the Appendix 2.8.5.

A physical manifestation of topological phases with Chern number is, as is the case for one dimensional quantum walk, boundary states across the regions in which two different topological phases are realized. The existence of such bound states can be understood according to the argument given in Section 2.4.3; the band structures away from the boundary are gapped, but the band gap has to close near the boundary in order for the topological number, Chern

number, to change its value. Thus there is generically states in the gap of the bulk systems and these states are necessarily localized near the boundary.

These bound states that appear in systems with non-zero Chern number are known to propagate in unidirectional fashion without any backscattering. It is possible to confirm the existence of such unidirectional edge states by considering inhomogeneous quantum walk where the particle at sites with $0 \leq y$ evolves according to the two dimensional quantum walk with rotation angles θ_{1+} and θ_{2+}, and the particle at sites with $y < 0$ evolves according to the two dimensional quantum walk with rotation angles θ_{1-} and θ_{2-}. Such inhomogeneous quantum walk is illustrated in Fig. 2.5.2 b). If the Chern number of the phases corresponding to θ_{1+} and θ_{2+} and θ_{1-} and θ_{2-} are different, unidirectional edge states are expected to appear along $y = 0$.

Since these edge states exist, just like 0 and π energy states of one dimensional quantum walk, in the gap of the bulk states, it is easy to identify the existence of these states by numerically solving for the quasi-energy spectrum. In Fig. 2.5.2 c), we provided the plot of quasi-energy spectrum for a torus geometry with periodic boundary condition on both x and y direction. The system size is taken to be 100×100. In the upper half of the system between $0 \leq y < 50$, we implemented the quantum walk with $\theta_{1+} = 7\pi/6$ and $\theta_{2+} = 7\pi/6$, whereas in the lower half $-50 \leq y < 0$, the quantum walk corresponds to $\theta_{1-} = 3\pi/2$ and $\theta_{2-} = 3\pi/2$. Note that there are two boundaries in this system, corresponding to the lower edge at $y = 0$ and upper edge at $y = 50$. In the spectrum, there are clearly two edge states, colored as red and green, which run along the upper and lower edge, respectively. These chiral edge modes are the signature of Chern numbers in two dimensional quantum walk.

2.5.2 Unidirectionally propagating modes in quantum walks without Chern numbers

In the case of one dimensional quantum walk, we found the existence of two bound states at quasi-energy 0 and π near the boundary of the phases with zero winding number. This existence of two flavors of topologically protected bound states represented a phenomenon unique to periodically driven systems that do not exist in static systems, and thus the existence is not captured by the winding number of the effective Hamiltonian.

In a similar fashion, it is possible to have unidirectionally propagating modes across the boundary of the regions where quantum walks in each region have no Chern numbers associated with the phases. In the following, we show that such chiral propagating modes exist for even simpler version of two dimensional quantum walk protocols.

Here we consider the following simple two dimensional quantum walk with two rotations and two spin dependent translations, see Fig. 2.5.3;

1. Rotation of the spin around y axis by angle θ_1, given by $R_y(\theta_1) = e^{-i\theta_1\sigma_y/2}$.

2. Translation of the spin $\uparrow$ one lattice to the right, and translation of the spin $\downarrow$ one lattice to the left. Explicitly, $T_1 = \sum_{x,y} |x+1, y\rangle\langle x, y| \otimes |\uparrow\rangle\langle\uparrow| + |x-1, y\rangle\langle x, y| \otimes |\downarrow\rangle\langle\downarrow|$.

3. Rotation of the spin around y axis by angle θ_2, given by $R_y(\theta_2) = e^{-i\theta_2\sigma_y/2}$.

4. Translation of the spin $\uparrow$ one lattice to the up, and translation of the spin $\downarrow$ one lattice to the down. Explicitly,

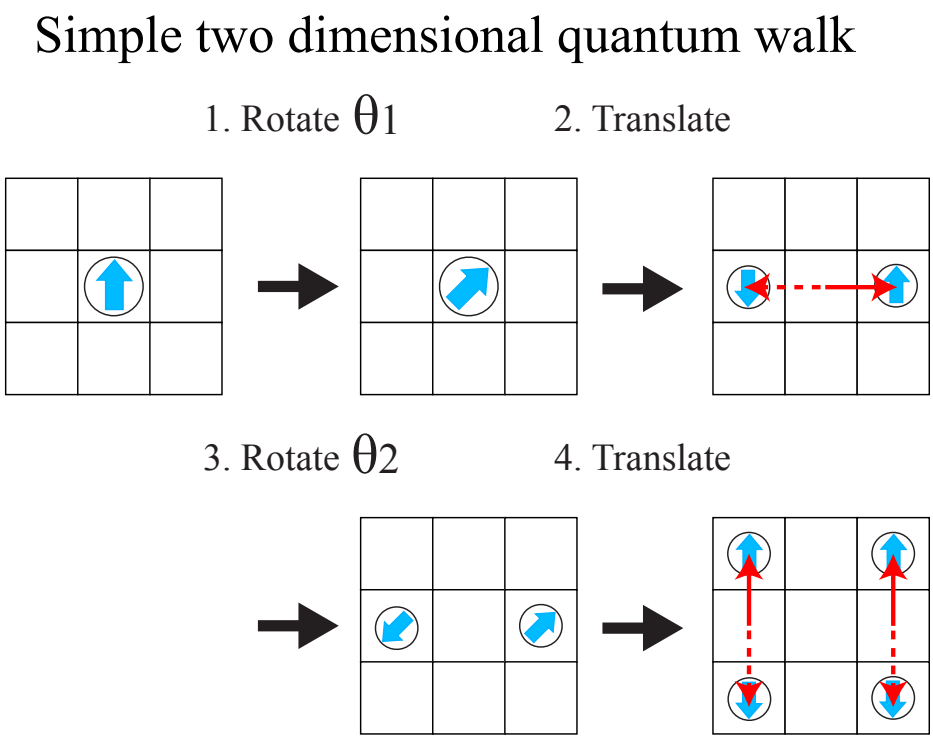

Figure 2.5.3: Protocol for the simple two dimensional quantum walk studied in Section 2.5.2. In this protocol, only four operations are applied during one step of quantum wallk. As before, the spin-dependent translation is indicated by red arrows, where solid arrow is for spin up and dotted arrow is for spin down. The explicit protocol is; 1. spin rotation around y axis by angle θ_1; 2. spin-dependent translation where spin up is move to right, and spin down to left; 3. spin rotation around y axis by angle θ_2; 4. spin-dependent translation where spin up is moved to up, and spin down to down.

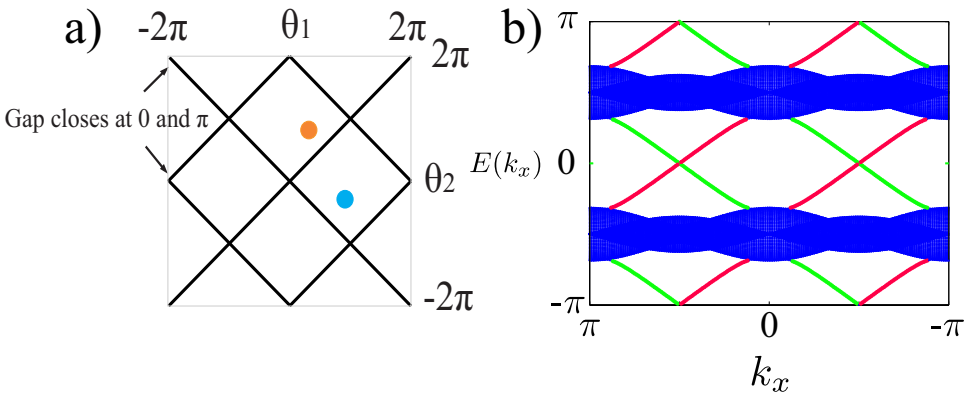

Figure 2.5.4: a) Phase diagram of simple two dimensional quantum walk studied in Section 2.5.2. The Chern number of the quantum walk is everywhere zero. Yet, there are topologically protected unidirectionally propagating modes in the inhomogeneous quantum walk. The existence of such unidirectional edge states are shown through analytical calculations for special values of quantum walks in the text. b) quasi-energy spectrum of the inhomogeneous quantum walks, where the two quantum walk protocols corresponding to the two regions are indicated as orange and blue dot in a). The bulk states are colored as blue, and unidirectionally propagating states are colored as green and red. Green states propagate along the lower edge of the boundary and red states along the upper edge. For a given edge, say, lower edge, the edge states have non-zero energy winding as k_x goes from $-\pi$ to π, and thus, such edge states cannot be removed under the continuous change of quantum walk protocols unless the bulk gap closes, where the upper edge and lower edge are allowed to mix.

$$T_2 = \sum_{x,y} |x, y+1\rangle\langle x, y| \otimes |\uparrow\rangle\langle\uparrow| + |x, y-1\rangle\langle x, y| \otimes |\downarrow\rangle\langle\downarrow|.$$

The effective Hamiltonian of this quantum walk is again given by the form $H_{\text{eff}} = \sum_{\mathbf{k}} E(\mathbf{k})\mathbf{n}(\mathbf{k}) \cdot \sigma \otimes |\mathbf{k}\rangle\langle\mathbf{k}|$. The spectrum of this quantum walk is given

$$\begin{aligned} \cos(E(\mathbf{k}) &= \cos(k_x + k_y)\cos(\theta_1/2)\cos(\theta_2/2) \\ &\quad - \cos(k_x - k_y)\sin(\theta_1/2)\sin(\theta_2/2) \end{aligned}$$

This quantum walk is described by Chern number zero phase everywhere, and the phase diagram is given in Fig. 2.5.4 a). All the gapless phases close their gap at both 0 and π energy. Now consider the inhomogeneous quantum walks in this protocol, where the particle is controlled by the quantum walk protocol with rotation angles θ_{1+} and θ_{2+} at sites $0 \leq y$, and the protocol at sites with $y < 0$ is given by the rotation angles θ_{1-} and θ_{2-}. If we choose the angles such that the two phases are separated by a single gapless phase, there are in fact two unidirectionally propagating modes at the boundary.

This can be most easily confirmed for the spacial rotation angles $\theta_{1+} = 0$ and $\theta_{2+} = \pi$ and $\theta_{1-} = \pi$ and $\theta_{2-} = 0$ by simply considering the evolution for spin up and down for a few steps. Near the boundary, the evolution is

$$\begin{aligned} &|j, 0\rangle \otimes |\uparrow\rangle \xrightarrow{R} |j, 0\rangle \otimes |\uparrow\rangle \xrightarrow{T_1} |j+1, 0\rangle \otimes |\uparrow\rangle \\ &\xrightarrow{R} |j+1, 0\rangle \otimes |\downarrow\rangle \xrightarrow{T_3} |j+1, -1\rangle \otimes |\downarrow\rangle \\ &|j, -1\rangle \otimes |\downarrow\rangle \xrightarrow{R} -|j, -1\rangle \otimes |\uparrow\rangle \xrightarrow{T_1} -|j+1, -1\rangle \otimes |\uparrow\rangle \\ &\xrightarrow{R} -|j+1, -1\rangle \otimes |\uparrow\rangle \xrightarrow{T_3} -|j+1, 0\rangle \otimes |\downarrow\rangle \end{aligned}$$

Thus we see that spin up states at site $y = 0$ and spin down state at site $y = -1$ both propagate to the right during the evolution.

By Fourier transform in x coordinate, it is clear that the walk takes $|k_x, y = 0\rangle \otimes |\uparrow\rangle \to e^{ik_x}|k_x, y = -1\rangle \otimes |\downarrow\rangle$ and $|k_x, y = -1\rangle \otimes |\downarrow\rangle \to -e^{ik_x}|k_x, y = 0\rangle \otimes |\uparrow\rangle$. Thus we conclude there are two unidirectionally propagating modes

$$\begin{aligned} |\psi_1\rangle &= \frac{1}{\sqrt{2}}\left(|k_x, y = 0\rangle \otimes |\uparrow\rangle + i|k_x, y = -1\rangle \otimes |\downarrow\rangle\right) \\ E(k_x) &= k_x - \frac{\pi}{2} \\ |\psi_2\rangle &= \frac{1}{\sqrt{2}}\left(|k_x, y = 0\rangle \otimes |\uparrow\rangle - i|k_x, y = -1\rangle \otimes |\downarrow\rangle\right) \\ E(k_x) &= k_x + \frac{\pi}{2} \end{aligned}$$

On the other hand, other states in the system evolve as, for $l > 0$

$$\begin{aligned} &|j, l > 0\rangle \otimes |\uparrow\rangle \xrightarrow{R} |j, l\rangle \otimes |\uparrow\rangle \xrightarrow{T_1} |j+1, l\rangle \otimes |\uparrow\rangle \\ &\xrightarrow{R} |j+1, l\rangle \otimes |\downarrow\rangle \xrightarrow{T_2} |j+1, l-1\rangle \otimes |\downarrow\rangle \\ &\xrightarrow{R} |j+1, l-1\rangle \otimes |\downarrow\rangle \xrightarrow{T_1} |j, l-1\rangle \otimes |\uparrow\rangle \\ &\xrightarrow{R} -|j, l-1\rangle \otimes |\uparrow\rangle \xrightarrow{T_2} -|j, l\rangle \otimes |\uparrow\rangle \end{aligned}$$

Thus we conclude that the states $\frac{1}{2}\left(|j, l\rangle \otimes |\uparrow\rangle + i|j+1, l-1\rangle \otimes |\downarrow\rangle\right)$ are eigenstates of the system with the flat quasi-energy $E = -\pi/2$ and $\frac{1}{2}\left(|j, l\rangle \otimes |\uparrow\rangle - i|j+1, l-1\rangle \otimes |\downarrow\rangle\right)$ are another set of eigenstates with quasi-energy $E = \pi/2$. In a similar fashion, it is straightforward to show that the bulk states in $l < -1$ have energies $\pm\pi/2$.

Notice that the edge states obtained above has a non-zero winding in the energy direction as k_x goes from $-\pi$ to π *i.e.* the states run from quasi-energy $E = -\pi$ to $E = \pi$ as k_x goes from $-\pi$ to π. it is straightforward to convince oneself, by drawing the spectrum, that such energy winding cannot be removed under the continuous change

of quantum walk protocols unless the bulk gap closes. Thus, the existence of these states is guaranteed for the inhomogeneous quantum walk which has θ_{1+} and θ_{2+} that are continuously connected with $\theta_{1+} = 0$ and $\theta_{2+} = \pi$ and θ_{1-} and θ_{2-} that are continuously connected with $\theta_{1-} = \pi$ and $\theta_{2-} = 0$, without crossing the gapless phase.

As an example, we plot the quasi-energy spectrum of inhomogeneous quantum walk with $\theta_{1+} = \pi/8$ and $\theta_{2+} = 7\pi/8$ from $0 \leq y < 50$, and $\theta_{1-} = 7\pi/8$ and $\theta_{2-} = -\pi/4$ from $-50 \leq y < 0$, and we again take periodic boundary condition for both x and y direction with system size 100×100. These two phases are connected with the limit $\theta_{1+} = 0$ and $\theta_{2+} = \pi$, and $\theta_{1-} = \pi$ and $\theta_{2-} = 0$ in a continuous fashion, as one can check. The spectrum of this system is plotted in Fig. 2.5.4 b), and one can see the existence of unidirectionally propagating modes on the two edges, colored as red and blue. One observes these edge modes in fact winds in the energy direction with non-trivial winding number. Such energy winding is in fact closely related to the phenomenon of Thouless pump[155], and we refer the interested readers to the detailed analysis in [86].

2.6 Other topological phases

Different class of topological phases exist in various symmetries and dimensions, as is classified for non-interacting static Hamiltonian[84, 126, 142]. Quantum walks as understood through the effective Hamiltonian are nothing but the quantum simulator for these static effective Hamiltonians and thus, a part of the classification scheme of quantum walks is the same as the classification of non-interacting static Hamiltonian given in Ref. [84, 126, 142]. As we have illustrated the ideas through a few examples in this chapter, it is possible to realize any of the topological phases in 1 and 2 dimension through the variations of quantum walk protocols. We refer the

interested readers to the article Ref.[87] for more complete analysis.

However, the topological phases given in the classification scheme according to the static effective Hamiltonian is not the only topological phases that can be realized in quantum walks. In previous sections, we have given two examples of topological phenomena that are unique to periodically driven systems; 0 and π energy bound states in zero winding number phases and energy winding unidirectional edge states in zero Chern number phases[86, 92]. These phenomena can also be extended to other classes of driven systems with other symmetries. Recently it has been proposed that two flavors of Majorana Fermions can be realized at 0 and π energies in cold atoms[77], in a similar fashion as 0 and π energy states of quantum walks.

The classification table of topological phenomena unique to driven systems in quantum walks is expected to be the shift of the classification table of static systems by one dimension, since periodical drives lead to a dimensional increase of static systems[92, 126]. The detailed study of such classification schemes is an interesting future work. In particular, it is of great interests to study if other types of topological phenomena unique to driven systems can be realized in quantum walks.

2.7 Conclusion and open questions

In this chapter, we studied topological phases appearing in quantum walks. After the introduction of quantum walks, we provided a thorough explanation of topological nature of quantum walks. We first associated the quantum walks with winding numbers, and gave an intuitive argument for the existence of bound states across the boundary of the regions that belong to different topological phases. We argued for the topological protection of bound states in two

different point of view; one from the spectrum (gap) in the system and another from topological invariant associated with the bound states. These physics are illustrated through the explicit example of quantum walks in one and two dimensions. We also explicitly demonstrated the existence of topological phenomena unique to periodically driven systems in one and two dimensions.

There are many open questions that one can study in the field of quantum walks. For example, there is not yet an example of three dimensional quantum walks that realizes non-trivial topological phase. A simple example of such quantum walks are of interests, considering the excitement in the field of three dimensional topological insulators[59, 125]. Moreover, three dimensional quantum walks with spin 1/2 has the possibility to realize Hopf-insulator first proposed by [111]. Since the realization of this topological phase is very difficult in condensed matter materials, it is of great interests to explore the possibility of realizations in artificial systems such as quantum walks.

Other open direction is provided by quantum walks in different geometries, such as hexagonal lattice. Since hexagonal lattice has three neighbors, study of hexagonal lattice quantum walk with spin 1 might provide interesting platform to explore unique quantum phenomena.

Less concretely, the study of quantum walks with a few to many particles with strong correlation would be interesting to investigate. In particular, in the presence of frustrated hopping, there may be unique quantum phenomena such as the formation of spin-liquid phase.

2.8 Appendix

2.8.1 Asymptotic distribution of quantum walk

In this section, we derive the intuitive result Eq. (2.21) which gives the asymptotic distribution of quantum walks. Here we consider a quantum walk initially prepared at site $x = o$ with initial spin state $|s\rangle$ such that the total initial state is written as $|i\rangle = |x = o\rangle \otimes |s\rangle$. The evolution of a particle after each step is dictated by the effective Hamiltonian given by $H_{\text{eff}} = \int dk E(k)\mathbf{n}(k) \cdot \sigma \otimes |k\rangle\langle k|$ as in Eq. (2.5).

Since the particle is propagating under the non-interacting Hamiltonian H_{eff}, it is natural to expect that the particle propagates in a ballistic fashion. Thus, the particle distribution has a well-defined form in terms of the variable $X = x/N$ in the asymptotic limit. The distribution of X, $P(X)$, can be computed through

$$\begin{aligned} P(X) &= \langle \delta(\hat{x}/N - X) \rangle \\ &= \left\langle \int_{-\infty}^{\infty} ds\, e^{is(X-\hat{x}/N)} \right\rangle \\ &= \int_{-\infty}^{\infty} ds\, e^{isX} \left\langle e^{-is\hat{x}/N} \right\rangle \end{aligned} \tag{2.20}$$

Here the expectation is taken with the state after evolving the initial state $|i\rangle$ for Nth steps under the quantum walk. Thus we aim to obtain the expectation of so-called characteristic function $e^{-is\hat{x}/N}$ after Nth steps as $N \to \infty$.

We first note that $\hat{x} = \sum_j j|j\rangle\langle j|$, and thus

$$\begin{aligned} e^{-is\hat{x}/N} &= 1 + \sum_j (-is)\frac{j}{N}|j\rangle\langle j| + (-is)^2\frac{(j/N)^2}{2!}|j\rangle\langle j| + \cdots \\ &= 1 + \sum_j \left(e^{-isj/N} - 1\right)|j\rangle\langle j| \\ &= \sum_j e^{-isj/N}|j\rangle\langle j| \\ &= \int dk\, |k + s/N\rangle\langle k| \end{aligned}$$

Now we evaluate $\left\langle e^{-is\hat{x}/N}\right\rangle = \langle i|e^{iH_{\text{eff}}N}e^{-is\hat{x}/N}e^{-iH_{\text{eff}}N}|i\rangle$. Since H_{eff} is diagonal in quasi-momentum space, the evaluation is straightforward. First of all,

$$\begin{aligned} & e^{iH_{\text{eff}}N}e^{-is\hat{x}/N}e^{-iH_{\text{eff}}N} \\ = & \int dk\, |k + s/N\rangle\langle k| \otimes e^{iNE(k+s/N)\mathbf{n}(k+s/N)\cdot\sigma} \\ & \times e^{-iNE(k)\mathbf{n}(k)\cdot\sigma} \\ = & \int dk\, |k + s/N\rangle\langle k| \otimes e^{isv_k\mathbf{n}(k)\cdot\sigma} \end{aligned}$$

In the last line, we took the expression in the lowest order in s/N. This can be confirmed through the expansion
$\exp\{NE(k+s/N)\mathbf{n}(k+s/N)\cdot\sigma\} =$
$\cos\{NE(k+s/N)\} + i\sin\{NE(k+s/N)\}\,\mathbf{n}(k+s/N)\cdot\sigma \approx$
$\cos(NE(k) + sv_k) + i\sin(NE(k) + sv_k)\,\mathbf{n}(k)\cdot\sigma$ to the lowest order in $\frac{s}{N}$.

It is now straightforward to evaluate the expectation value of above expression in the initial state $|i\rangle = \int_{-\pi}^{\pi}\frac{dk}{\sqrt{2\pi}}|k\rangle \otimes |s\rangle$. Using the expression Eq. (2.20), we obtain the final expression

$$\begin{aligned} P(X) &= \int_{-\pi}^{\pi}\frac{dk}{2\pi}\frac{1}{2}\left(1 + \langle\mathbf{n}(k)\cdot\sigma\rangle\right)\delta(v_k - X) \\ &\quad + \frac{1}{2}\left(1 - \langle\mathbf{n}(k)\cdot\sigma\rangle\right)\delta(v_k + X) \end{aligned}$$

2.8.2 Sublattice (chiral) symmetry of inhomogeneous quantum walk

In this section, we give the explicit proof of sublattice (chiral) symmetry for inhomogeneous split-step quantum walks. In Eq. (2.8), we defined the sublattice (chiral) symmetry in terms of Hamiltonian. This definition directly translates to the sublattice (chiral) symmetry on the evolution operator after one period U as

$$\Gamma^{-1} U \Gamma = U^{\dagger} \tag{2.21}$$

We have shown in Section 2.4.2 that the (homogeneous) split-step quantum walk, $U = T_{\downarrow} R_y(\theta_2) T_{\uparrow} R_y(\theta_1)$ possesses the symmetry with the operator $\Gamma_{\theta_1} = e^{-i\pi \mathbf{A}\cdot\boldsymbol{\sigma}/2}$ where $\mathbf{A} = (\cos\theta_1/2, 0, -\sin\theta_1/2)$. Here we write the subscript θ_1 on the symmetry operator to emphasize the dependence on θ_1.

Here Γ_{θ_1} is a local operator and thus, we expect that the chiral symmetry is preserved even if θ_2 becomes inhomogeneous in space.

In order to explicitly check this, we expand the evolution operator $U = T_{\downarrow} R_y(\theta_2) T_{\uparrow} R_y(\theta_1)$ in the position basis, where we take the general case that θ_2 depends on space in an arbitrary fashion. For example, $T_{\uparrow} = \sum_x (1+\sigma_z)/2 |x+1\rangle\langle x| + (1-\sigma_z)/2 |x\rangle\langle x|$. After the expansion, one obtains

$$\begin{aligned} U &= \sum_x \frac{1+\sigma_z}{2} R_y(\theta_2(x+1)) \frac{1+\sigma_z}{2} R_y(\theta_1) \otimes |x+1\rangle\langle x| \\ &\quad + \frac{1-\sigma_z}{2} R_y(\theta_2(x+1)) \frac{1-\sigma_z}{2} R_y(\theta_1) \otimes |x\rangle\langle x+1| \\ &\quad + \left(\frac{1-\sigma_z}{2} R_y(\theta_2(x+1)) \frac{1+\sigma_z}{2} R_y(\theta_1) \right. \\ &\quad \left. + \frac{1+\sigma_z}{2} R_y(\theta_2(x)) \frac{1-\sigma_z}{2} R_y(\theta_1) \right) |x\rangle\langle x| \end{aligned}$$

Now the sublattice (chiral) symmetry condition $\left(\Gamma'_{\theta_1}\right)^{-1} U \Gamma_{\theta_1} = U^\dagger$ can be checked by comparing both sides of the equation for each position operators of the form $|x\rangle\langle x+a|$ with $a = -1, 0, 1$. For example, comparing the both sides of the equation for the coefficients of $|x+1\rangle\langle x|$, sublattice (chiral) symmetry requires that

$$\begin{aligned}
&(\Gamma_{\theta_1})^{-1} \frac{1+\sigma_z}{2} R_y(\theta_2(x+1)) \frac{1+\sigma_z}{2} R_y(\theta_1) \Gamma_{\theta_1} \\
&\stackrel{?}{=} R_y^{-1}(\theta_1) \frac{1-\sigma_z}{2} R_y^{-1}(\theta_2(x+1)) \frac{1-\sigma_z}{2}
\end{aligned}$$

It is straightforward to check that this equality indeed holds for any rotation θ_1 and $\theta_2(x+1)$. Repeating such process for the coefficients of $|x\rangle\langle x+1|$ and $|x\rangle\langle x|$, one confirms the existence of sublattice (chiral) symmetry for inhomogeneous quantum walks.

Notice that the split step quantum walk with $\theta_1 = 0$ is effectively the conventional quantum walk described in Section 2.2.1. The quantum walk becomes $U = T_\downarrow R_y(\theta_2) T_\uparrow$, which is unitarily related to the conventional quantum walk $U_{\text{con}} = T R_y(\theta_2) = T_\uparrow T_\downarrow R_y(\theta_2)$ by the shift of time. Therefore, the explanation above also provides the proof that the disordered conventional quantum walk where the rotation angle at each site is random possesses sublattice (chiral) symmetry.

2.8.3 Analytic solution of the bound state for quantum walks with reflecting boundary condition

In this section, we give the analytical solution of bound states for quantum walks with reflecting boundary condition studied in Section 2.4.4. Given the quantum walk with reflecting boundary condition whose evolution operator is $U_{x \le 0}$ in Section 2.4.4, we look for the bound states near $x = 0$. Generally, such bound state can be

written as

$$|\psi_b\rangle = \sum_{j\leq 0} \left(c_{j,\downarrow}|\downarrow\rangle + c_{j,\uparrow}|\uparrow\rangle \right) |j\rangle \tag{2.22}$$

The approach we take is to directly solve the eigenvalue problem

$$U_{x\leq 0}|\psi_b\rangle = e^{-iE_b}|\psi_b\rangle \tag{2.23}$$

where E_b is the quasi-energy of the bound state. Comparison of the two sides of the equation above together with the normalizability of the bound state wavefunction allows the solution of the problem.

The left-hand side of the equation gives

$$\begin{aligned} & U_{x\leq 0}|\psi_b\rangle \\ = & \sum_{j\leq 0} \tilde{c}_{j,\downarrow}|j-1,\downarrow\rangle + \sum_{j\leq -1} \tilde{c}_{j,\uparrow}|j+1,\uparrow\rangle + e^{i\phi}\tilde{c}_{0,\uparrow}|0,\downarrow\rangle \\ = & \sum_{j\leq -1} \tilde{c}_{j+1,\downarrow}|j,\downarrow\rangle + \sum_{j\leq 0} \tilde{c}_{j-1,\uparrow}|j,\uparrow\rangle + e^{i\phi}\tilde{c}_{0,\uparrow}|0,\downarrow\rangle \end{aligned}$$

where the tilde coefficients $\tilde{c}_{j,\uparrow,\downarrow}$ are related to the original coefficients $c_{j,\uparrow,\downarrow}$ through the rotation $R_y(\theta)$ as

$$\begin{aligned} \begin{pmatrix} \tilde{c}_{j,\uparrow} \\ \tilde{c}_{j,\downarrow} \end{pmatrix} &= R_y(\theta) \begin{pmatrix} c_{j,\uparrow} \\ c_{j,\downarrow} \end{pmatrix} \\ &= \begin{pmatrix} \cos(\theta/2) & -\sin(\theta/2) \\ \sin(\theta/2) & \cos(\theta/2) \end{pmatrix} \begin{pmatrix} c_{j,\uparrow} \\ c_{j,\downarrow} \end{pmatrix} \end{aligned}$$

Comparison of the equation above with the right hand side of

Eq. (2.22) immediately gives

$$\begin{aligned} e^{-iE_b}c_{j,\downarrow} &= \tilde{c}_{j+1,\downarrow} \quad j \leq -1 \\ e^{-iE_b}c_{j,\uparrow} &= \tilde{c}_{j-1,\uparrow} \quad j \leq 0 \\ e^{-iE_b}c_{0,\downarrow} &= e^{i\phi}\tilde{c}_{0,\uparrow} \end{aligned} \tag{2.24}$$

In matrix form, the first two equations can be rewritten as

$$\begin{aligned} &\begin{pmatrix} 0 & e^{-iE_b} \\ \cos(\theta/2) & -\sin(\theta/2) \end{pmatrix} \begin{pmatrix} c_{j,\uparrow} \\ c_{j,\downarrow} \end{pmatrix} = \\ &\begin{pmatrix} \sin(\theta/2) & \cos(\theta/2) \\ e^{-iE_b} & 0 \end{pmatrix} \begin{pmatrix} c_{j+1,\uparrow} \\ c_{j+1,\downarrow} \end{pmatrix} \quad \text{for } j \leq -1 \\ \rightarrow \quad &\begin{pmatrix} c_{j,\uparrow} \\ c_{j,\downarrow} \end{pmatrix} = \\ &e^{iE_b} \begin{pmatrix} \frac{\sin^2(\theta/2)}{\cos(\theta/2)} + \frac{1}{\cos(\theta/2)}e^{-2iE_b} & \sin(\theta/2) \\ \sin(\theta/2) & \cos(\theta/2) \end{pmatrix} \begin{pmatrix} c_{j+1,\uparrow} \\ c_{j+1,\downarrow} \end{pmatrix} \quad \text{for } j \leq -1 \end{aligned} \tag{2.25}$$

This last equation is a recursive equation that relates the coefficients at site $j+1$ to site j. We denote the matrix that relates them as $\mathbf{K}$, which is a matrix that appears on the right hand side of Eq. (2.25).

The behavior of wavefunction in the limit of $x \to -\infty$ is determined by the eigenvalues of the matrix $\mathbf{K}$. They are given by

$$\begin{aligned} \mathbf{K} &= \begin{pmatrix} \mathbf{v}_+ & \mathbf{v}_- \end{pmatrix} \begin{pmatrix} \lambda_+ & 0 \\ 0 & \lambda_- \end{pmatrix} \begin{pmatrix} \mathbf{v}_+^T \\ \mathbf{v}_-^T \end{pmatrix} \\ \mathbf{v}_\pm &= \frac{1}{N_\pm} \begin{pmatrix} \frac{e^{-2iE_b} - \cos(\theta) \pm e^{-iE_b}\sqrt{e^{-2iE_b} + e^{2iE_b} - 2\cos(\theta)}}{\sin(\theta)} \\ 1 \end{pmatrix} \\ \lambda_\pm &= \frac{\cos(E_b) \pm \sqrt{\cos^2(E_b) - \cos^2(\theta/2)}}{\cos(\theta/2)} \end{aligned}$$

where $N_\pm$ in the expression of $\mathbf{v}_\pm$ are the normalization factors.

Then, the amplitude of bound states wavefunction at site $-j$ is given by

$$\begin{pmatrix} c_{-j,\uparrow} \\ c_{-j,\downarrow} \end{pmatrix} = Q \begin{pmatrix} \lambda_+^j & 0 \\ 0 & \lambda_-^j \end{pmatrix} Q^{-1} \begin{pmatrix} c_{0,\uparrow} \\ c_{0,\downarrow} \end{pmatrix} \quad j \leq -1$$

where $Q = \begin{pmatrix} \mathbf{v}_+ & \mathbf{v}_- \end{pmatrix}$. One crucial observation is $\lambda_+\lambda_- = 1$, and therefore $|\lambda_+| \leq 1$ when $\cos(E_b) \leq 0$ and $|\lambda_-| \leq 1$ when $\cos(E_b) \geq 0$. The normalizability of the bound state wavefunction requires that the amplitude $(c_{0,\uparrow}, c_{0,\downarrow})^T$ is proportional to $\mathbf{v}_+(\mathbf{v}_-)$ when $\cos(E_b) \leq 0 (\cos(E_b) \geq 0)$. No normalizable bound state wavefunction exists when $|\lambda_+| = |\lambda_-| = 1$, or $\cos^2(E_b) - \cos^2(\theta/2) < 0$.

Additional constraint on the amplitudes $c_{0,\uparrow}, c_{0,\downarrow}$ comes from the equation Eq. (2.24), namely, $e^{-iE_b} c_{0,\downarrow} = e^{i\phi} \tilde{c}_{0,\uparrow}$. Solving these two conditions give us

$$\sin(\theta/2) e^{-i\phi} = -i \sin(E_b) \mp \sqrt{\cos^2(E_b) - \cos^2(\theta/2)}$$

where minus sign is for v_- or when $\cos(E_b) \geq 0$ and plus sign is for v_+ or when $\cos(E_b) \leq 0$.

When $\phi = 0$ and $0 < \theta < 2\pi$, the solution exists at energy $E_b = \pi$ with $(c_{0,\uparrow}, c_{0,\downarrow})^T \propto v_+$. For $\phi = 0$ and $2\pi < \theta < 4\pi$, the bound state energy is $E_b = 0$ and $(c_{0,\uparrow}, c_{0,\downarrow})^T \propto v_-$.

On the other hand, when $\phi = \pi$ and $0 < \theta < 2\pi$, the bound state energy is $E_b = 0$ with $(c_{0,\uparrow}, c_{0,\downarrow})^T \propto v_-$, whereas when $\phi = \pi$ and $2\pi < \theta < 4\pi$, the bound state energy is $E_b = \pi$ with $(c_{0,\uparrow}, c_{0,\downarrow})^T \propto v_+$.

The bound state wave function found above decays on the length scale of $\sim 1/|\log(\lambda_-)| = \frac{1}{|\log(1-|\sin(\theta/2)|)-\log(\cos(\theta/2))|}$. Thus the extent of bound state approaches ∞ as $\theta \to 0, 2\pi$. On the other hand, the bound state becomes most localized when $\theta = \pi$.

2.8.4 Spectrum of two dimensional quantum walk

Here we give the details of how to compute the spectrum of two dimensional quantum walk introduced in Section 2.5.1. The method introduced here is general and can be easily extended to other protocols of quantum walks in, say, higher dimensions.

The evolution operator of one step for the two dimensional quantum walk can be written, in the quasi-momentum space, as

$$\begin{aligned} U(k_x, k_y) = e^{ik_x\sigma_z} e^{-i\theta_1\sigma_y/2} e^{ik_y\sigma_z} e^{-i\theta_2\sigma_y/2} \\ \times e^{i(k_x+k_y)\sigma_z} e^{-i\theta_1\sigma_y/2} \end{aligned}$$

Most general form of the effective Hamiltonian resulting from spin $1/2$ system is given by

$$H_{\text{eff}}(\mathbf{k}) = E_0(\mathbf{k}) + E(\mathbf{k})\mathbf{n}(\mathbf{k}) \cdot \sigma \tag{2.26}$$

This is true because a generator of two by two unitary matrix is 1 and Pauli matrices $\boldsymbol{\sigma}$.

Then the spectrum can be identified by considering the trace of evolution operator because

$$\begin{aligned} & \text{Tr}(U(k_x, k_y)) \equiv \text{Tr}\left(\exp(-iH_{\text{eff}}(\mathbf{k}))\right) \\ = \; & \text{Tr}\left\{e^{-iE_0(\mathbf{k})}\left(\cos\left(E(\mathbf{k})\right) - i\sin\left(E(\mathbf{k})\right)\mathbf{n}(\mathbf{k}) \cdot \sigma\right)\right\} \\ = \; & 2e^{-iE_0(\mathbf{k})}\cos\left(E(\mathbf{k})\right) \end{aligned}$$

The explicit evaluation of the trace of $U(k_x, k_y)$ shows that $E_0(\mathbf{k}) = 0$ for all $\mathbf{k}$ and

$$\begin{aligned} \cos\left(E(\mathbf{k})\right) = \; & \cos(k_x)\cos(k_x + 2k_y)\cos(\theta_1)\cos(\theta_2/2) \\ & - \sin(k_x)\sin(k_x + 2k_y)\cos(\theta_2/2) \\ & - \cos^2(k_x)\sin(\theta_1)\sin(\theta_2/2) \end{aligned}$$

2.8.5 GAPLESS PHASE OF TWO DIMENSIONAL QUANTUM WALK

In this section, we detail the calculation to obtain the line of gapless phase in the phase diagram of Fig. 2.5.2 a). The two bands of the system closes the gap when the two eigenvalues of Hamiltonian

$$H_{\text{eff}}(\mathbf{k}) = E(\mathbf{k})\mathbf{n}(\mathbf{k}) \cdot \sigma \tag{2.27}$$

becomes degenerate. Since the eigenvalues of $\mathbf{n}(\mathbf{k}) \cdot \sigma$ is ± 1, the quasi-energy of the states become degenerate if $E(\mathbf{k}) = -E(\mathbf{k})$, which happens if $E(\mathbf{k}) = 0$ or π due to the periodicity of the quasi-energy.

The gapless phase occurs at the values of θ_1 and θ_2 such that the equation Eq. (2.17) has a solution of $E(\mathbf{k}) = 0$ or π for some value of k_x and k_y. On the other hand, at $E(\mathbf{k}) = 0$ or π, the evolution operator $U(k_x, k_y)$ takes the value 1 or -1, respectively.

A simple way to obtain such values of θ_1 and θ_2 is to look at $(1, 1)$ component of the evolution operator $a_{11} = U(k_x, k_y)[1, 1]$. First we study the lines of gapless phases where the gap is closed at the quasi-energy 0. Then the equation $1 = a_{11}$ gives the condition

$$\begin{aligned} 1 = e^{ik_x} \big\{ & i \sin(k_x + 2k_y) \cos(\theta_2/2) \\ & + \cos(k_x + 2k_y) \cos\theta_1 \cos(\theta_2/2) \\ & - \cos k_x \sin\theta_1 \sin(\theta_2/2) \big\} \end{aligned} \tag{2.28}$$

Note that 1 is the maximum magnitude that RHS of the above equation attains for any values of k_x, k_y, θ_1 and θ_2. Therefore, we can simply maximize the RHS in terms of the variables k_x and k_y or alternatively the variables $k_x + 2k_y$ and k_x. The argument separates few cases.

If $\sin\theta_1 \sin(\theta_2/2)$ is non-zero, then $\cos k_x = \pm 1$. If we take the two orthogonal variables $k_1 = k_x + 2k_y$ and $k_2 = 2k_x - k_y$, then the first two terms of the RHS of Eq. (2.28) is only a function of k_1. By

differentiating the absolute square of RHS in terms of k_2, one can show that the extremum of this value is taken when $\cos k_x = \pm 1$.

Suppose $\cos k_x = 1$. Then $e^{ik_x} = 1$ and the equation Eq. (2.28) requires the first term $\sin(k_x + 2k_y)\cos(\theta_2/2)$ to be zero. If we take $\sin(k_x + 2k_y)$ to be zero, then $\cos(k_x + 2k_y) = \pm 1$, and the condition is reduced to $1 = \cos(\theta_1 + \theta_2/2)$ for plus sign and $-1 = \cos(\theta_1 - \theta_2/2)$ for minus sign. Thus the gapless phase exist whenever $\theta_1 + \theta_2/2 = 2\pi n$ and $\theta_1 - \theta_2/2 = 2\pi n + \pi$. If $\cos(\theta_2/2) = 0$, then the equation is solved only at discrete points of $\theta_1 = \pi/2 + 2\pi n$ with $\theta_2 = 3\pi + 4\pi n$ or $\theta_1 = 3\pi/2 + 2\pi n$ with $\theta_2 = \pi + 4\pi n$. These cases are already included in the condition above.

Similarly consider $\cos k_x = -1$. Then $e^{ik_x} = -1$ and the equation Eq. (2.28) again requires the first term $\sin(k_x + 2k_y)\cos(\theta_2/2)$ to be zero. If we take $\sin(k_x + 2k_y)$ to be zero, then $\cos(k_x + 2k_y) = \pm 1$, and the condition is reduced to $-1 = \cos(\theta_1 - \theta_2/2)$ for plus sign and $1 = \cos(\theta_1 + \theta_2/2)$ for minus sign. Thus the gapless phase exist whenever $\theta_1 - \theta_2/2 = \pi + 2\pi n$ and $\theta_1 + \theta_2/2 = 2\pi n$. Thus these conditions give exactly the same gapless phases as for $\cos k_x = 1$.

Now suppose that $\sin\theta_1 \sin(\theta_2/2)$ is zero. A new condition appears when $\sin(\theta_2/2) = 0$. Then $\cos(\theta_2/2) = \pm 1$. But now, we can satisfy the condition Eq. (2.28) by setting $\cos(k_x + 2k_y) = 0$. Since this does not require for θ_1 to take any particular value, we conclude that gap closes for the line of $\theta_2 = n\pi$.

A similar consideration for quasi-energy $E = \pi$ gives the condition that the gap closes at $E = \pi$ for $\theta_1 + \theta_2/2 = 2\pi n + \pi$, $\theta_1 - \theta_2/2 = 2\pi n$ and $\theta_2 = n\pi$. These results lead to the gapless phases plotted in Fig. 2.5.2 a).

3

The dynamics and prethermalization of one dimensional quantum systems probed through the full distributions of quantum noise

Transient dynamics of quantum systems is yet poorly understood after more than 100 years of development of quantum theory. The full descriptions of many-body quantum dynamics is difficult because 1. analytical solutions of many-body quantum systems are not readily

available 2. the descriptions and observations of dynamical states require going much beyond thermodynamical variables such as temperature and density. In this chapter, we study two equivalent one dimensional many-body quantum systems whose low-energy descriptions are simple enough to allow analytical solutions; one is the dynamics of spins after the Ramsey sequence of one dimensional, two-component bosons; the other is the evolution of interference patterns between two one dimensional quasi-condensates created from a single condensate through splitting. In order to reveal the rich properties of dynamical states, we compute full distribution functions of quantum variables such as spins or interference patterns. The full distribution functions contain information about all orders of the observables such as average, fluctuation, skewness etc and thus fully capture the quantum fluctuations of the states during the dynamics. Using the tools developed in this chapter, we demonstrate that one dimensional dynamics in these systems exhibits the phenomenon known as "prethermalization", where the observables of *non-equilibrium*, long-time transient states become indistinguishable from those of thermal *equilibrium* states.

3.1 Introduction

Probabilistic character of Schrödinger wavefunctions manifests itself most directly in quantum noise. In many-body systems, shot-to-shot variations of experimental observables contain rich information about underlying quantum states. Measurements of quantum noise played crucial role in establishing nonclassical states of photons in quantum optics[4], demonstrating quantum correlations and entanglement in electron interferometers[82], and verifying fractional charge of quasi-particles in quantum Hall systems[33, 35, 139]. In atomic physics so far, noise experiments focused on systems in equilibrium.

Recent work includes analysis of counting statistics in atom lasers[121], establishing Hanbury-Brown-Twiss effect for both bosons and fermions[3], analysis of quantum states in optical lattices[38, 53, 55, 134, 149], observation of momentum correlations in Fermi gases with pairing[47] and investigation of thermal and quantum fluctuations in one and two dimensional condensates[17, 27, 56, 61, 65, 69, 106, 129]. In this chapter we demonstrate that analysis of quantum noise should also be a powerful tool for analyzing non-equilibrium dynamics of strongly correlated systems. Here we study the two equivalent dynamical phenomena; one given by the interaction induced decoherence dynamics in Ramsey type interferometer sequences for two component Bose mixtures in one dimension[164], and another given by the evolution of interference patterns of two one dimensional condensate created through the splitting of a single condensate[60]. We obtain a complete time evolution of the full distribution function of the amplitude of Ramsey fringes or interference patterns. In the case of Ramsey fringes, the average amplitude of Ramsey fringes measures only the average value of the transverse spin component. On the other hand, full distribution functions are determined by higher order correlation functions of the spins. Hence full distribution functions contain considerably more information about the time evolution of the system[68, 99, 124] and provide a powerful probe for the nature of the quantum dynamics under study. In particular, we use the simple expressions of full distribution functions to demonstrate the phenomena of "prethermalization" in these one dimensional systems, where observables in non-equilibrium long-time transient states become indistinguishable from those in thermal equilibrium states.

One dimensional systems with continuous symmetries, including superfluids and magnetic systems, have a special place in the family of strongly correlated systems. Quantum and thermal fluctuations are so

extreme that long range order is not possible in equilibrium. Such systems can not be analyzed using standard mean-field approaches, yet they can be studied through the application of methods specific to one dimension such as exact Bethe ansatz solutions[12, 26, 40, 43, 45, 64, 66, 67, 101, 102, 119, 157], effective description using Tomonaga-Luttinger and sine-Gordon models[9, 32, 46, 52, 70], and numerical analysis using density-matrix renormalization group(DMRG) and matrix product state (MPS) methods[143]. Such systems are often considered as general paradigms for understanding strongly correlated systems. One dimensional systems also give rich examples of integrable systems, where due to the existence of infinite number of conserved quantities, equilibration does not take place[25, 83, 130]. Hence the problem we consider in this chapter is important for understanding fundamental issues such as the quantum dynamics of strongly correlated systems and equilibration/non-equilibration of many-body systems, as well as for possible applications of spinor condensates in spectroscopy, interferometry, and quantum information processing [87, 147, 167].

Our work is motivated by recent experiments of Widera *et al.*[164] who used two hyperfine states of ^{87}Rb atoms confined in 2D arrays of one dimensional tubes to perform Ramsey type interferometer sequences. They observed rapid decoherence of Ramsey fringes and the near absence of spin echo. Their results could not be explained within the single mode approximation which assumes a macroscopic Bose condensation into a single orbital state, but could be understood in terms of the multi-mode Tomonaga-Luttinger type model. Yet the enhanced decoherence rate and suppression of spin echo do not provide unambiguous evidences for what the origin of decoherence is. In this chapter, we suggest that the crucial evidence of the multi-mode dynamics as a source of decoherence should come from the time evolution of the full distribution functions of the Ramsey

fringe amplitude. Such distribution functions should be accessible in experiments on Atom Chips[13, 39, 61, 128, 163] from the analysis of shot-to-shot fluctuations.

This chapter is organized as follows. In Section 3.2, we describe the dynamics of Ramsey sequence and define the distribution functions for spins, the central objects we study in this chapter. Then, we give a short summary of the central results of this chapter. In Section 3.3, we formally give the Hamiltonian of the one dimensional system based on Tomonaga-Luttinger approach. In Section 3.4, we derive the analytical expression for the time evolution of the full distribution function for a simple case in which charge and spin degrees of freedom decouple. This decoupling limit gives a good approximation to the experimental situation of Widera *et al*[164]. A short summary of the result in this decoupling limit has been already reported in Ref [87]. More general case in which spin and charge degrees of freedom mix is studied in Section 3.5. Such mixing introduces the dependence of spin distribution functions on the initial temperature of the system. The dynamics of Ramsey sequence with two component bosons is mathematically equivalent to the dynamics of the interference of split one dimensional condensates, and we describe the mapping between these systems in Section 3.6. In Section 3.7, we demonstrate the phenomenon of prethermalization and show that the interference contrasts of split condensates in a steady state have indistinguishable distributions from those of thermal condensates at some effective temperature T_{eff}. We conclude in Section 3.8 with a discussion of possible extensions of this work.

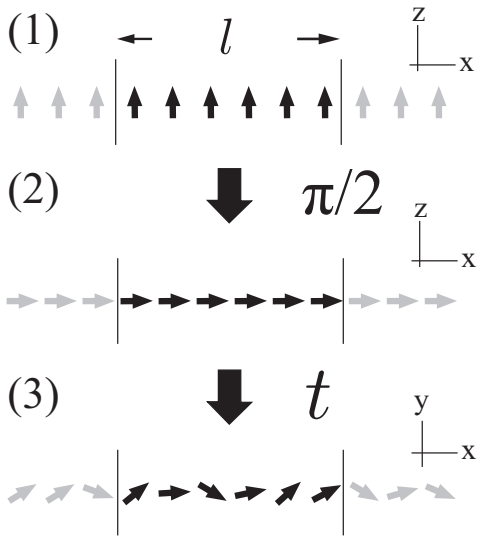

Figure 3.2.1: Ramsey sequence for one dimensional system with two component bosons considered in this chapter. (1) All atoms are prepared in spin up state; (2) $\pi/2$ pulse is applied to rotate each atom into the x direction; (3) spins freely evolve for time t. In actual experiments, final $\pi/2$ pulse is applied to measure the x component of spin. The imaging step (4) is omitted in the illustration. In this chapter, spin operators refer to the ones before the final $\pi/2$ pulse.

3.2 Description of Ramsey dynamics and summary of results

In this chapter, we study the dynamics of one dimensional, interacting two-component Bose mixtures in the Ramsey-type sequence. In analogy with spin-$1/2$ particles, we refer to one component to be spin-up and the other component to be spin-down. In the experiment of cold atoms in Ref [164], two hyperfine states are used for these two components. In the following, we consider a generic situation where there is no symmetry that relates spin-up and spin-down. In particular, unlike fermions with spin-$1/2$, there is no SU(2) symmetry. In a typical experimental setup with cold atoms, there is a harmonic confinement potential along the longitudinal direction of condensates, but here we assume the absence of such a harmonic trap potential. Our consideration gives a good approximation for the central region of cold atom experiments in the presence of such potentials.

Ramsey-type sequence is described as follows(Figure 3.2.1):

1. All atoms are prepared in spin up state at low temperature
2. $\pi/2$ pulse is applied to rotate the spin of each atom into the x direction
3. Spins evolve for time t
4. Spins in the transverse direction ($x-y$ plane) are measured

In a typical experimental situations[164], the last measurement step is done by applying a $\pi/2$ pulse to map the transverse spin component into z direction, which then can be measured. In the following discussions, we describe the dynamics in the rotating frame of Larmer frequency in which the chemical potentials of spin-up and spin-down are the same in the absence of interactions. In this frame, the

evolution of spins in the third step is dictated by the diffusion dynamics coming from interactions. Unlike the conventional use of the Ramsey sequence in the context of precision measurements, here we employ the Ramsey sequence as a probe of correlation functions in one dimensional system.

The description of the spin dynamics starts from the highly excited state prepared after the $\pi/2$ pulse of step 2. The subsequent dynamics during step 3 crucially depends on the nature of excitations in the system. In particular, the dynamics of two-component Bose mixture in one dimension is quite different from those in three dimension. In three dimensions, bosons form a Bose-Einstein condensate(BEC) at low temperature, and particles occupy a macroscopic number of $k = 0$ mode. Then, the spin diffusion of three dimensional BEC is dominated by the *spatially homogeneous* dynamics coming from the single $k = 0$ mode at sufficiently low temperatures. On the other hand, bosonic systems in one dimension do not have the macroscopic occupancy of the $k = 0$ mode, and their physics is dominated by the strong fluctuations, to the extent that the system cannot retain the long range phase coherence even at zero temperature[46]. Thus, the spin dynamics of one dimensional bosonic system necessarily involves a large number of modes with different momenta and the spin becomes *spatially inhomogeneous* during the step 3 above.

Such dynamics unique to one dimension can be probed through the observation of transverse spin components in the fourth step. Since we aim to capture the multi-mode nature of the dynamics in one dimension, we consider the observation of spins at length scale l, given by

$$\hat{S}_l^a(t) = \int_{-l/2}^{l/2} dr \hat{S}^a(r,t) \tag{3.1}$$

where $\hat{S}^a(r,t)$ with $a = x, y$ are the transverse components of spin operators after time evolution of step 3 of duration t. We assume that l is much larger than the spin healing length ξ_s, and much smaller than the system size L to avoid finite size effects. Furthermore, we assume that the number of particles within the length l, N_l, is large, so that the simultaneous measurements of $\hat{S}_l^x(t)$ and $\hat{S}_l^y(t)$ are in principle possible. For large N_l, the non-commutativity of $\hat{S}_l^x$ and $\hat{S}_l^y$ gives corrections of the order of $1/\sqrt{N_l}$ compared to the average values. In this situation, it is also possible to measure the magnitude of transverse spin components, $\hat{S}_l^\perp = \sqrt{\left(\hat{S}_l^x\right)^2 + \left(\hat{S}_l^y\right)^2}$, which we will extensively study in the later sections.

Due to quantum and thermal fluctuations, the measurements of $\hat{S}_l^a(t)$ give different values from shot-to-shot. After the $\pi/2$ pulse of step 2, the spins are prepared in x direction, so the average value yields $\left\langle \hat{S}_l^x(t=0) \right\rangle \approx N_l/2$ and $\left\langle \hat{S}_l^y(t=0) \right\rangle \approx 0$. In the rotating frame of Larmer frequency, the subsequent evolution does not change the expectation value of the y component so that $\left\langle \hat{S}_l^y(t) \right\rangle \sim 0$ throughout. The decay of the average $\left\langle \hat{S}_l^x(t) \right\rangle$ during the evolution in step 3 tells us the strength of spin diffusion in the system. The behaviors of $\left\langle \hat{S}_l^a(t) \right\rangle$ due to spin diffusion are similar for one and three dimensions, and the difference is quantitative, rather than qualitative. On the other hand, a richer information about the dynamics of one dimensional system is contained in the noise of $\hat{S}_l^a(t)$. Such noise inherent to quantum systems is captured by higher moments $\langle \left(\hat{S}_l^a(t) \right)^n \rangle$. In this chapter, we obtain the expression for the full distribution function $P_l^a(a,t)$ which can produce any moments of $\hat{S}_l^a(t)$ through the relation

$$\langle \left(\hat{S}_l^a(t) \right)^n \rangle = \int da\, P_l^a(a,t) a^n, \tag{3.2}$$

where $P_l^a(a,t)da$ represents the probability that the measurement of $\hat{S}_l^a(t)$ gives the value between a and $a + da$. We will see in Section 3.4

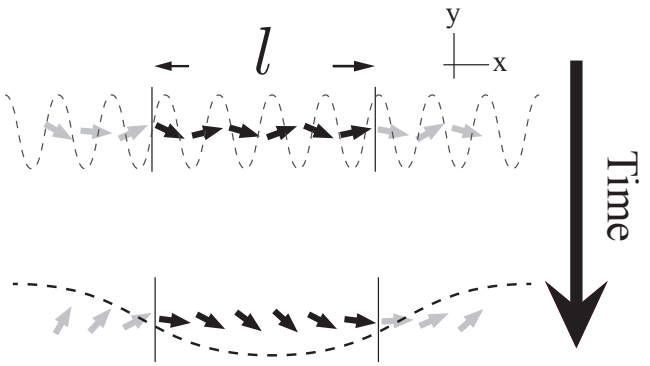

Figure 3.2.2: Illustration of the dynamics of spins in the presence of spin wave excitations. At short times(top), high momenta excitations contribute to fluctuations of the spins, but their effect is weak. At long times(bottom), low momenta excitations lead to the strong fluctuations of the spins. Such fluctuations with wavelengths larger than l rotate the regions of length l as a whole so that they do not lead to the decay of the magnitude of spin $\hat{S}_l^{\perp}$, but result in diffusion of $\hat{S}_l^x$.

that it is also possible to obtain the joint distributions $P_l^{x,y}(a,\beta,t)$ of $\hat{S}_l^x(t)$ and $\hat{S}_l^y(t)$ as well as the distribution $P_l^{\perp}(a,t)$ of the squared transverse magnitude $\left(\hat{S}_l^{\perp}\right)^2$.

Now we summarize the main results of this chapter, and give a qualitative description of spin dynamics in the Ramsey sequence. Elementary excitations of spin modes in the system are described in terms of linearly dispersing spin waves with momenta k and excitation energies $c_s|k|$, where c_s is the spin wave velocity. When certain symmetry conditions are satisfied(see discussion in Section 3.4), spin and charge degrees of freedom decouple, and these spin waves are free and they do not interact among themselves in the low energy descriptions within so-called Tomonaga-Luttinger theory[46]. Here, we describe the result in this decoupling limit, but the qualitative picture does not change even after the coupling between spin and charge is introduced, as we will see in Sec. 3.5.

The initial state prepared after $\pi/2$ pulse in step 2 in which all spins point in the x direction is far from the equilibrium state of the system because interactions of spins are not symmetric in terms of spin rotations. Thus, the initial state contains many excitations and the subsequent dynamics of spins is determined by time evolution of the spin waves. A spin wave excitation with momentum k rotates spins with length scale $\sim 2\pi/k$ and time scale $\sim 1/(c_s|k|)$. The amplitude of fluctuations coming from the spin wave with momentum k is determined by the initial state as well as the nature of spin wave excitations. We find that the energy stored in each mode is approximately the same(see discussion in Sec. 3.4.2), thus the amplitude of fluctuations for wave vector k scales as $1/k^2$. Therefore, the fluctuation of spins is weak at short wave lengths and short times, and strong at long wave lengths and long times. In Fig.3.2.2, we illustrate such dynamics of spins due to fluctuations of spin wave excitations. It leads to the distributions presented in Fig.3.2.3 and Fig.3.2.4. Here, we have plotted distribution function of the squared transverse magnitude of spins $\left(\hat{S}_l^{\perp}\right)^2$(Fig.3.2.3) and the joint distribution function(Fig.3.2.4) with $L = 200$, $K_s = 20$ and various integration length $l/\xi_s = 20, 30, 40$. K_s is the spin Luttinger parameter, which measures the strength of interactions and correlations in 1D system (see Eq. (3.8) below), and ξ_s is a spin healing length which gives a characteristic length scale in the low energy theory of spin physics.

The multi-mode nature of one dimensional system, in which spin correlations at different length scales are destroyed in qualitatively different fashion during the dynamics, can be revealed most clearly in the squared transverse magnitude of spins $\left(\hat{S}_l^{\perp}\right)^2$, plotted in Fig.3.2.3. In the initial state, all the spins are aligned in the x direction, so the distribution of $\left(\hat{S}_l^{\perp}\right)^2$ is a delta function peak at its maximum value, $\sim (\rho l)^2$, where ρ is the average density of spin-up or spin-down. The

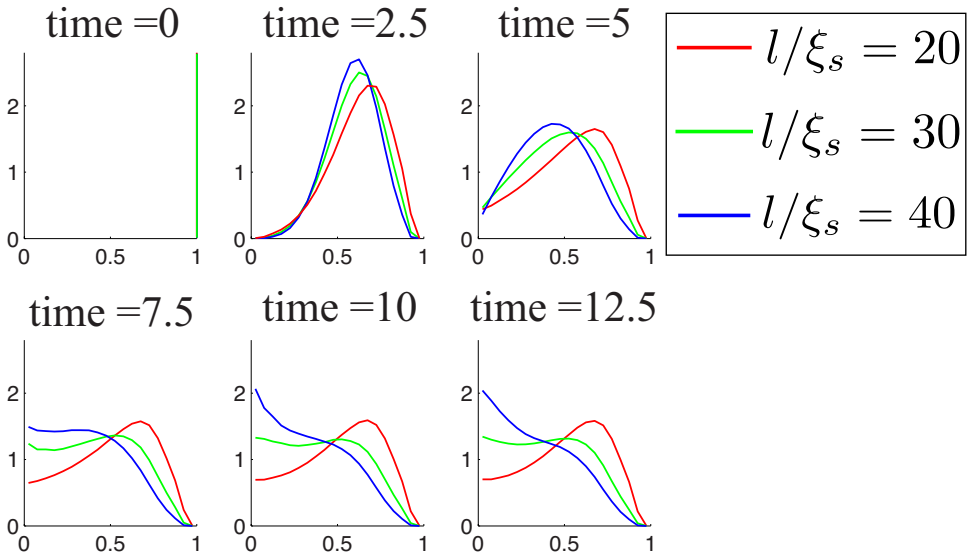

Figure 3.2.3: Time evolution of the distribution $P_l^{\perp}(a)$ of the squared transverse magnitude of spins, $\left(\hat{S}_l^{\perp}\right)^2$, for the system size $L/\xi_s = 200$, the spin Luttinger parameter $K_s = 20$ and various integration length $l/\xi_s = 20, 30, 40$. Here ξ_s is the spin healing length, and the x axis is scaled such that the maximum value of a is 1. Time is measured in units of ξ_s/c_s where c_s is the spin sound wave velocity. The evolution of the distribution crucially depends on the integration length. The steady state of the distribution of the squared transverse magnitude has a peak at a finite value for short integration length $l/\xi_s = 20$, whereas the peak is at 0 for long integration length $l/\xi_s = 40$.

evolution of spin waves lead to the fluctuations of spins and thus to the decay of the integrated magnitude of the transverse spin. How the spin waves affect the integrated magnitude of spins strongly depends on the wavelength of the excitations. Spin excitations with momenta much smaller than $\sim 2\pi/l$ do not affect $\left(\hat{S}_l^{\perp}\right)^2$ since these spin waves rotate the spins within l as a whole, while spin excitations with higher momenta lead to the decay of the magnitude. This is in stark contrast with the x component of the spin $\hat{S}_l^x$, which receives contributions from spin waves of all wavelengths.

As a result of different contributions of spin wave excitations with different wavelengths to the integrated spin magnitude, there are two distinct behaviors of the distributions of $\left(\hat{S}_l^{\perp}\right)^2$; one for short integration length l, which we call "spin diffusion regime" and another for long integration length l, which we call "spin decay regime."

For short integration length l, the distribution function of $\left(\hat{S}_l^{\perp}\right)^2$ is always peaked near its maximum value $(\rho l)^2$ during the dynamics because the strengths of fluctuations coming from spin waves with high momenta are suppressed by $1/k^2$(Fig.3.2.3, $l/\xi_s = 20$). While the magnitude of spins does not decay in this regime, fluctuations still lead to a diffusion of $\hat{S}_l^x$, thus, we call this regime the "spin diffusion regime."

On the other hand, for long integration length, spin waves lead to fluctuations of the spins within the integration region, and the spins are randomized after a long time. This randomization of spins leads to the development of a Gaussian-like peak near $\left(S_l^{\perp}\right)^2 = 0$(Fig.3.2.3, $l/\xi_s = 40$). During the intermediate time, both peaks at 0 and the maximum value $(\rho l)^2$ are present, and one can observe the double peak structure. Because of the strong decaying behavior of the magnitude of spin, we call this regime the "spin decay regime."

More complete behaviors of distribution functions can be captured by looking at the joint distribution functions from which we can read off the distributions of both $\left(\hat{S}_l^{\perp}\right)^2$ and $\hat{S}_l^x$, see Fig.3.2.4. In the "spin diffusion regime" with short l, the joint distributions form a "ring" during the time evolution, whereas in the "spin decay regime" with long l, they form a "disk"-like structure in the long time limit. As we will see later, a dimensionless parameter given by $l_0 \sim \frac{\pi^2 l}{4K_s\xi_s}$ determines whether the dynamics belongs to the "spin diffusion regime"($l_0 \leq 1$) or the "spin decay regime"($l_0 \gg 1$).

We emphasize that in three dimensions, spin waves are dominated

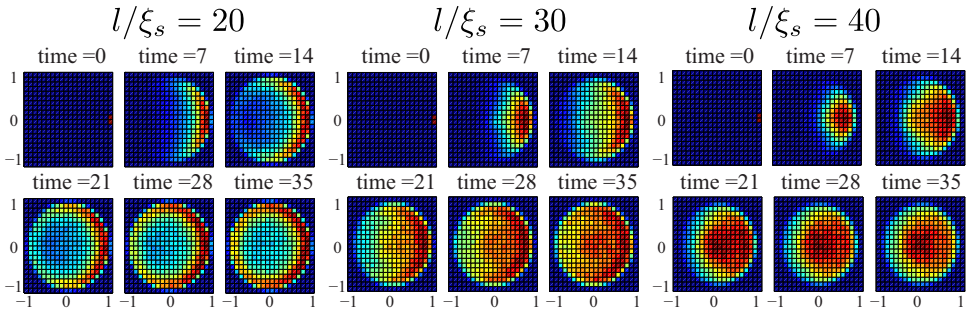

Figure 3.2.4: Time evolution of the joint distribution function $P^{x,y}(\alpha, \beta)$ for the system size $L/\xi_s = 200$, the spin Luttinger parameter $K_s = 20$ and various integration lengths $l/\xi_s = 20$(left),30(middle), and 40(right). Time is measured in units of ξ_s/c_s where c_s is the spin sound wave velocity. Here axes are scaled such that the maximum value of α and β are 1. For for short integration length $l/\xi_s = 20$, the dynamics leads to the distribution with the "ring"-like structure, showing that the magnitude of spins does not decay much (spin diffusion regime). On the other hand, for longer integration lengths, the magnitude of spins decays quickly and the distribution forms a "disk"-like structure(spin decay regime).

by $k = 0$ mode and therefore, there is almost no decay in the magnitude of spins throughout the dynamics. Therefore, the existence of two qualitatively different behaviors of distribution functions of $\left(\hat{S}_l^{\perp}\right)^2$ unambiguously distinguishes the dynamics in one and three dimensions.

3.3 Two component Bose mixtures in one dimension: Hamiltonian

In this chapter, we study the dynamics of two-component Bose mixtures in one dimension through Tomonaga-Luttinger formalism[46]. As we have stated before, we assume the rotating frame, in which spin-up and spin-down particles have the same chemical potential in the absence of interactions. The Hamiltonian of

two component Bose mixtures in one dimension is given by

$$\mathcal{H} = \int_{-L/2}^{L/2} dr \left[\sum_i \frac{1}{2m_i} \nabla\psi_i^\dagger(r)\nabla\psi_i(r) + \sum_{ij} g_{ij}\,\psi_i^\dagger(r)\psi_j^\dagger(r)\psi_j(r)\psi_i(r) \right] \tag{3.3}$$

Here ψ_i with $i = \uparrow, \downarrow$ describe two atomic species with masses m_i and g_{ij} are the interaction strengths given by $g_{ij} = \nu_\perp a_{ij}$[117] where $\nu_\perp$ is the frequency of transverse confinement potential and a_{ij} are the scattering lengths between spin i and j. System size is taken to be L, and we take the periodic boundary condition throughout the chapter. In addition, we use the unit in which $\hbar = 1$.

In the low energy description, the Hamiltonians for weakly interacting bosons after the initial $\pi/2$ rotation can be written in quadratic form, and given by

$$\begin{aligned} H &= H_\uparrow + H_\downarrow + H_{int}, \\ H_\uparrow &= \int_{-L/2}^{L/2} dr \left[\frac{\rho}{2m_\uparrow} (\nabla\hat{\phi}_\uparrow(r))^2 + g_{\uparrow\uparrow}(\hat{n}_\uparrow(r))^2 \right], \\ H_\downarrow &= \int_{-L/2}^{L/2} dr \left[\frac{\rho}{2m_\downarrow} (\nabla\hat{\phi}_\downarrow(r))^2 + g_{\downarrow\downarrow}(\hat{n}_\downarrow(r))^2 \right], \\ H_{int} &= 2\int_{-L/2}^{L/2} dr(r) \left[g_{\uparrow\downarrow}\hat{n}_\uparrow\hat{n}_\downarrow(r) + g^{\phi}_{\uparrow\downarrow}\nabla\hat{\phi}_\uparrow\nabla\hat{\phi}_\downarrow(r) \right], \end{aligned} \tag{3.4}$$

where ρ is the average density of each species and $\hat{n}_\sigma$ are variables representing the phase and density fluctuation for the particle with spin σ. These variables obey a canonical commutation relation $[\hat{n}_\sigma(r), \hat{\phi}_\sigma(r')] = -i\delta(r - r')$. The variables $\hat{\phi}_\sigma$ and $\hat{n}_\sigma$ are "coarse-grained" in the sense that they represent the operators in the long wavelength beyond the spin healing length ξ_s. ξ_s is determined

from microscopic physics and gives the length below which the kinetic energy wins over the interaction energy and the particles start behaving like free particles. For weakly interacting bosons with $m_\uparrow = m_\downarrow = m$, it is given by $\xi_s = \pi/\sqrt{m\rho(g_{\uparrow\uparrow} + g_{\downarrow\downarrow} - 2g_{\uparrow\downarrow})}$.

In the following, we assume that the number of particles within the spin healing length is large, *i.e.* $\xi_s \rho \gg 1$. This condition is always satisfied for weakly interacting bosons. We note, that in the weakly interacting case one can obtain the parameters of the Hamiltonian in Eq. (3.4) such as g_{ij} and m_i through hydrodynamic linearization of the microscopic Hamiltonian. Here we consider a general form of the Hamiltonian allowed by symmetry such as inversion.

In order to describe the spin dynamics, we define spin and charge operators as the difference and the sum of spin up and down operators, *i.e.* $\hat{\phi}_s = \hat{\phi}_\uparrow - \hat{\phi}_\downarrow$, $\hat{\phi}_c = \hat{\phi}_\uparrow + \hat{\phi}_\downarrow$, $\hat{n}_s = \frac{1}{2}(\hat{n}_\uparrow - \hat{n}_\downarrow)$, $\hat{n}_c = \frac{1}{2}(\hat{n}_\uparrow + \hat{n}_\downarrow)$. In this representation, the Hamiltonian in Eq. (3.4) becomes

$$
\begin{aligned}
H &= H_s + H_c + H_{mix} \\
H_s &= \int_{-L/2}^{L/2} dr \left[\frac{\rho}{2m_s} (\nabla \hat{\phi}_s(r))^2 + g_s (\hat{n}_s(r))^2 \right] && (3.5) \\
H_c &= \int_{-L/2}^{L/2} dr \left[\frac{\rho}{2m_c} (\nabla \hat{\phi}_c(r))^2 + g_c (\hat{n}_c(r))^2 \right] && (3.6) \\
H_{mix} &= 2 \int_{-L/2}^{L/2} dr \left[g_{mix} \hat{n}_s(r) \hat{n}_c(r) + g^{\phi}_{mix} \nabla \hat{\phi}_s(r) \nabla \hat{\phi}_c(r) \right] && (3.7)
\end{aligned}
$$

where interaction strengths are given by $g_c = g_{\uparrow\uparrow} + g_{\downarrow\downarrow} + 2g_{\uparrow\downarrow}$, $g_s = g_{\uparrow\uparrow} + g_{\downarrow\downarrow} - 2g_{\uparrow\downarrow}$, $g_{mix} = g_{\uparrow\uparrow} - g_{\downarrow\downarrow}$, $g^{\phi}_{mix} = \rho/(8m_\uparrow) - \rho/(8m_\downarrow)$. The masses are given by the relations $\rho/(2m_c) = \rho/(8m_\uparrow) + \rho/(8m_\downarrow) + g^{\phi}_{\uparrow\downarrow}/2$ and $\rho/(2m_s) = \rho/(8m_\uparrow) + \rho/(8m_\downarrow) - g^{\phi}_{\uparrow\downarrow}/2$

In the next section, we consider the case $g_{mix} = 0$ and $g^{\phi}_{mix} = 0$, in

which spin and charge degree of freedom decouple. Then the dynamics of spins is completely described by the spin Hamiltonian in Eq. (3.5). The general case in which $g_{mix} \neq 0$ and $g^{\phi}_{mix} \neq 0$ will be treated in Sec 3.5.

3.4 Dynamics of Full Distribution Function for decouped spin and charge degrees of freedom

3.4.1 Hamiltonian and initial state

The experiment of Widera *et al.*[164] used $F = 1, m_F = +1$ and $F = 2, m_F = -1$ states of ^{87}Rb for spin-up and spin-down particles, respectively. These hyperfine states have the scattering lengths $a_{\sigma\sigma'}$ such that $a_{\uparrow\uparrow} \approx a_{\downarrow\downarrow}$. Consequently, the mixing Hamiltonian in Eq.(3.7) approximately vanishes for weak interactions. Motivated by this experiment, here we consider the decoupling of spin and charge degrees of freedom[87]. Spin dynamics in this case is completely determined by the spin Hamiltonian

$$H_s = \frac{c_s}{2} \int \left[\frac{K_s}{\pi} (\nabla \hat{\phi}_s(r))^2 + \frac{\pi}{K_s} \hat{n}_s^2(r) \right] dr \tag{3.8}$$

where K_s is the spin Luttinger parameter representing the strength of interactions, and c_s is spin sound velocity. K_s and c_s are directly related to the spin healing length ξ_s in the weak interaction limit, given by $2K_s = \rho\xi_s$ and $c_s = \frac{\pi}{2m_s\xi_s}$. $\hat{n}_s(r,t)$ is the local spin imbalance $\hat{n}_s = \psi^\dagger_\alpha(\frac{1}{2}\sigma^z_{\alpha\beta})\psi_\beta$ and $\hat{\phi}_s(r,t)$ is related to the direction of the transverse spin component $\rho e^{i\hat{\phi}_s} = \psi^\dagger_\alpha \sigma^+_{\alpha\beta}\psi_\beta$. Here, $\psi^\dagger_\alpha$ is the creation operator of spin $\alpha = \uparrow, \downarrow$. These variables $\hat{n}_s$ and $\hat{\phi}_s$ obey a canonical commutation relation $[\hat{n}_s(r), \hat{\phi}_s(r')] = -i\delta(r - r')$.

Other spin variables can be similarly defined in terms of coarse

grained spin variables $\hat{n}_s$ and $\hat{\phi}_s$. In the following, we consider the general transverse spins pointing in the direction $(x, y, z) = (\cos\theta, \sin\theta, 0)$ integrated over l given by

$$\begin{aligned} \hat{S}_l^\theta &= \int_{-l/2}^{l/2} dr\, \psi_a^\dagger(r,t) \left(\cos\theta \frac{\sigma^x_{a\beta}}{2} + \sin\theta \frac{\sigma^y_{a\beta}}{2} \right) \psi_\beta(r,t) \\ &= \int_{-l/2}^{l/2} dr \frac{\rho}{2} \left(e^{i(\hat{\phi}_s(r)-\theta)} + e^{-i(\hat{\phi}_s(r)-\theta)} \right) \end{aligned} \tag{3.9}$$

where σ^a with $a = x, y$ are Pauli matrices. Here $\hat{S}_l^\theta$ with $\theta = 0$ corresponds to spin x operator and $\theta = \pi/2$ corresponds to spin y operator. In order to explore the one dimensional dynamics resulting from Hamiltonian in Eq.(3.8), we analytically compute the mth moment of the spin operator $\hat{S}_l^\theta$, $\left\langle \left(\hat{S}_l^\theta\right)^m \right\rangle$, after time t of the $\pi/2$ pulse of the Ramsey sequence. Then, the full distribution functions of $\hat{S}_l^x$ and $\hat{S}_l^y$, as well as the joint distribution of these will be obtained from $\left\langle \left(\hat{S}_l^\theta\right)^m \right\rangle$.

In order to study the dynamics of Ramsey interferometer in terms of low energy variables $\hat{n}_s$ and $\hat{\phi}_s$, we need to write down an appropriate state after the $\pi/2$ pulse in terms of $\hat{n}_s$ and $\hat{\phi}_s$. If pulse is sufficiently strong, each spin is independently rotated into x direction after the $\pi/2$ pulse. Naively, this prepares the initial state in the eigenstate of $\hat{S}^x(r) = \rho\cos\hat{\phi}_s(r)$ with eigenvalue $\hat{\phi}_s(r) = 0$. However, due to the commutation relation between $\hat{n}_s$ and $\hat{\phi}_s$, such an initial state has an infinite fluctuation in $\hat{n}_s$ and therefore, the state has an infinite energy according to Eq.(3.8). This unphysical consequence comes about because the low energy theory in Eq.(3.8) should not be applied to the physics of short time scale given by $1/E_c$ where E_c is the high energy cutoff of Tomonaga-Luttinger theory. During this short time dynamics, the initial state establishes the correlation at the length scale of spin healing length ξ_s. The state after this short time

dynamics can now be described in terms of the coarse-grained variables $\hat{n}_s(r)$ and $\hat{\phi}_s(r)$. The variables $\hat{n}_s(r)$ and $\hat{\phi}_s(r)$ are defined on the length scale larger than the spin healing length ξ_s. Since the z component of spins are still uncorrelated beyond ξ_s after the initial short time dynamics, the appropriate initial condition of the state is written as

$$\langle S^z(r)S^z(r')\rangle = \langle \hat{n}_s(r)\hat{n}_s(r')\rangle = \frac{\rho\eta}{2}\delta(r-r') \tag{3.10}$$

where the delta function $\delta(r-r')$ should be understood as a smeared delta function over the scale of ξ_s. Because the state after the short time dynamics is still close to the eigenstate of the $\hat{S}^x(r)$ operator, spins are equal superpositions of spin-up and spin-down. Then the distribution of $\hat{S}^z_l = \int_0^l \hat{S}^z(r)dr$ is determined through random picking of the values $\pm 1/2$ for $2\rho l$ particles. Due to the central limit theorem, the distribution of $\hat{S}^z_l = \int_0^l \hat{S}^z(r)dr$ is Gaussian, *i.e.* $\left\langle \left(\hat{S}^z_l\right)^{2n}\right\rangle = \frac{(2n)!}{2^n n!}(\rho l\eta)^n$. In particular, $\left\langle \left(\hat{S}^z_l\right)^2\right\rangle = \rho l\eta/2$, which determines the magnitude of the fluctuation for $\hat{S}^z(r)$ in Eq.(3.10). In Eq.(3.10), we also introduced the phenomenological parameter η which accounts for the decrease and increase of fluctuations coming from, for example, imperfections of $\pi/2$ pulse. The ideal, fast application of $\pi/2$ pulse corresponds to $\eta = 1$. In the experimental realization of Ref. [164], η was determined to be between 0.8 and 1.3 through the fitting of the experiment with Tomonaga-Luttinger theory for the time evolution of the average x component of the spin, $\left\langle \hat{S}^x_l\right\rangle$. Through engineering of the initial state such as the application of a weak $\pi/2$ pulse, η can also be made intentionally smaller than 1.

A convenient basis to describe the initial state of the dynamics above is the basis that diagonalizes the spin Hamiltonian of Eq.(3.8). The phase and density of the spins $\hat{\phi}_s(r)$ and $\hat{n}_s(r)$ can be written in terms of the creation $b^\dagger_{s,k}$ and annihilation $b_{s,k}$ operators of elementary

excitations for the spin Hamiltonian in Eq.(3.8) as

$$\begin{aligned}
\hat{\phi}_s(r) &= \frac{1}{\sqrt{L}} \sum_k \hat{\phi}_{s,k} e^{ikr} \\
&= \frac{1}{\sqrt{L}} \left(\sum_{k\neq 0} -i\sqrt{\frac{\pi}{2|k|K_s}} (b^\dagger_{s,k} - b_{s,-k}) e^{ikr} + \hat{\phi}_{s,0} \right) \\
\hat{n}_s(r) &= \frac{1}{\sqrt{L}} \sum_k \hat{n}_{s,k} e^{ikr} \\
&= \frac{1}{\sqrt{L}} \left(\sum_{k\neq 0} \sqrt{\frac{|k|K_s}{2\pi}} (b^\dagger_{s,k} + b_{s,-k}) e^{ikr} + \hat{n}_{s,0} \right) \\
\mathcal{H}_s &= \sum_{k\neq 0} c_s |k| b^\dagger_{s,k} b_{s,k} + \frac{\pi c_s}{2K_s} \hat{n}^2_{s,0}
\end{aligned} \tag{3.11}$$

where we defined $\hat{\phi}_{s,k}$ and $\hat{n}_{s,k}$ to be the Fourier transform of operators $\hat{\phi}_s(r)$ and $\hat{n}_s(r)$. $b^\dagger_{s,k}$ creates a collective mode with momentum k and follows a canonical commutation relation $[b_{s,k}, b^\dagger_{s,k}] = 1$. Note that $k = 0$ mode has no kinetic energy, and it naturally has different evolution from $k \neq 0$ modes.

The Gaussian state determined by Eq.(3.10) takes the form of a squeezed state of operators $b_{s,k}$, and it is given by

$$\begin{aligned}
|\psi_0\rangle &= \frac{1}{\mathcal{N}} \exp\left(\sum_{k\neq 0} W_k b^\dagger_{s,k} b^\dagger_{s,-k} \right) |0\rangle |\psi_{s,k=0}\rangle \\
\langle n_{s,0} | \psi_{s,k=0} \rangle &= \exp\left(-\frac{1}{2\rho\eta} n^2_{s,0} \right)
\end{aligned} \tag{3.12}$$

where $2W_k = \frac{1-a_k}{1+a_k}$, $a_k = \frac{|k|K_s}{\pi\rho\eta}$. Here the state $|n_{s,0}\rangle$ is the normalized eigenstate of the operator $\hat{n}_{s,0}$ with eigenvalue $n_{s,0}$. The summation of k in the exponent has a ultraviolet cutoff around $k_c = 2\pi/\xi_s$. $\mathcal{N}$ is the overall normalization of the state. It is easy to check that $\langle \psi_0 | \hat{n}_{s,k} \hat{n}_{s,k'} | \psi_0 \rangle = \frac{\rho\eta}{2} \delta_{k,-k'}$, which corresponds to Eq. (3.10).

3.4.2 Moments and full distribution functions of spins

After free evolution of the initial state $|\psi_0\rangle$ for time t, the state becomes $|\psi(t)\rangle = e^{-iH_s t}|\psi_0\rangle$. We characterize the state at time t by the mth moments of spin operators, $\left\langle (\hat{S}_l^\theta)^m \right\rangle$. As we will see below, the full distribution function can be constructed from the expression of $\left\langle (\hat{S}_l^\theta)^m \right\rangle$ [69].

We consider the evaluation of moments $\left\langle (\hat{S}_l^\theta)^m \right\rangle$ at time t, $|\psi(t)\rangle$. Each momentum k component of the initial state $|\psi_0\rangle$ independently evolves in time. Since $k = 0$ mode has a distinct evolution from other $k \neq 0$ modes, we separately consider $k = 0$ and $k \neq 0$ modes.

$k = 0$ mode

The Hamiltonian of $k = 0$ mode is given by $H_{s,k=0} = \frac{\pi c_s}{2K_s} \hat{n}_{s,0}^2$ in Eq. (3.11). Therefore, in the basis of $n_{s,0}$, $k = 0$ part of the state $|\psi(t)\rangle$ is given by

$$\begin{aligned} &\langle n_{s,0}|e^{-iH_{s,k=0}t}|\psi_{k=0}\rangle = \\ &\frac{1}{\mathcal{N}_{k=0}} \exp\left\{\left(-\frac{1}{(2\rho\eta)} - i\frac{\pi c_s t}{2K_s}\right) n_{s,0}^2\right\}, \end{aligned} \tag{3.13}$$

where $\mathcal{N}_{k=0}$ is the normalization of the state. The initial Gaussian state of $\hat{n}_{s,0}$ stays Gaussian at all times, and any analytic operator of $\phi_{s,0}$ and $n_{s,0}$ can be exactly evaluated through Wick's theorem. For example, $k = 0$ part contributes to the decay of the average of the x component of spin $\left\langle \hat{S}_l^x \right\rangle_{k=0} = l\rho \mathrm{Re}\left(\left\langle e^{i\phi_{s,0}/\sqrt{L}} \right\rangle\right)$ as

$$\begin{aligned} \left\langle \hat{S}_l^x \right\rangle_{k=0} &= l\rho e^{-\frac{1}{2L}\left\langle \phi_{s,0}^2 \right\rangle_t} \\ \left\langle \phi_{s,0}^2 \right\rangle_t &= \frac{1}{2\rho\eta} + \left(\frac{c_s \pi t}{K_s}\right)^2 \frac{\eta\rho}{2} \end{aligned} \tag{3.14}$$

This diffusion of the spin from $k = 0$ contribution is generally present in any dimensional systems, and not particular to one dimension.

Physical origin of this diffusion is the interaction dependent on the total spin , $\hat{S}_z^2$. The eigenstate of $\hat{S}_x$ with eigenvalue ρl is the superposition of different eigenstates of $\hat{S}_z$ with eigenvalues m_z, and they accumulate different phases $e^{-itm_z^2}$ in time. This leads to the decay of $\langle \hat{S}_x \rangle$. In the thermodynamic limit $L \to \infty$, the uncertainty of $\hat{S}_z$ becomes diminishingly small, and therefore, the decay of $\langle \hat{S}_x \rangle$ coming from $k = 0$ goes to zero. More interesting physics peculiar to one dimensional systems comes from $k \neq 0$ modes. In the case of three dimensional systems, macroscopic occupancy of a single particle state is absent in one dimension, so $k \neq 0$ momentum excitations have much more significant effect in one dimensional dynamics.

$k \neq 0$ CONTRIBUTION

The exact evaluation of spin moments $\langle (\hat{S}_l^\theta)^m \rangle$ for $k \neq 0$ is possible through the following trick. Consider the annihilation operator $\gamma_{s,k}(t)$ for the state $|\psi(t)\rangle$ such that $\gamma_{s,k}(t)|\psi(t)\rangle = 0$. If we write the operators $\hat{\phi}_s(r)$ in terms of $\gamma_{s,k}(t)$ and $\gamma_{s,k}^\dagger(t)$, then $k \neq 0$ part of the mth moment schematically takes the form $\langle (\hat{S}_l^\theta)^m \rangle \sim \left\langle \exp(i \sum_{k\neq 0} C_{s,k}\gamma_{s,k} + C_{s,k}^* \gamma_{s,k}^\dagger) \right\rangle$ (Here and in the following, we drop the time dependence of $\gamma_{s,k}(t)$ from the notation). Using the property
$e^{\gamma_{s,k}}|\psi(t)\rangle = (1 + \gamma_{s,k} + \cdots)|\psi(t)\rangle = |\psi(t)\rangle$ and the identity
$e^{A+B} = e^A e^B e^{-\frac{1}{2}[A,B]}$ where $[A, B]$ is a c-number, we can evaluate mth moments as
$\langle (S_l^\theta)^m \rangle \sim \left\langle e^{iC_{s,k}^* \gamma_{s,k}^\dagger} e^{-\frac{1}{2}\sum_{k\neq 0}|C_{s,k}|^2} e^{iC_{s,k}\gamma_{s,k}} \right\rangle = \exp(-\frac{1}{2}\sum_{k\neq 0}|C_{s,k}|^2)$.

It is straightforward to check that $\gamma_{s,k}$ operator is given by the linear combination of $b_{s,k}$ and $b_{s,-k}^\dagger$ as follows,

$$\begin{pmatrix} \gamma_{s,-k}^\dagger(t) \\ \gamma_{s,k}(t) \end{pmatrix} = \begin{pmatrix} \frac{e^{-ic_s|k|t}}{\sqrt{1-4|W_k|^2}} & \frac{-2W_k e^{ic_s|k|t}}{\sqrt{1-4|W_k|^2}} \\ \frac{-2W_k e^{-ic_s|k|t}}{\sqrt{1-4|W_k|^2}} & \frac{e^{ic_s|k|t}}{\sqrt{1-4|W_k|^2}} \end{pmatrix} \begin{pmatrix} b_{s,-k}^\dagger \\ b_{s,k} \end{pmatrix}. \tag{3.15}$$

$\gamma_{s,k}$ and $\gamma_{s,k}^\dagger$ obey a canonical commutation relation $[\gamma_{s,k}, \gamma_{s,k}^\dagger] = 1$. In terms of these $\gamma_{s,k}$, the expression of $\hat{\phi}_{s,k}(t)$ becomes

$$\begin{aligned} \frac{1}{\sqrt{L}}\hat{\phi}_{s,k} &= C_{s,k}\gamma_{s,k}^\dagger + C_{s,k}^*\gamma_{s,-k} \\ C_{s,k} &= -i\sqrt{\frac{\pi}{2|k|K_sL}}\frac{e^{ic_s|k|t} - 2W_ke^{-ic_s|k|t}}{\sqrt{1-4|W_k|^2}}. \end{aligned} \tag{3.16}$$

$C_{s,k}(t)$ measures the fluctuation, or variance, of phase in the kth mode at time t, given by $\left\langle |\hat{\phi}_{s,k}(t)|^2 \right\rangle = \left\langle \hat{\phi}_{s,k}(t)\hat{\phi}_{s,-k}(t) \right\rangle$. Indeed, since $\gamma_{s,k}$ is the annihilation operator of our state at time t, we immediately conclude that $\left\langle |\hat{\phi}_{s,k}(t)|^2 \right\rangle / L = |C_{s,k}(t)|^2$.

Using the technique described above, mth moment of $\hat{S}_l^\theta$ becomes (we include both $k = 0$ and $k \neq 0$ contributions in the expression below)

$$\begin{aligned} &\langle\psi(t)| \left(\int_{-l/2}^{l/2} S^\theta(r)dr \right)^m |\psi(t)\rangle \\ &= \left\langle \prod_i^m \left(\int_{-l/2}^{l/2} \frac{\rho}{2} dr_i \sum_{s_i=\pm 1} e^{is_i(\hat{\phi}_s(r_i)-\theta)} \right) \right\rangle \\ &= \sum_{\{s_i=\pm 1\}} \prod_{i=1}^m \int_{-l/2}^{l/2} \frac{\rho dr_i}{2} \left\langle e^{\left(i(s_1\hat{\phi}_s(r_1)+\ldots+s_m\hat{\phi}_s(r_m))\right)} \right\rangle \\ &\quad \times e^{-i\left(\sum_i s_i\right)\theta} \\ &= \sum_{\{s_i=\pm 1\}} \prod_{i=1}^m \int_{-l/2}^{l/2} \frac{\rho dr_i}{2} \exp\left(-\frac{1}{2} \sum_k \xi_{s,k}^{\{s_i,r_i\}} (\xi_{s,k}^{\{s_i,r_i\}})^* \right) \\ &\quad \times e^{-i\left(\sum_i s_i\right)\theta}, \end{aligned} \tag{3.17}$$

where $\xi_{s,k}^{\{s_i,r_i\}} = \sqrt{\frac{\left\langle |\hat{\phi}_{s,k}(t)|^2 \right\rangle}{L}}(s_1e^{ikr_1} + \ldots + s_me^{ikr_m})$. s_i takes either the value 1 or -1, and $\sum_{\{s_i\}}$ sums over all possible set of values. Note that L is the total system size and l is the integration range.

Full Distribution Function

Calculation of the full distribution functions from moments in Eq. (3.17) is studied by the techniques introduced in Ref. [69] through mapping to the statistics of random surfaces. In this subsection, we provide the details of the calculation.

Eq. (3.17) is simplified if the integrations for each r_i can be independently carried out. This is not possible in Eq. (3.17) because e^{ikr_i} and e^{ikr_j} for $i \neq j$ are coupled in $\left|\xi_{s,k}^{\{s_i,r_i\}}\right|^2 = \left(\mathrm{Re}\xi_{s,k}^{\{s_i,r_i\}}\right)^2 + \left(\mathrm{Im}\xi_{s,k}^{\{s_i,r_i\}}\right)^2$. To unentangle this, we introduce Hubbard-Stratonovich transformation, $e^{-\frac{x^2}{2}} = \frac{1}{\sqrt{2\pi}}\int_{-\infty}^{\infty} e^{-\frac{\lambda^2}{2}} e^{ix\lambda}$, for example,

$$e^{-\frac{1}{2}\left(\mathrm{Re}(\xi_{s,k}^{\{s_i,x_i\}})\right)^2} = \int_{-\infty}^{\infty} \frac{d\lambda_{1sk}}{\sqrt{2\pi}} e^{-\lambda_{1sk}^2/2} e^{i\lambda_{1sk}\mathrm{Re}\left(\xi_{s,k}^{\{s_i,x_i\}}\right)}.$$

We apply a similar transformation for $\mathrm{Im}\xi_{s,k}$. This removes the cross term between e^{ikr_i} and e^{ikr_j} for $i \neq j$ and allows us to independently integrate over r_i's. Associated with each transformation, we introduce auxiliary variables λ_{1sk} for $\mathrm{Re}(\xi_{s,k})$, λ_{2sk} for $\mathrm{Im}(\xi_{s,k})$. Then, mth moment becomes

$$\begin{aligned}
&\langle\psi(t)|\left(\int_{-l/2}^{l/2} S^{\theta}(r)dr\right)^m |\psi(t)\rangle = \\
&\sum_{\{s_i\}}\prod_k \int_{-\infty}^{\infty} e^{-(\lambda_{1sk}^2+\lambda_{2sk}^2)/2}\frac{d\lambda_{1sk}}{\sqrt{2\pi}}\frac{d\lambda_{2sk}}{\sqrt{2\pi}} \\
&\left[\prod_{i=1}^{m}\int_{-l/2}^{l/2}\frac{\rho dr_i}{2}\exp\left(is_i\sum_k\left\{\lambda_{1sk}\mathrm{Re}(\xi_{s,k}^{r_i}) + \lambda_{2sk}\mathrm{Im}(\xi_{s,k}^{r_i}) - \theta\right\}\right)\right],
\end{aligned}$$

where we introduced $\xi_{s,k}^{\{r_i\}} = \sqrt{\frac{\left\langle|\hat{\phi}_{s,k}(t)|^2\right\rangle}{L}}e^{ikr_i}$. Summation over $\{s_i = \pm 1\}$ can now be carried out. Furthermore, we introduce a new

variables λ_{rsk} and $\lambda_{\theta sk}$, and replace λ_{1sk} and λ_{2sk} through the relation $\lambda_{rsk} = \sqrt{\lambda_{1sk}^2 + \lambda_{2sk}^2}$ and $\cos(\lambda_{\theta sk}) = \lambda_{2sk}/\sqrt{\lambda_{1sk}^2 + \lambda_{2sk}^2}$. These operations result in the simplified expression,

$$\langle\psi(t)|\left(\int_{-l/2}^{l/2} S^{\theta}(r)dr\right)^m |\psi(t)\rangle = \prod_{k,a=r,\theta} \frac{1}{2\pi}\int d\lambda_{ask} \times \lambda_{rsk} e^{-\frac{\lambda_{rsk}^2}{2}} \left(\rho\int_{-l/2}^{l/2} dr\cos\left[\chi(r,\{\lambda_{jsk}\}) - \theta\right]\right)^m, \tag{3.18}$$

where

$$\chi(r,\{\lambda_{jsk}\}) = \sum_k \sqrt{\frac{\left\langle|\hat{\phi}_{s,k}|^2\right\rangle}{L}}\lambda_{rsk}\sin(kr + \lambda_{\theta sk}), \tag{3.19}$$

$$\begin{aligned}\left\langle|\hat{\phi}_{s,k}|^2\right\rangle =& \frac{\pi}{2|k|K_s}\frac{\sin^2(c_s|k|t) + a_k^2\cos^2(c_s|k|t)}{a_k}(k\neq 0),\\ \left\langle\phi_{s,0}^2\right\rangle_t =& \frac{1}{2\rho\eta} + \left(\frac{c_s\pi t}{K_s}\right)^2\frac{\eta\rho}{2} \quad (k=0),\end{aligned} \tag{3.20}$$

with $a_k = \frac{|k|K_s}{\pi\rho\eta}$. The integration over λ_{rsk} and $\lambda_{\theta sk}$ in Eq.(3.18) extends from 0 to ∞ and from $-\pi$ to π, respectively.

Comparing the expression in Eq.(3.18) and the implicit definition of a distribution function in Eq.(3.2), it is easy to identify the distribution function as

$$P_l^{\theta}(a) = \prod_k \int_{-\pi}^{\pi}\frac{d\lambda_{\theta sk}}{2\pi}\int_0^{\infty}\lambda_{rsk}e^{-\lambda_{rsk}^2/2}d\lambda_{rsk} \times\delta\left(a - \rho\int_{-l/2}^{l/2} dr\cos\left[\chi(r,\{\lambda_{jsk}\}) - \theta\right]\right). \tag{3.21}$$

This function can be numerically evaluated through Monte Carlo method with weight $\lambda_{rsk}e^{-\lambda_{rsk}^2/2}$ for λ_{rsk} and equal unity weight for $\lambda_{\theta sk}$.

While we have assumed that the chemical potentials of spin-up and spin-down atoms are the same in the absence of interactions by going to the rotating frame, it is easy to obtain the expression for distribution functions in the lab frame. The energy difference E between spin-up and spin-down atoms results in the rotation of the spin in the $x-y$ plane at a constant angular velocity E. Therefore, the distribution in the lab frame is obtained by replacing $\theta \to \theta + Et$ in Eq. (3.21).

In this section, we have focused on the distribution function of spins in $x-y$ plane, but it is also possible to obtain the distribution function of z component of the spin, and we present the result in the Appendix 3.54.

Joint Distribution Function

From the expression for the spin operators in Eq. (3.9), we observe that the spin operators for the x and y directions commute in the low energy description. This is because spin operators in Tomonaga-Luttinger theory are coarse-grained over $\sim \rho\xi_s$ particles, and since for weak interactions $\rho\xi_s \gg 1$, the uncertainty of measurements coming from non-commutativity of $\hat{S}_l^x$ and $\hat{S}_l^y$ becomes suppressed. The possibility of simultaneous measurements of spin x and y operators implies the existence of joint distribution functions $P_l^{x,y}(\alpha,\beta)$, where $P_l^{x,y}(\alpha,\beta)d\alpha d\beta$ is the probability that the simultaneous measurements of $\hat{S}_l^x$ and S_l^y give the values between α and $\alpha+d\alpha$, and β and $\beta+d\beta$, respectively. Here we provide the expression for $P_l^{x,y}(\alpha,\beta)$ and proves that this is indeed the unique solution.

The joint distribution function $P_l^{x,y}(\alpha,\beta)$ is given by the following

expression

$$P_l^{x,y}(\alpha,\beta) = \prod_k \int_{-\pi}^{\pi} \frac{d\lambda_{\theta sk}}{2\pi} \int_0^{\infty} \lambda_{rsk} e^{-\lambda_{rsk}^2/2} d\lambda_{rsk}$$
$$\times \delta\left(\alpha + i\beta - \rho \int_{-l/2}^{l/2} dr e^{i\chi(r,\{\lambda_{jsk}\})}\right) \tag{3.22}$$

where the expression for $\chi(r,\{\lambda_{jsk}\})$ is given in Eq.(3.19). To prove it, we first show that Eq.(3.22) reproduces the distribution function $P_l^{\theta}(\alpha)$ in Eq.(3.21) for all θ. Then, we show that a function with this property is unique, and therefore the expression in Eq.(3.21) is necessarily the joint distribution function.

Given a joint distribution function $P_l^{x,y}(\alpha,\beta)$, we can determine the distribution function $P_l^{\theta}(\gamma)$ of a spin pointing in the direction $(\cos\theta, \sin\theta, 0)$. Consider the spin $\mathbf{S}$ in the $x-y$ plane with $\mathbf{S} = (\alpha,\beta,0)$ whose probability distribution is given by $P_l^{x,y}(\alpha,\beta)$. The projection of the spin $\mathbf{S}$ onto the axis pointing in the direction $(\cos\theta,\sin\theta,0)$ is given by $|S|\cos(\phi-\theta)$ where $|S| = \sqrt{\alpha^2+\beta^2}$ is the magnitude of spin and ϕ is the angle $\mathrm{Arg}(\alpha+i\beta)$. After a simple algebra, we find $|S|\cos(\phi-\theta) = \alpha\cos\theta + \beta\sin\theta$. Then given a spin $\mathbf{S} = (\alpha,\beta,0)$, if one measures the spin along the direction $(\cos\theta,\sin\theta,0)$, the measurement result gives γ if and only if $\gamma = \alpha\cos\theta + \beta\sin\theta$. From this consideration, the probability distribution that the measurement along the direction $(\cos\theta,\sin\theta,0)$ gives the value γ is given by

$$P_l^{\theta}(\gamma) = \int d\alpha d\beta P_l^{x,y}(\alpha,\beta)\delta(\gamma - \alpha\cos\theta - \beta\sin\theta). \tag{3.23}$$

Now, if we plug in the expression of Eq.(3.22) in Eq. (3.23), we see that $P_l^{\theta}(\gamma)$ agrees with Eq. (3.21) for all θ.

Now we prove the uniqueness of a function with the above property, *i.e.* a function that reproduces Eq. (3.21) through the relation

Eq.(3.23). Suppose you have another distribution $\tilde{P}_l^{x,y}(a,\beta)$ that satisfies Eq.(3.23) for all θ. We define $Q(a,\beta) = P_l^{x,y}(a,\beta) - \tilde{P}_l^{x,y}(a,\beta)$. Our goal is to show that $Q(a,\beta)$ must be equal to zero. By definition, we have the equality

$$0 = \int da d\beta Q(a,\beta)\delta(\gamma - a\cos\theta - \beta\sin\theta), \tag{3.24}$$

for all θ and γ. If we take the Fourier transform of both sides of Eq. (3.24) in terms of γ, we obtain

$$\begin{aligned} 0 &= \int d\gamma \int da d\beta Q(a,\beta)\delta(\gamma - a\cos\theta - \beta\sin\theta)e^{iw\gamma} \\ &= \int d\boldsymbol{\alpha} Q(\boldsymbol{\alpha})e^{i\mathbf{w}\cdot\boldsymbol{\alpha}}. \end{aligned}$$

In the last line, we defined $\mathbf{w} = w(\cos\theta, \sin\theta)$ and $\boldsymbol{\alpha} = (a,\beta)$. Notice that this equation holds for any $\mathbf{w}$. Then this last expression is just like (two-dimensional) Fourier transform of Q. By taking the inverse fourier transform of the last expression in terms of $\mathbf{w}$, we find

$$0 = \int_{-\infty}^{\infty} d\mathbf{w} \int d\boldsymbol{\alpha} Q(\boldsymbol{\alpha})e^{i\mathbf{w}\cdot(\boldsymbol{\alpha}-\boldsymbol{\alpha}')}Q(\boldsymbol{\alpha}'),$$

thereby proving the uniqueness of the joint distribution $P_l^{x,y}(a,\beta)$.

From the joint distribution function in Eq.(3.22), one can also obtain other distributions, such as the distribution $P_l^{\perp}(\gamma)$ of the square of the transverse spin magnitude, $\left(S_l^{\perp}(t)\right)^2$, which is given by

$$\begin{aligned} P_l^{\perp}(\gamma) &= \int_{-\infty}^{\infty} da d\beta P_l^{x,y}(a,\beta)\delta\left(\gamma - a^2 - \beta^2\right) \\ &= \prod_k \int_{-\pi}^{\pi} \frac{d\lambda_{\theta sk}}{2\pi} \int_0^{\infty} \lambda_{rsk} e^{-\lambda_{rsk}^2/2} d\lambda_{rsk} \\ &\quad \times\delta\left(\gamma - \left|\rho \int_{-l/2}^{l/2} dr e^{i\chi(r,\{\lambda_{jsk}\})}\right|^2\right) \end{aligned} \tag{3.25}$$

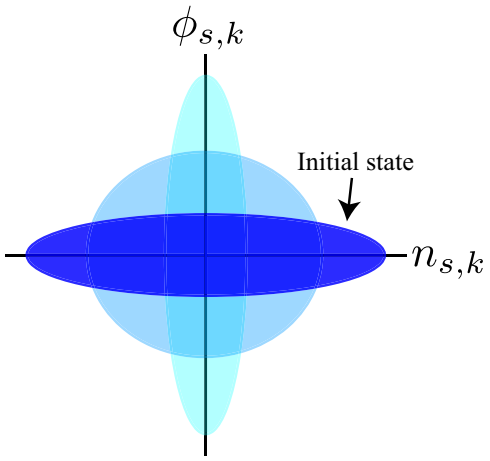

Figure 3.4.1: The illustration of the dynamics for each harmonic oscillator mode, described by the Hamiltonian Eq.(3.8). The initial state contains a large fluctuation of density difference $\hat{n}_{s,k}$ given by $\langle \hat{n}_{s,k}\hat{n}_{s,-k}\rangle = \eta\rho/2$(see Eq.(3.10)), and its conjugate variable, the phase difference $\hat{\phi}_{s,k}$, has a small fluctuations. In the subsequent dynamics, such squeezed state evolves and energy oscillates between the fluctuations of the density difference and phase difference.

Interpretation of the distribution dynamics

The form of the distribution function in Eq. (3.22) encapsulates the interpretation in terms of dynamics originating from spin waves explained in Sec 3.2. Here $e^{i\chi(r,\{t_{jsk}\})}$ represents the spin direction at coordinate r, where the $x-y$ plane of the spin component is taken to be a complex plane. Then Eq.(3.22) suggests that for a given instance of the set $\{\lambda_{jsk}\}$, $(S_l^x + iS_l^y)$ is simply the sum of the local spin directions $e^{i\chi(r,\{\lambda_{jsk}\})}$ over the integration length l. The local spin direction at position r are determined by the phase $\chi(r,\{t_{jsk}\})$, which receives contributions from each spin wave of momentum k with strength $A_k(t) = \lambda_{rsk}\sqrt{\left\langle |\hat{\phi}_{s,k}(t)|^2 \right\rangle}$. Spin waves with momenta k rotate the spins as $\sin(kr + \lambda_{\theta sk})$ (see the expression of $\chi(r,\{\lambda_{jsk}\})$ in Eq.(3.19)). The rotation strength $A_k(t) \propto \lambda_{rsk}$ has the distribution

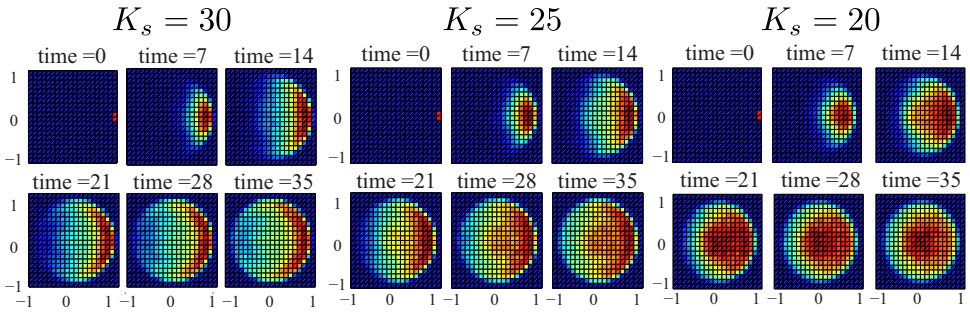

Figure 3.4.2: The dynamics of the joint distributions for $L/\xi_s = 200$, $\xi_s = 40$ and various spin Luttinger parameters $K_s = 30, 25$, and 20. Here axes are scaled such that the maximum value of a and β are 1. Smaller value of K_s enhances the spin fluctuations, leading to a stronger diffusion and decay. Time is measured in units of ξ_s/c_s.

$\lambda_{rsk} e^{-\lambda_{rsk}^2/2}$, which represents the quantum fluctuation of the spins. On the other hand, $\lambda_{\theta sk}$ is distributed uniformly between $-\pi$ and π.

The dynamics of phase fluctuations $\left\langle |\hat{\phi}_{s,k}(t)|^2 \right\rangle$ can in fact be easily understood by considering the Hamiltonian given by Eq.(3.8) as a harmonic oscillator for each k(Fig. 3.4.1). We first note that the initial state has a large fluctuation of density $\hat{n}_{s,k}$ because the initial $\pi/2$ pulse prepares the state in the (almost) eigenstate of $S^x = \rho \cos(\hat{\phi}_{s,k})$ with a small fluctuation of $\hat{\phi}_{s,k}$, the conjugate variable of $\hat{n}_{s,k}$. The fluctuation of $\hat{n}_{s,k}$ is given by $\langle \hat{n}_{s,k} \hat{n}_{s,-k} \rangle = \eta\rho/2$ (see Eq.(3.10)). Because of this large fluctuation in the density, almost all the energy of the initial state is stored in the interaction term $|n_{s,k}|^2$ in Eq. (3.8). Therefore, the total energy of each harmonic oscillator can be estimated as $\frac{\pi c_s \rho \eta}{4K_s}$. During the dynamics dictated by the harmonic oscillator Hamiltonian, this energy oscillates between the density fluctuations and phase fluctuations in a sinusoidal fashion, see Fig. 3.4.1. In the dephased limit of the dynamics, approximately equal energy of the system is distributed to the phase and density fluctuations, and from the conservation of energy, we conclude that the characteristic magnitude

of phase fluctuation is given by $\left\langle |\phi_{s,k}(t)|^2 \right\rangle \sim \frac{\pi^2 \rho \eta}{4K_s^2 k^2}$. Such $1/k^2$ dependence of $\left\langle |\hat{\phi}_{s,k}(t)|^2 \right\rangle$ agrees with the more rigorous result in Eq.(3.20). Therefore the spin fluctuations dominantly come from spin waves with long wavelengths, as we have stated in Section 3.2. Moreover, the weak dependence of spin dynamics on high momenta contributions justifies the use of Tomonaga-Luttinger theory for describing the dynamics. We will more carefully analyze the dependence of distributions on the high momentum cutoff in Sec 3.4.4.

From the simple argument above, it is also clear that the spin fluctuations coming from spin waves with momenta k have the time scales associated with the harmonic oscillators given by $\frac{1}{|k|c_s}$. Again, this rough argument agrees with the more rigorous result presented in Eq.(3.20). Therefore, the fast dynamics is dominated by spin waves with high momenta and slow dynamics is dominated by low momenta. These considerations lead to the illustrative picture of Fig.3.2.2. Furthermore, this implies that the dynamics of the magnitude of spin $\left(\hat{S}_l^{\perp}\right)^2$ reaches a steady state around the time $\frac{l}{4c_s}$ since spin waves with wavelength longer than l do not affect the magnitude. This should be contrasted with the evolution of the x component of spin which, in principle, keeps evolving until the time scale of $\sim \frac{L}{4c_s}$(see Fig.3.2.4).

The strength of interactions and correlations are associated with Luttinger parameter, K_s. K_s influences the spin fluctuations $\left\langle |\phi_{s,k}(t)|^2 \right\rangle$ at all wavelength, and $\left\langle |\phi_{s,k}(t)|^2 \right\rangle$ depends on K_s as $1/K_s^2$ for a fixed density. As is expected, in the limit of the weak interaction corresponding to large K_s, the amplitude of spin fluctuation decreases. In Fig. 3.4.2, we have plotted the time evolution of the joint distributions for $L/\xi_s = 200$, $l/\xi_s = 40$, and $K_s = 20, 25$ and 30. For larger K_s, we see that the spin fluctuations get quickly suppressed.

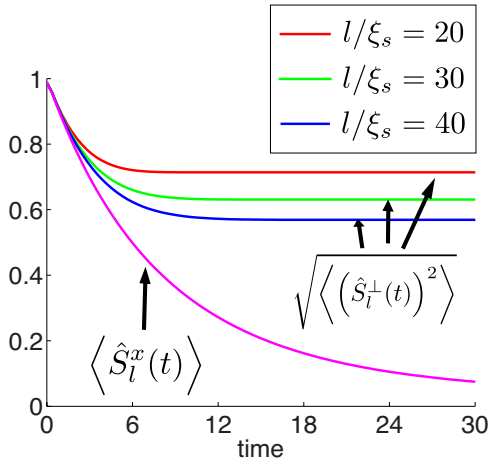

Figure 3.4.3: The dynamics of the average value of the magnitude of spins, $\sqrt{\left\langle \left(\hat{S}_l^{\perp}(t)\right)^2 \right\rangle}$, and the average of the x component of spins $\left\langle \hat{S}_l^x(t) \right\rangle$. Here y axis is scaled such that the initial values take the maximum value of 1. Here we took $L/\xi_s = 200$, $K_s = 20$ and the integration lengths $l/\xi_s = 20, 30, 40$. The magnitude of spins decays only due to the spin waves with wavelengths shorter than the integration length l, and the decay of the magnitude stops around the time scale of $\sim \frac{l}{4c_s}$. On the other hand, all spin waves contribute to the evolution of the of the x component of magnetization, which keeps decaying[20].

3.4.3 Dynamics of the expectation value of the magnitude of spin $\left\langle \left(\hat{S}_l^{\perp}(t)\right)^2 \right\rangle$

In order to illustrate the dynamics of the Ramsey sequence further, it is helpful to study the dynamics of the expectation value of the squared transverse magnitude, given by $\left\langle \left(\hat{S}_l^{\perp}(t)\right)^2 \right\rangle$.

In Fig.3.4.3, we plot the evolution of $\sqrt{\left\langle \left(\hat{S}_l^{\perp}(t)\right)^2 \right\rangle}$ with $K_s = 20$, $L/\xi_s = 200$ and $l/\xi_s = 20, 30, 40$. We also plotted $\left\langle \hat{S}_l^x(t) \right\rangle$ along with $\sqrt{\left\langle \left(\hat{S}_l^{\perp}(t)\right)^2 \right\rangle}$ with the same parameters. It is easy to verify that $\langle S_l^x(t) \rangle$ is independent of integration length l[20]. As we have discussed in the previous section, $\sqrt{\left\langle \left(\hat{S}_l^{\perp}(t)\right)^2 \right\rangle}$ reach the steady states at the

time scale of $\frac{l}{4c_s}$ with finite values, while $\left\langle \hat{S}_l^x(t) \right\rangle$ keeps decaying for much longer time.

It is interesting to ask if the long time limit of $\sqrt{\left\langle \left(\hat{S}_l^\perp(t)\right)^2 \right\rangle}$ for sufficiently large integration length l attains the value which corresponds to the one expected from the randomization of spin patches of size ξ_s. At low energies, spins within the length $\sim \xi_s$ are aligned in the same direction, but spin waves can randomize the direction of the spin for each of l/ξ_s patches. Since the magnitude of spin within ξ_s is $\xi_s\rho$, if the patches are completely randomized, the result of the random walk predicts that $\sqrt{\left\langle \left(\hat{S}_l^\perp\right)^2 \right\rangle} \sim (\xi_s\rho)^2(l/\xi_s)$. We will see below that, due to the properties of correlations in one dimension, the integrated magnitude of spin $\sqrt{\left\langle \left(\hat{S}_l^\perp\right)^2 \right\rangle}$ never attains this form, albeit a similar expression is obtained (see Eq.(3.26)). Moreover, we identify the integration length $\tilde{l}$ which separates the "spin diffusion regime" and the "spin decay regime" by finding the decaying length scale for $\sqrt{\left\langle \left(\hat{S}_l^\perp\right)^2 \right\rangle}$.

The results for the long time limit of $\left\langle \left(\hat{S}_l^\perp(t)\right)^2 \right\rangle$ can be analytically computed. Following similar steps leading to Eq.(3.17), we find

$$\begin{aligned} \left\langle \left(\hat{S}_l^\perp(t)\right)^2 \right\rangle &= \left\langle \left| \int dr \rho e^{i\phi(s,r)} \right|^2 \right\rangle \\ &= \prod_{i=1}^{2} \int_{-l/2}^{l/2} \rho dr_i \exp\left(-\frac{1}{2} \sum_{k\neq 0} \xi_{s,k}^{\{r_i\}} (\xi_{s,k}^{\{,r_i\}})^* \right). \end{aligned}$$

Here $\xi_{s,k}^{\{r_i\}} = |C_{s,k}|(e^{ikr_1} - e^{ikr_2})$. We introduce dimensionless variables $r_i' = r_i/l, k' = kl$ and the integration over k in the exponent can be

carried out as

$$\begin{aligned}
&\int dk' \frac{L}{2\pi l} \xi_{s,k'}^{\{r_i'\}} (\xi_{s,k'}^{\{,r_i'\}})^* = \\
&\frac{2}{\pi} \int_{k'_{min}}^{k'_c} dk' \left(\frac{1}{\rho\eta l} \cos^2(|k|c_s t) + \frac{\pi^2 \rho\eta l}{k'^2 K_s^2} \sin^2(|k|c_s t) \right) \\
&\times \sin^2 \left(\frac{r_1' - r_2'}{2} |k'| \right) \\
&\approx \frac{k'_c}{2\rho\pi l\eta} + \frac{\pi\eta\rho l}{2K_s} |r_1' - r_2'| \int_0^\infty dy \frac{\sin^2(y)}{y^2}.
\end{aligned}$$

In the second line, we approximated $\cos^2(|k|c_s t) \approx \sin^2(|k|c_s t) \approx 1/2$, which is appropriate for long time. In the last line, we extended the upper limit of the integration for the second term to ∞ and the lower limit to 0. The former is justified because we know that high momentum contribution is suppressed by $1/k^2$, and the latter is justfied because we also know low momenta excitations with wavelengths larger than l do not affect $\hat{S}_l^\perp$. Since $\int_0^\infty dy \frac{\sin^2(y)}{y^2} = \pi/2$, we find, in the long time limit,

$$\begin{aligned}
&\left\langle \left(\hat{S}_l^\perp (t = \infty) \right)^2 \right\rangle / \left\langle \left(\hat{S}_l^\perp (t \approx 0) \right)^2 \right\rangle \\
&= 2 \left\{ \frac{1}{l_0} - \left(\frac{1}{l_0} \right)^2 (1 - \exp(-l_0)) \right\},
\end{aligned} \tag{3.26}$$

where we expressed the result as a ratio of the asymptotic value and the value at shortest time scale of the theory given by $t \sim 1/\mu$. $l_0 = \frac{\pi^2 \eta\rho l}{8K_s^2}$ is the dimensionless integration length that controls the value of $\left\langle \left(\hat{S}_l^\perp \right)^2 \right\rangle$ in the long time limit. As soon as l_0 becomes larger than 1, the long time value of $\left\langle \left(\hat{S}_l^\perp \right)^2 \right\rangle$ quickly approach the long integration limit, $\propto 2 \left\{ \frac{1}{l_0} - \left(\frac{1}{l_0} \right)^2 \right\}$. Therefore, $l_0 \approx 1$ separates the "spin diffusion regime" and the "spin decay regime."

An intuition behind the expression for l_0 can be explained through the following heuristic argument. The system enters the spin decay

regime when the spins within the integration length l rotates by 2π across l. The angle difference between the spins at $r = 0$ and $r = l$ in the long time limit is roughly given by $\Delta\chi = \frac{1}{\sqrt{L}} \sum_k \lambda_{rsk} \sqrt{\left\langle |\hat{\phi}_{s,k}|^2 \right\rangle_{mean}} \sin(kl)$ where $\left\langle |\hat{\phi}_{s,k}|^2 \right\rangle_{mean}$ is the characteristic magnitude of $\left\langle |\hat{\phi}_{s,k}(t)|^2 \right\rangle$ in Eq.(3.20), which is given by the half of the maximum magnitude of $\left\langle |\hat{\phi}_{s,k}(t)|^2 \right\rangle$. Now the expectation of magnitude $\langle (\Delta\chi)^2 \rangle$ over the quantum fluctuations represented by λ_{rsk} can be computed, and it yields $\langle (\Delta\chi)^2 \rangle \approx \frac{\pi^2 \eta \rho l}{4K_s^2}$. When $\sqrt{\langle (\Delta\chi)^2 \rangle}$ becomes of the order of 1, the system enters the spin decay regime. This estimate gives the boundary between the two regimes $l_0 = \frac{\pi^2 \eta \rho l}{8K_s^2} \approx 1$ apart from an unimportant numerical factor.

It is notable that the Eq. (3.26) approaches the random walk behavior $\propto (\xi_s \rho)^2 (l/\xi_s)$ very slowly, *i.e.* in an algebraic fashion. Therefore, even in the steady state, the system retains a strong correlation among spins. Moreover, Eq. (3.26) in the limit of $l_0 \to \infty$ is not just the random walk value, but is proportional to K_s, which measures the strength of fluctuations.

The calculation above shows that the spin diffusion regime and the spin decay regime are separated at the integration length scale of $\tilde{l} \approx \frac{8K_s^2}{\pi^2 \eta \rho}$. This length scale is nothing but the correlation length of spins in the long time limit. The calculation of the spin correlation length, for example, between $S^x(r)$ and $\hat{S}^x(r')$ can be done similarly to the calculation of $\left\langle \left(\hat{S}_l^{\perp}\right)^2 \right\rangle$. The result in the long time limit is

$$\left\langle \hat{S}^x(r) \hat{S}^x(r') \right\rangle \approx C \frac{\rho^2}{2} e^{-|r-r'|/\tilde{l}}, \tag{3.27}$$

where $C = e^{-k_c/(4\pi\rho\eta)}$ is a small reduction of the spins due to the contributions from high energy sector. Thus, one expects qualitatively different behaviors of distribution functions for integration lengths $l < \tilde{l}$ and $l > \tilde{l}$.

3.4.4 Momentum cut-off dependence

The description of dynamics presented above uses the low energy effective theory. In order to confirm the self-consistency of our approach, we check that the distributions of spins are not strongly affected by high energy physics, *i.e.* they weakly depend on high momentum cut-off. We have seen an indication that this is indeed the case through the weak fluctuations of phases for large k, $\left\langle |\hat{\phi}_{s,k}| \right\rangle \propto 1/k^2$, in Sec 3.4.2.

First of all, we analyze the high momentum cut-off $k_c \sim 2\pi/\xi_s$ dependence of the average value of $\hat{S}_l^x$. From the discussion in Sec 3.4.2, it is straightforward to obtain that(here we ignore $k = 0$ contribution)

$$\begin{aligned}
\left\langle \hat{S}_l^x \right\rangle &= \int_{-l/2}^{l/2} \frac{\rho}{2} dx \left\langle e^{i\phi(x)} + e^{-i\phi(x)} \right\rangle \\
&= \rho l \exp\left(-\frac{1}{2} \sum_{k\neq 0} |C_{s,k}|^2 \right), \\
\sum_{k\neq 0} |C_{s,k}|^2 &= \int_{-k_c}^{k_c} dk \left(\frac{\cos^2(|k|c_s t)}{4\pi\rho\eta} + \frac{\pi\rho\eta}{4k^2 K_s^2} \sin^2(|k|c_s t) \right) \\
&\approx \frac{k_c}{2\pi\rho\eta} + \frac{\rho c_s t \eta}{(2K_s/\pi)^2},
\end{aligned} \tag{3.28}$$

where in the last line, we took the long time limit $t \gg \xi_s/c_s$ [20]. In this limit, only the first term in Eq.(3.28) depends on the cutoff k_c, and moreover, the cutoff dependence is independent of time. The effect is to reduce the value of $\left\langle \hat{S}_l^x \right\rangle$ through the multiplication of a number close to one in the weakly interacting limit. For example, if we take $k_c = 2\pi/\xi_c$, then the cut-off dependent term reduces the value by multiplying $\exp\left(-\frac{k_c}{4\pi\rho\eta}\right) \approx e^{-1/(4K_s)} \approx 1$.

In a similar fashion, higher moments of spin operators can be shown to have a weak dependence on the cutoff momentum k_c, as long

as the integration length is much larger than the healing length, $l/\xi_s \gg 1$. In this limit, m moments of, for example, $\hat{S}_l^x$ is reduced by $\exp\left(-m\frac{k_c}{4\pi\rho\eta}\right)$. Therefore, the full distribution function is simply reduced by the multiplication of a number close to one $\exp\left(-\frac{k_c}{4\pi\rho\eta}\right) \approx e^{-1/(4K_s)} \approx 1$ in the weakly interacting regime. This gives the self-consistency check of our results in Sec 3.4.2

3.5 Dynamics of Full Distribution Function in the presence of mixing between spin and charge degrees of freedom

In this section, we extend the analysis in Sec 3.4 to a more general case, in which spin and charge degrees of freedom mix. We will see that the distribution functions even for this more general case have essentially the same structure as in Eq. (3.21), and are described by spin waves with fluctuations whose amplitude is determined by the fluctuations of phase $\left\langle |\hat{\phi}_{s,k}|^2 \right\rangle$. One important difference from the decoupling case is the dependence of spin distributions on the initial temperature of the system. The thermal excitations are present in the charge degrees of freedom in the initial state, and such thermal fluctuations increase the value of $\left\langle |\hat{\phi}_{s,k}|^2 \right\rangle$ through the coupling between spin and charge during the evolution.

3.5.1 Hamiltonian and initial state

In a generic system of two component bosons in one dimension, spin and charge degrees of freedom couple through the mixing Hamiltonian in Eq.(3.7). Yet, Hamiltonian in Eq.(3.4) is still quadratic and it can

be diagonalized. We define new operators $\hat{\phi}_1, \hat{\phi}_2, \hat{n}_1, \hat{n}_2$ by

$$\begin{pmatrix} \hat{\phi}_1 \\ \hat{\phi}_2 \end{pmatrix} = \begin{pmatrix} \cos\kappa & \sin\kappa \\ -\sin\kappa & \cos\kappa \end{pmatrix} \begin{pmatrix} \sqrt{s_c}\hat{\phi}_c \\ \hat{\phi}_s \end{pmatrix}, \tag{3.29}$$

$$\begin{pmatrix} \hat{n}_1 \\ \hat{n}_2 \end{pmatrix} = \begin{pmatrix} \cos\kappa & \sin\kappa \\ -\sin\kappa & \cos\kappa \end{pmatrix} \begin{pmatrix} \frac{1}{\sqrt{s_c}}\hat{n}_c \\ \hat{n}_s \end{pmatrix}. \tag{3.30}$$

Mixing angle κ and scaling parameter s_c are chosen so that the Hamiltonian is written in the following diagonal form

$$\begin{aligned} H &= H_1 + H_2, \\ H_1 &= \int_{-L/2}^{L/2} dr \frac{\rho}{2m_1} (\nabla\hat{\phi}_1(r))^2 + g_1(\hat{n}_1)^2, \\ H_2 &= \int_{-L/2}^{L/2} dr \frac{\rho}{2m_2} (\nabla\hat{\phi}_2)^2 + g_2(\hat{n}_2)^2. \end{aligned} \tag{3.31}$$

Explicitly, κ and s_c are given by

$$\begin{aligned} s_c &= \frac{\frac{g_{mix}\rho}{2m_c} + g_s g^{\phi}_{mix}}{g_c g^{\phi}_{mix} + \frac{g_{mix}\rho}{2m_s}}, \quad \tan\kappa = \frac{-\kappa_0 \pm \sqrt{\kappa_0^2 + 4}}{2}, \\ \kappa_0 &= \frac{s_c g_c - g_s}{\sqrt{s_c} g_{mix}} = \frac{\frac{\rho}{2m_c} - s_c \frac{\rho}{2m_s}}{g^{\phi}_{mix}\sqrt{s_c}}, \end{aligned}$$

where $\pm$ in the expression of $\tan\kappa$ is $+$ when $\kappa_0 > 0$ and $-$ when $\kappa_0 < 0$. We defined κ such that $\kappa = 0$ corresponds to decoupling of charge and spin, i.e. to $g_{mix} = 0$ and $g^{\phi}_{mix} = 0$ in Eq.(3.7). Parameters

g_1, g_2, $\frac{\rho}{2m_1}$ and $\frac{\rho}{2m_2}$ are given by

$$\begin{aligned} g_1 &= s_c g_c + \sqrt{s_c}\tan\kappa g_{mix}, \\ g_2 &= g_s - \sqrt{s_c}\tan\kappa g_{mix}, \\ \frac{\rho}{2m_1} &= \frac{\rho}{2m_c s_c} + \tan\kappa \frac{g^{\phi}_{mix}}{\sqrt{s_c}}, \\ \frac{\rho}{2m_2} &= \frac{\rho}{2m_s} - \tan\kappa \frac{g^{\phi}_{mix}}{\sqrt{s_c}}. \end{aligned}$$

In the weakly interacting systems which we study in this chapter, Luttinger parameters K_i and sound velocities c_i are determined for each Hamiltonian H_i, $i = \uparrow, \downarrow, c, s, 1, 2$ through

$$K_i = \pi\sqrt{\frac{\rho}{2m_i g_i}}, \quad c_i = \sqrt{\frac{\rho g_i}{m_i}}. \tag{3.32}$$

At finite temperature, the state before the first $\pi/2$ pulse contains excitations, and these excitations are carried over to the charge degrees of freedom after the pulse. Pulse only acts on the spin degrees of freedom, and the local sum density of spin-up and down is left untouched as long as the pulse is applied in a short time compared to the inverse of typical excitation energies, $\beta = 1/(k_B T)$. In other words, the local density fluctuation of spin-up, $\hat{n}_\uparrow(r)$, before $\pi/2$ pulse is converted to the sum of the local density fluctuation of spin-up and spin-down, $\hat{n}_\uparrow(r) + \hat{n}_\downarrow(r)$ after $\pi/2$ pulse. In this strong pulse limit, then, the distribution of $\hat{n}_\uparrow(r)$ before $\pi/2$ pulse is the same as the distribution of $\hat{n}_\uparrow(r) + \hat{n}_\downarrow(r)$ after $\pi/2$ pulse.

The distribution of the local density for spin-up atoms before $\pi/2$ pulse is determined by the density matrix for spin-up given by $e^{-\beta H'_\uparrow}$, where in the weak interaction regime we have (see Eq.(3.4))

$$H'_\uparrow = \int_{-L/2}^{L/2} dr \left[\frac{2\rho}{2m_\uparrow}(\nabla\hat{\phi}_\uparrow(r))^2 + g_{\uparrow\uparrow}(\hat{n}_\uparrow(r))^2\right].$$

Then, the density matrix which produces the distribution of $\hat{n}_\uparrow(r) + \hat{n}_\downarrow(r)$ required above is given by $e^{-\beta H_{c\uparrow}}$ where

$$\begin{aligned} H_{\uparrow c} = & \int_{-L/2}^{L/2} dr \left[\frac{2\rho}{2m_\uparrow} \left\{ (\nabla\hat{\phi}_\uparrow(r) + \nabla\hat{\phi}_\downarrow(r))/2 \right\}^2 , \right. \\ & \left. + g_{\uparrow\uparrow}(\hat{n}_\uparrow(r) + \hat{n}_\downarrow(r))^2 \right] \\ = & \frac{c_{c\uparrow}}{2} \int_{-L/2}^{L/2} dr \left[\frac{K_{c\uparrow}}{\pi} (\nabla\hat{\phi}_c)^2 + \frac{\pi}{K_{c\uparrow}} \hat{n}_c^2 \right] . \end{aligned} \tag{3.33}$$

where $K_{c\uparrow} = \frac{\pi}{4}\sqrt{\frac{\rho}{m_\uparrow g_{\uparrow\uparrow}}}$ and $c_{c\uparrow} = \sqrt{\frac{2\rho g_{\uparrow\uparrow}}{m_\uparrow}}$.

The initial state for spins is determined by the $\pi/2$ pulse, and we obtained the state in Eq.(3.12). Then, the complete initial density matrix after the first $\pi/2$ pulse is given by

$$\hat{\rho}_0 = |\psi_0\rangle\langle\psi_0| \otimes e^{-\beta H_{c\uparrow}} / \mathrm{Tr}\left(e^{-\beta H_{c\uparrow}}\right) . \tag{3.34}$$

This density matrix evolves in time as $\hat{\rho}(t) = e^{-itH}\hat{\rho}_0 e^{itH}$. Since we assume that the preparation of the initial state is done through a strong, short pulse, the spin and charge degrees of freedom are unentangled in the initial state.

3.5.2 Time evolutions of operators

In order to calculate the distribution function of $\hat{S}_l^\theta$, we again start from the calculation of mth moments, $\mathrm{Tr}\left(\hat{\rho}(t)\left(\hat{S}_l^\theta\right)^m\right)$. Evaluation of moments can be done through a similar technique used in Sec 3.4.2.

In the following, we describe convenient, time-dependent operators $\gamma_{s,k}(t)$ and $\gamma_{c,k}(t)$ used to evaluate spin operators such as $e^{i\hat{\phi}_{s,k}}$. The first operator resides in the spin sector and it is again the annihilation operator of the initial spin state such that $\mathrm{Tr}\gamma_{s,k}(0)\hat{\rho}_0 = 0$. This

operator is given in Eq. (3.15), which is

$$\begin{aligned} \gamma_{s,k}(t) &= e^{-itH}\gamma_{s,k}(0)e^{itH}, \\ \begin{pmatrix} \gamma^{\dagger}_{s,-k}(0) \\ \gamma_{s,k}(0) \end{pmatrix} &= \begin{pmatrix} \frac{1}{\sqrt{1-4|W_k|^2}} & \frac{-2W_k}{\sqrt{1-4|W_k|^2}} \\ \frac{-2W_k}{\sqrt{1-4|W_k|^2}} & \frac{1}{\sqrt{1-4|W_k|^2}} \end{pmatrix} \begin{pmatrix} b^{\dagger}_{s,-k} \\ b_{s,k} \end{pmatrix}, \end{aligned}$$

with $2W_k = \frac{1-a_k}{1+a_k}$ and $a_k = \frac{|k|K_s}{\pi\rho\eta}$ as before. The second operator is the operator of charge degrees of freedom, and it is given by

$$\begin{aligned} \gamma_{c,k}(t) &= e^{-itH}\gamma_{c,k}(0)e^{itH}, \\ \gamma_{c,k}(0) &= b_{c\uparrow,k}. \end{aligned}$$

where $b_{c\uparrow,k}$ is an annihilation operator for the elementary excitations in $H_{c\uparrow}$. Since $\gamma_{s,k}(t)$ and $\gamma_{c,k}(t)$ commute at $t = 0$, they commute at any time t. We will drop the time dependence of $\gamma_{a,k}(t)$ in the notation from now on.

From the expression of initial density matrix $\hat{\rho}_0$ in Eq. (3.34), it is easy to check that the density matrix at time t given by $\hat{\rho}(t) = e^{-itH}\hat{\rho}_0 e^{itH}$ can be written as the tensor product of the density matrix of operators $\gamma_{s,k}(t)$ and that of $\gamma_{c,k}(t)$. This is because $\hat{\rho}_0$ is a tensor product of the density matrices of $\gamma_{s,k}(t = 0)$ and that of $\gamma_{c,k}(t = 0)$. This structure of the density matrices at time t allows the independent evaluation of $\gamma_{s,k}(t)$ and $\gamma_{c,k}(t)$ operators, and it is advantageous to express spin operators in terms of these operators.

As we show in the Appendix 3.9.2, we can write $\hat{\phi}_{s,k}$ in terms of $\gamma_{c,k}(t)$ and $\gamma_{s,k}(t)$ as follows.

$$\frac{1}{\sqrt{L}}\hat{\phi}_{s,k} = C^*_{s,k}\gamma^{\dagger}_{s,-k} + C_{s,k}\gamma_{s,k} + C^*_{c,k}\gamma^{\dagger}_{c,-k} + C_{c,k}\gamma_{c,k}, \tag{3.35}$$

where explicit expression of $C_{s,k}$ and $C_{c,k}$ are given by

$$
\begin{aligned}
C_{s,k} &= i\sqrt{\frac{1}{2L\rho\eta}} \\
&\times (\cos^2\theta\cos(c_2|k|t) + \sin^2\theta\cos(c_1|k|t) \\
&-i\frac{K_s}{a_k}\left\{\frac{\cos^2\theta\sin(c_2|k|t)}{K_2} + \frac{\sin^2\theta\sin(c_1|k|t)}{K_1}\right\}\Bigg), \\
C_{c,k} &= \cos\theta\sin\theta\sqrt{\frac{\pi}{2L|k|s_c\tilde{K}_{c\uparrow}}} \\
&\times \left(i\left\{\cos(c_1|k|t) - \cos(c_2|k|t)\right\} - \tilde{K}_{c\uparrow}\left\{\frac{\sin(c_2|k|t)}{K_2} - \frac{\sin(c_1|k|t)}{K_1}\right\}\right),
\end{aligned}
\tag{3.36}
$$

where $\tilde{K}_{c\uparrow} = K_{c\uparrow}/\sqrt{s_c}$.

Using Eq.(3.35), we find an expression for $(\hat{S}_l^\theta)^m$ in terms of $\gamma_{a,k}$ with $a = s, c$ as follows

$$
\begin{aligned}
(\hat{S}_l^\theta)^m &= \prod_{i=1}^{m}\int_{-l/2}^{l/2} dr_i \frac{\rho}{2}\sum_{\{s_i\}} e^{i\sum_{k\neq 0}(\xi^*_{s,k}\gamma^\dagger_{s,k} + \xi_{s,k}\gamma_{s,k})} \\
&\times e^{i\sum_{k\neq 0}(\xi^*_{c,k}\gamma^\dagger_{c,k} + \xi_{c,k}\gamma_{c,k})} e^{i(\sum_i s_i)\phi_{s,0}/\sqrt{L}} e^{-i(\sum_i s_i)\theta},
\end{aligned}
$$

where $\xi_{a,k} = (\sum_i^m s_i e^{ir_i k})C_{a,k}$. In the following, we separately evaluate three contributions; $k = 0$ component given by $e^{i(\sum_i s_i)\phi_{s,0}/\sqrt{L}}$; the charge component of $k \neq 0$ given by $e^{i\sum_{k\neq 0}(\xi^*_{c,k}\gamma^\dagger_{c,k} + \xi_{c,k}\gamma_{c,k})}$; the spin component of $k \neq 0$ given by $e^{i\sum_{k\neq 0}(\xi^*_{s,k}\gamma^\dagger_{s,k} + \xi_{s,k}\gamma_{s,k})}$.

$k = 0$ CONTRIBUTION

The initial state of $k = 0$ spin sector in Eq.(3.12) as well as that of the charge sector in Eq. (3.33) both have a Gaussian form so that calculation of the trace Tr $\left\{e^{i(\sum_i s_i)\phi_{s,0}/\sqrt{L}}\hat{\rho}(t)\right\}$ is straightforward. We

leave the details to the Appendix 3.9.3, and the result is

$$\left\langle e^{i(\sum_i s_i)\phi_{s,0}/\sqrt{L}} \right\rangle = \exp\left(-\left(\sum_i s_i\right)^2 \frac{\left\langle \phi_{s,0}^2 \right\rangle_t}{2L} \right)$$
$$\left\langle \phi_{s,0}^2 \right\rangle_t = \frac{1}{2\rho\eta} + \left(\sin^2\theta \frac{\pi c_1}{K_1} + \cos^2\theta \frac{\pi c_2}{K_2} \right)^2 \frac{\rho\eta}{2} t^2$$
$$+ \sin^2\theta \cos^2\theta \left(\frac{\pi c_1}{K_1} - \frac{\pi c_2}{K_2} \right)^2 \frac{\tilde{K}_{c\uparrow}}{\pi c_{c\uparrow}\beta} t^2. \tag{3.37}$$

$k \neq 0$, SPIN SECTOR

This calculation is analogous to Eq.(3.17) and the result can be directly read off from Eq.(3.17), and it is

$$\left\langle e^{i\sum_{k\neq 0}(\xi_{s,k}^* \gamma_{s,k}^\dagger + \xi_{s,k}\gamma_{s,k})} \right\rangle = \exp\left(-\frac{1}{2} \sum_{k\neq 0} \xi_{s,k}^* \xi_{s,k} \right). \tag{3.38}$$

$k \neq 0$, CHARGE SECTOR

We first rewrite the density matrix at time t as

$$\begin{aligned} \hat{\rho}_{c,k\neq 0}(t) &= e^{-itH} e^{-\beta c_{c\uparrow} \sum_{k\neq 0} |k| b_{c\uparrow,k}^\dagger b_{c\uparrow,k}} e^{itH} / \mathcal{N} \\ &= e^{-\beta c_{c\uparrow} \sum_{k\neq 0} |k| \gamma_{c,k}^\dagger(t)\gamma_{c,k}(t)} / \mathcal{N}, \end{aligned}$$

where $\mathcal{N}_c$ is normalization given by $\mathcal{N}_c = \mathrm{Tr} e^{-\beta c_{c\uparrow} \sum_{k\neq 0} |k| \gamma_{c,k}^\dagger(t)\gamma_{c,k}(t)} = \prod_{k\neq 0} -1/\lambda_k$ with $\lambda_k = e^{-\beta c_{c\uparrow}|k|} - 1$.

Then the trace of $\left(\hat{S}_l^\theta\right)^m$ for $k \neq 0$ spin sector is

$$\left\langle e^{i\sum_{k\neq 0}(\xi_{c,k}^* \gamma_{c,k}^\dagger + \xi_{c,k}\gamma_{c,k})} \right\rangle = \tag{3.39}$$
$$\prod_{k\neq 0} \mathrm{Tr}\left(e^{i(\xi_{c,k}^* \gamma_{c,k}^\dagger + \xi_{c,k}\gamma_{c,k})} e^{-\beta|k|c_{c\uparrow}\gamma_{c,k}^\dagger \gamma_{c,k}} \right) / \mathcal{N}$$

We can evaluate this by taking the trace in the basis of normalized

coherent states $|a_k\rangle$ such that $\gamma_{c,k}|a_k\rangle = a_k|a_k\rangle$. The use of the identity $1 = \frac{1}{\pi}\int d^2a_k|a_k\rangle\langle a_k|$ as well as of an important equality $e^{va^\dagger a} =: e^{(e^v-1)a^\dagger a}$:[69], where $:\mathcal{O}:$ is a normal ordering of $\mathcal{O}$, leads to

$$\begin{aligned}\left\langle e^{i\sum_{k\neq 0}(\xi^*_{c,k}\gamma^\dagger_{c,k}+\xi_{c,k}\gamma_{c,k})}\right\rangle =& \frac{1}{\mathcal{N}}\prod_{k\neq 0}\frac{1}{\pi}\int d^2a_k\langle a_k|e^{i(\xi^*_{c,k}\gamma^\dagger_{c,k}+\xi_{c,k}\gamma_{c,k})}e^{-\beta|k|c_{c\uparrow}\gamma^\dagger_{c,k}\gamma_{c,k}}|a_k\rangle \\ =& \frac{1}{\mathcal{N}}\prod_{k\neq 0}\frac{1}{\pi}\int d^2a_k e^{-1/2\xi^*_{c,k}\xi_{c,k}}\langle a_k|e^{i\xi^*_{c,k}a^*_k}e^{i\xi_{c,k}\gamma_{c,k}}:e^{\lambda_k\gamma^\dagger_{c,k}\gamma_{c,k}}:|a_k\rangle \\ =& \prod_{k\neq 0}e^{-\frac{1}{2}\frac{1+e^{-\beta|k|c_{c\uparrow}}}{1-e^{-\beta|k|c_{c\uparrow}}}\xi^*_{c,k}\xi_{c,k}}.\end{aligned}$$

Full distribution function

We can summarize the results above as

$$\begin{aligned}\left\langle(\hat{S}^\theta_l)^n\right\rangle &= \sum_{\{s_i\}}\prod_{i=1}^{m}\int dr_i\frac{\rho}{2}\exp\left(-\frac{1}{2}\sum_{k\neq 0}\xi^*_{s,k}\xi_{s,k}\right) \\ &\quad\times\exp\left(-\frac{1}{2}\sum_{k\neq 0}M_{c,k}\xi^*_{c,k}\xi_{c,k}\right)\exp\left(-\frac{1}{2}\left(\sum_i s_i\right)^2\frac{\left\langle\phi^2_{s,0}\right\rangle_t}{L}\right)e^{-i(\sum_i s_i)\theta}\end{aligned} \tag{3.40}$$

Here, $M_{c,k} = \frac{1+e^{-\beta|k|c_{c\uparrow}}}{1-e^{-\beta|k|c_{c\uparrow}}}$. As before, we introduce the auxiliary variables to separate spatial integrations over r_i. We can combine $\xi^*_{s,k}\xi_{s,k}$ and $M_{c,k}\xi^*_{c,k}\xi_{c,k}$ so that we only need to introduce three sets of variables, $\lambda_{1,s,k}, \lambda_{2,s,k}, \lambda_0$ for Hubbard-Stratonovich transformation. Summing over $\{s_i\}$ simplifies the result, leading to the following

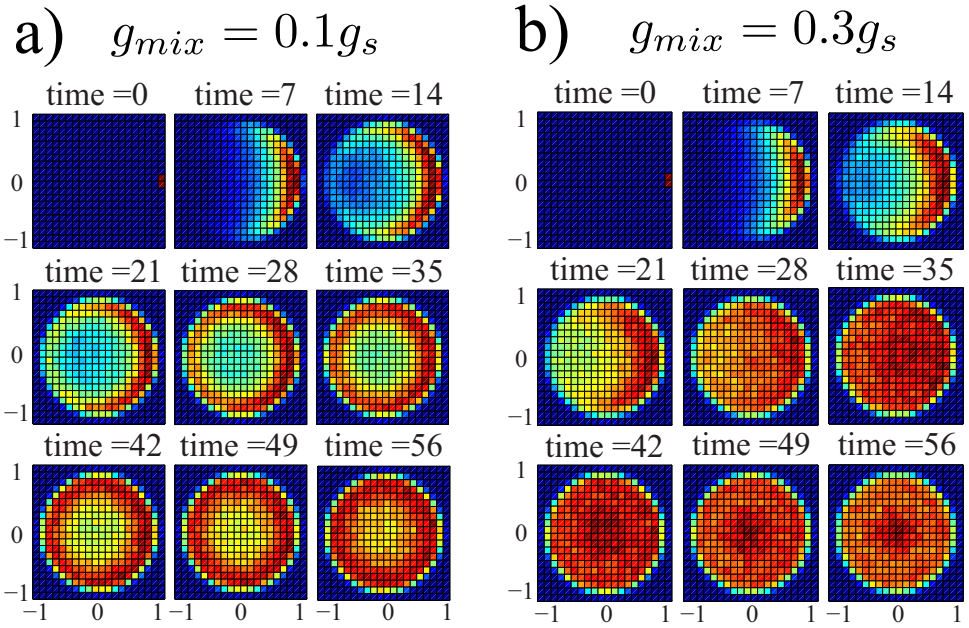

Figure 3.5.1: Time evolution of the joint distribution function $P^{x,y}(\alpha, \beta)$ for the system size $L/\xi_s = 400$, the spin Luttinger parameter $K_s = 20$ and integration length $l//\xi_s = 20$ in the presence of mixing between the spin and charge modes. For a), the interaction strength ratio is taken to be $g_c : g_s : g_{mix} = 1 : 1 : 0.1$, and for b), $g_c : g_s : g_{mix} = 1 : 1 : 0.3$. Time is measured in units of ξ_s/c_s where c_s is the spin sound wave velocity. Here axes are scaled such that the maximum value of α and β are 1. With increasing strength of mixing, the large initial temperature affects the spin dynamics at earlier time more strongly.

expression for the full distribution function

$$\begin{aligned} P_l^{\theta}(a) = & \quad \prod_k \int_{-\pi}^{\pi} \frac{d\lambda_{\theta sk}}{2\pi} \int_0^{\infty} \lambda_{rsk} e^{-\lambda_{rsk}^2/2} d\lambda_{rsk}, \\ & \times \quad \delta\left(a - \rho \int_{-l/2}^{l/2} dr \cos\left[\chi(r, \{\lambda_{jsk}\}) - \theta\right]\right) \\ \chi(r, \{\lambda_{jsk}\}) = & \quad \sum_k \sqrt{\frac{\left\langle |\hat{\phi}_{s,k}|^2 \right\rangle}{L}} \lambda_{rsk} \sin(kr + \lambda_{\theta sk}), \\ \left\langle |\hat{\phi}_{s,k}|^2 \right\rangle / L = & \quad |C_{s,k}|^2 + \frac{1+e^{-\beta|k|c_{c\uparrow}}}{1-e^{-\beta|k|c_{c\uparrow}}} |C_{c,k}|^2, \quad k \neq 0. \end{aligned} \tag{3.41}$$

The last line can be confirmed by directly computing $\left\langle |\hat{\phi}_{s,k}|^2 \right\rangle$, using the expression in Eq. (3.35). The expression for $\left\langle |\phi_{s,0}|^2 \right\rangle$ is given by Eq. (3.37). As before, the joint distributions as well as the distributions of squared transverse magnitude can be obtained through the same procedure as in Sec 3.4.2.

The spin distribution in the presence of mixing between spin and charge degrees of freedom resembles the one in the absence of such mixing, and the only change is the additional contributions to phase fluctuations coming from the thermal excitations, represented by $\frac{1+e^{-\beta|k|c_{c\uparrow}}}{1-e^{-\beta|k|c_{c\uparrow}}} |C_{c,k}|^2$ in Eq. (3.41). $|C_{c,k}|$ is proportional to $\sin^2 \kappa$ as one can see from Eq. (3.36). Thus, for weak coupling of $\kappa \sim 0$, the contribution is diminished by a factor of κ^2.

In the experiment by Widera *et al.*, they used Rb^{87} in the presence of Feshbach resonance. They employed the theory which assumes the absence of mixing between spin and charge degrees of freedom to analyze the decay of the Ramsey fringes. The ratio of interaction strengths in their experiment can be roughly estimated as $g_c : g_s : g_{mix} \approx 3.66 : 0.34 : 0.06$ which leads to the value of $\kappa \approx 2 \times 10^{-2}$. Therefore, the thermal contributions are diminished by about four order of magnitude and thus, their assumption of decoupling between spin and charge is justified.

In Fig.3.5.1, we have plotted the evolution of the joint distribution

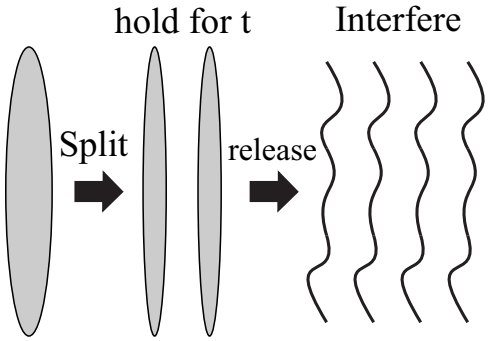

Figure 3.6.1: The interference of two quasi-condensates that are created by splitting one single quasi-condensate. After the splitting, the quasi-condensates are held for time t and then the transverse confinement is released. The two condensates interfere with each other after the release and the position of constructive interference is denoted by solid line in the figure. This interference pattern contains the information about the local phase difference between the two quasi-condensate at the time of release.

functions for different strength of the coupling g_{mix} at a relatively large initial temperature $k_B T = 0.4 \times 2\pi c_{c\uparrow}/\xi_s$ where $2\pi c_{c\uparrow}/\xi_s$ is approximately the high energy cut-off of Tomonaga-Luttinger theory. Here we took the system size $L/\xi_s = 400$, the Luttinger parameter $K_s = 20$, integration length $l = 20\xi_s$. For Fig.3.5.1 a), the ratio of interaction is taken to be $g_c : g_s : g_{mix} = 1 : 1 : 0.1$, and for For Fig.3.5.1 b), $g_c : g_s : g_{mix} = 1 : 1 : 0.3$. One can see that with increasing strength of mixing, the large initial temperature affects the spin dynamics at earlier time more strongly. For comparison, also see Fig. 3.2.4.

3.6 Interference of two one-dimensional condensates

3.6.1 Dynamics of interference pattern

The dynamics of Ramsey sequence considered in this chapter can be directly mapped to the dynamics of interference pattern of split one dimensional quasi-condensate[146]. More specifically we consider the following sequence of operations(see Fig.3.6.1). First, we prepare one-component 1D quasi-condensate in equilibrium. At time $t = 0$, the quasi-condensate is quickly split along the axial direction, and the resulting two quasi-condensates are completely separated. The two quasi-condensates freely evolve for a hold time of t, and they are released from transverse traps to observe the interference pattern between these two quasi-condensates[60].

Such dynamics can be mapped to the dynamics of the Ramsey interferometer studied in this chapter. The splitting of a quasi-condensate corresponds to the initial $\pi/2$ pulse in the Ramsey sequence. If we call one of the quasi-condensates to be L for left and another to be R for right, $L(R)$-condensate corresponds to spin-up (spin-down) component. Therefore, the "spin" variable corresponds to the difference of variables such as phases and densities for the two quasi-condensates, and "charge" variable corresponds to the sum of variables. For example, the local phase difference $\hat{\phi}_L(r) - \hat{\phi}_R(r)$ between L-condensate and R-condensate plays the role of the "spin phase," denoted by $\hat{\phi}_s(r)$ in the main text.

Immediately after the splitting, the phases of the two quasi-condensates at the same coordinate along the axial direction are the same. We see that the splitting effectively amounts to the $\pi/2$ pulse in the Ramsey sequence. The interference of two quasi-condensates measures the local phase difference at time t. If the

phases of L and R condensates are the same, the interference pattern has a peak in the middle of the two condensates, which we call $x = 0$. Therefore, the deviation of the peak from $x = 0$ measures the local phase difference $\hat{\phi}_s(r)$[124], which yields the information about $\hat{S}^x(r) = \rho \cos(\hat{\phi}_s(r))$ as well as $\hat{S}^y(r) = \rho \sin(\hat{\phi}_s(r))$ studied in previous sections.

The low energy effective Hamiltonian of two quasi-condensates after splitting is given by

$$\begin{aligned} H &= H_L + H_R, \\ H_L &= \int_{-L/2}^{L/2} dr \left[\frac{\rho_L}{2m} (\nabla \hat{\phi}_L(r))^2 + \frac{g}{2} (\hat{n}_L(r))^2 \right], \\ H_R &= \int_{-L/2}^{L/2} dr \left[\frac{\rho_R}{2m} (\nabla \hat{\phi}_R(r))^2 + \frac{g}{2} (\hat{n}_R(r))^2 \right]. \end{aligned} \tag{3.42}$$

where we assumed weakly interacting bosons with a possible density difference $\rho_R - \rho_L \neq 0$ between the two condensates. Here and in the following, we consider the rotating frame and ignore the chemical potential difference $g/2(\rho_R^2 - \rho_L^2)$ between left and right condensates arising from interactions.

The interference pattern measures the phase difference $\hat{\phi}_L - \hat{\phi}_R$. As before, we describe the system in terms of the "spin" variables that are the difference of left and right condensates and "charge" variables that are the sum of the two. Using the variables $\hat{\phi}_s = \hat{\phi}_R - \hat{\phi}_L$, $\hat{\phi}_c = \hat{\phi}_R + \hat{\phi}_L$, $\hat{n}_s = (\hat{n}_R - \hat{n}_L)/2$, $\hat{n}_c = (\hat{n}_R + \hat{n}_L)/2$, we find the

Hamiltonian of the system to be

$$
\begin{aligned}
H &= H_s + Hc + H_{int} && (3.43)\\
H_s &= \int dx \left[\frac{\rho_R + \rho_L}{8m} (\partial_x \hat{\phi}_s)^2 + g\hat{n}_s^2 \right], && (3.44)\\
H_c &= \int dx \left[\frac{\rho_R + \rho_L}{8m} (\partial_x \hat{\phi}_c)^2 + g\hat{n}_c^2 \right], && (3.45)\\
H_{int} &= \int dx \left[\frac{\rho_R - \rho_L}{4m} \partial_x \hat{\phi}_c \partial_x \hat{\phi}_s \right]. && (3.46)
\end{aligned}
$$

Therefore, when the splitting makes two identical quasi-condensates with equal density, "spin" and "charge" degrees of freedom decouple and we can use a simpler theory derived in Sec 3.4.2. On the other hand, when the splitting makes two condensates with unequal densities, more general theory of Sec 3.5 needs to be employed. In any case, the full time evolution of the distributions of interference patterns can be obtained, which in principle can be compared with experiments.

It is notable that the mixing of the "spin" and "charge" degrees of freedom for small density difference $\rho_R - \rho_L$ is not "small," in the sense that the mixing angle κ defined in section 3.5 takes the maximum value $\pi/4$. The spin decoupling in the limit of $\rho_R - \rho_L \to 0$ is recovered not by taking $\kappa \to 0$, but rather, by taking the time at which the effect of the coupling takes place to infinity. This is most explicitly shown in Eq. (3.36) where the charge contributions of fluctuations go to zero as $c_1 \to c_2$ which is attained in the limit $\rho_R - \rho_L = 0$.

3.6.2 Interference patterns in equilibrium

The techniques to calculate the full distribution functions presented in previous sections are directly applicable to also obtaining a simple form of the full distribution functions of the interference patterns between two independent, thermal quasi-condensates. This problem

has been previously analyzed in theory[51, 150] as well as in experiments[17, 61].

We consider the preparation of two independent one dimensional quasi-condensates. If they are prepared by cooling two independent quasi-condensates, the temperature of the left quasi-condensate T_L and that of right quasi-condensate T_R are generically different. The density matrix of the initial state is described by $\hat{\rho}_0 = e^{-(\beta_L H_L + \beta_R H_R)}$ where $\beta_a = 1/(k_B T_a)$ with $a = L, R$. It is important to note that the constant shift of phase $\phi_a \to \phi_a + \theta_{ac}$ does not change the energy of the system, so that for the average over thermal ensemble one has to integrate over θ_{ac}. Physically, this simply means that the phases of independent condensates are random. Then the only interesting distribution here is the distribution of the interference contrast [51, 61, 69, 124] given by,

$$\hat{C}^2 = \left| \int_{-l/2}^{l/2} e^{-i\hat{\phi}_s(r)} \right|^2 dr \tag{3.47}$$

which corresponds to, in spin language, the squared transverse magnitude of the spin $\left(\hat{S}_l^{\perp}\right)^2$. The analysis of the evaluation of distributions in the density matrix of thermal equilibrium state in Sec 3.5 can be directly extended to this case, and we obtain the

distribution

$$P_l^{\perp}(\gamma) = \prod_k \int_{-\pi}^{\pi} \frac{d\lambda_{\theta sk}}{2\pi} \int_0^{\infty} \lambda_{rsk} e^{-\lambda_{rsk}^2/2} d\lambda_{rsk} \times \delta\left(\gamma - \left|\rho \int_{-l/2}^{l/2} dr e^{i\chi(r,\{\lambda_{jsk}\})}\right|^2\right), \tag{3.48}$$

$$\chi(r,\{\lambda_{jsk}\}) = \sum_k \sqrt{\frac{\left\langle |\hat{\phi}_{s,k}|^2 \right\rangle}{L}} \lambda_{rsk} \sin(kr + \lambda_{\theta sk}),$$

$$\left\langle |\hat{\phi}_{s,k}|^2 \right\rangle = \frac{1 + e^{-\beta_L |k| c_L}}{1 - e^{-\beta_L |k| c_L}} \frac{\pi}{2|k|K_L} + \frac{1 + e^{-\beta_R |k| c_R}}{1 - e^{-\beta_R |k| c_R}} \frac{\pi}{2|k|K_R}, \tag{3.49}$$

where c_a and $K_a, a = L, R$ are the sound velocity and Luttinger parameters of left and right quasi-condensate.

3.7 Prethermalization of one-dimensional condensates

The equilibration and relaxation dynamics of generic many-body systems are fundamental open problems. Among possible processes, it has been suggested that the time evolution of some systems prepared in non-equilibrium states results in the reaching of quasi-steady states within much shorter time than equilibration time. This quasi-steady state is often not a true equilibrium state, but rather it is a dephased state, and true equilibration takes place at much longer time scale. Yet in some cases, the physical observables in the qausi-steady states take the value corresponding to the one in thermal equilibrium at some effective temperature T_{eff}, displaying disguised "thermalized" states. Such surprising non-equilibrium phenomena, called prethermalization, have been shown to occur in quantum as well as

classical many-body systems[11, 15, 107].

In particular, integrable one dimensional systems are known *not to* thermalize and indeed, experiments in Ref. [83] have observed an exceedingly long equilibration time. Yet even in this extreme case, we suggest in this section that many-body one dimensional systems can reach disguised "thermalized" states through prethermalization phenomena within a short time.

The sudden splitting of one dimensional condensates considered in the previous Sec 3.6 is a particular example of dynamics in which slow equilibration is expected because the system essentially consists of uncoupled harmonic oscillators in the low energy description. We demonstrate that the quasi-condensates reach a long-time transient state after the sudden splitting, and show that the distribution of the interference contrast amplitudes of the two *non-equilibrium* quasi-condensates are given by that of two *equilibrium* quasi-condensates at some effective temperature T_{eff}.

First we give a heuristic argument for the prethermalization phenomena and derive the estimate of T_{eff}. Long time after the splitting, the position of the interference peak becomes completely random, and yields no information. Therefore, we focus on the interference contrasts $\hat{C}^2$ in Eq.(3.47), which, translated to the language of spin dynamics, is the squared transverse magnitude of the spin $\left(\hat{S}_l^{\perp}\right)^2$. The interference contrast of the split condensates after a long time is determined by the "average" phase fluctuations present in the system. In the dephased limit, such fluctuations are determined by the total energy present in each mode labeled by momenta k. First we suppose that the splitting process prepares two identical quasi-condensates with the same density $\rho_L = \rho_R = \rho$, and consider the case of unequal densities later. Under this circumstances, the initial state of the phase difference is determined solely by the splitting process (see Eq.(3.12)), and moreover the subsequent

dynamics of the phase difference described by Eq.(3.44) decouples from the dynamics of the sum of the densities. Therefore, here the phase fluctuations, and thus interference contrast become independent of the initial temperatures of the quasi-condensates.

In Sec. 3.4.2, we gave an intuitive estimate of the energy stored in each mode in this decoupling case, and concluded that each mode contains the energy $\frac{\pi c_s \rho \eta}{4K_s}$. We remind the readers that the energy contained in each mode is independent of momenta because the density difference of quasi-condensates along the axial direction is uncorrelated in the initial state beyond the spin healing length ξ_s for a fast splitting process (see discussion below Eq. (3.10)). On the other hand, the interference contrast of *thermal* condensates at temperature T is determined by the thermal phase fluctuations caused by excitations whose energy is distributed according to equipartition theorem; each mode in the *thermal* condensates contains the equal energy of $k_B T$. Thus from this argument, we find that the interference contrast of split condensates after a long time becomes indistinguishable from the one resulting from thermal condensates at temperature $k_B T_{\text{eff}} = \frac{\pi c_s \rho \eta}{4K_s}$. We will show below that in fact, the *full distribution function* of interference contrast becomes indistinguishable for these two states. In the case of splitting two dimensional condensates, equipartition of energy and existence of "non-equilibrium temperature" was pointed out in Ref.[107].

In the following, we derive the result above through the formalism developed in the previous sections. The distribution of the interference contrast is determined by $\left\langle |\hat{\phi}_{s,k}|^2 \right\rangle$ given in Eq.(3.20). In the long time limit, we can take $\sin^2(c_s|k|t) \sim \cos^2(c_s|k|t) \sim 1/2$. Moreover, since the interference contrast is most affected by the excitations with small wave vectors k with $a_k = \frac{|k|K_s}{\pi \rho \eta} < 1$, we can

approximate the expression as

$$\left\langle |\hat{\phi}_{s,k}|^2 \right\rangle \approx \frac{\pi}{2|k|K_s} \frac{\pi\rho\eta}{2|k|K_s}. \tag{3.50}$$

On the other hand, for two quasi-condensates in thermal equilibrium, the position of the interference peaks is again random. The interference contrast is determined by $\left\langle |\hat{\phi}_{s,k}|^2 \right\rangle$ given in Eq.(3.49). Since the main contribution to the fluctuation comes from low momenta, we approximate $e^{-\beta|k|c} \approx 1 - \beta|k|c$. It is easy to check that the sound velocity and Luttinger parameters for each condensate is related to those of the difference mode (see Eqs.(3.44-3.46)) as $c_L = c_R = c_s$ and $K_L = K_R = 2K_s$. Thus we obtain

$$\left\langle |\hat{\phi}_{s,k}|^2 \right\rangle \approx \frac{2}{\beta|k|c_s} \frac{\pi}{2|k|K_s}. \tag{3.51}$$

Now the crucial observation is that our closed form expressions for distributions of interference contrasts of both split quasi-condensates and thermal quasi-condensates are determined solely by $\left\langle |\hat{\phi}_{s,k}|^2 \right\rangle$, and they take precisely the same form in terms of $\left\langle |\hat{\phi}_{s,k}|^2 \right\rangle$. Moreover, the expressions given by Eq.(3.50) and Eq.(3.51) have the same dependence on wave vectors $|k|$. Therefore, the *full* distribution of interference contrast of split condensates become indistinguishable from that of thermal condensates with temperature

$$k_B T_{\text{eff}} \approx \frac{\pi c_s \rho\eta}{4K_s} = \frac{\mu\eta}{2}, \tag{3.52}$$

where the second equality holds for weakly interacting bosons and the chemical potential of one quasi-condesate is given by $\mu = g\rho$. Thus, split one dimensional quasi-condensates indeed display the prethermalization phenomenon.

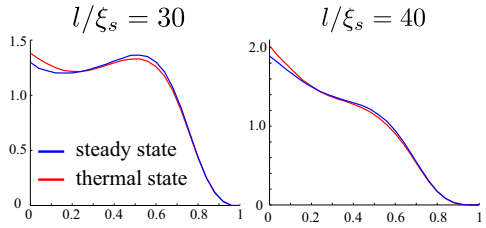

Figure 3.7.1: The distributions of interference contrast for steady states of split quasi-condensates and two thermal quasi-condensates. Here x axis is scaled such that the maximum value of interference contrast is 1. For the split condensates, we plot the distribution at time $t = 60\xi_s/c_s$ for Luttinger parameter $K_s = 20$, system size $L = 400\xi_s$ and two different integration length $l/\xi_s = 30, 40$. The thermal quasi-condensates are for temperature $\frac{\pi c_s}{2\xi_s}$ for the same integration length corresponding to the effective temperature obtained in Eq. (3.52).

In Fig. 3.7.1, we plot the interference contrast $P_l^{\perp}(\gamma)$ (see Eq.(3.25)) of split condensates in a steady state at time $t = 60\xi_s/c_s$ for Luttinger parameter $K_s = 20$, system size $L = 400\xi_s$ and two different integration lengths $l/\xi_s = 30, 40$. Also we plot the interference contrast of the thermal quasi-condensates (see Eq.(3.48)) at temperature $\frac{\pi c_s}{2\xi_s}$ for the same integration length. This temperature corresponds to the effective temperature obtained in Eq. (3.52). Indeed we see only a small difference between the distributions of steady states and thermal states for both integration lengths. The small difference comes from the approximations made in obtaining the expressions given by Eq.(3.50) and Eq.(3.51).

In the previous paragraphs, we assumed that the splitting prepares quasi-condensates with identical average densities. Here we briefly consider the case in which the splitting process prepares two quasi-condensates with slightly different densities. In this case, the temperature of the initial quasi-condensates affects the interference contrast around the time scale of $\frac{\xi_s}{(c_L - c_R)\pi} \approx \frac{\hbar}{\mu(\sqrt{\rho_L} - \sqrt{\rho_R})}$, whereas the prethermalized, long-time transient state is reached around $\frac{\hbar}{\mu}\frac{l}{\xi_s}$, where

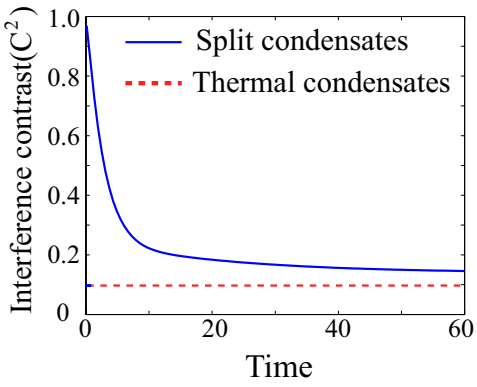

Figure 3.7.2: The evolution of the interference contrast $\hat{C}^2$ for system size $L = 500\xi_s$, integration length $l = 40\xi_s$, and the effective spin Luttinger parameter $K_s = 20$ with initial temperature corresponding to the chemical potential μ. Time is measured in units of ξ_s/c_s. Here we took the density $\rho_R = 1.2\rho$ and $\rho_L = 0.8\rho$. The magnitude of $\hat{C}^2$ for two thermal quasi-condensates at temperature $k_B T = \mu$ is plotted as red dotted line for comparison.

l is the integration length.

These analytic arguments can be confirmed through numerical simulations. In Fig. 3.7.2, we have plotted the evolution of the interference contrast $\hat{C}^2$ for system size $L = 500\xi_s$, integration length $l = 40\xi_s$, and Luttinger parameter $K_s = 20$ with initial temperature corresponding to the chemical potential μ. Here we consider a situation where the density of left quasi-condensate is different from that of right quasi-condensate by 20% such that $\rho_R = 1.2\rho$ and $\rho_L = 0.8\rho$ where $\rho_{R(L)}$ is the average density of the right (left) condensate, and 2ρ is the average density of the initial condensate before splitting. Also for comparison we have plotted the magnitude of interference contrast of two quasi-condensates in *thermal* states at temperature given by μ. From the plot, one can observe the existence of quasi-steady state plateau after short time. Notice that the magnitude of $\hat{C}^2$ in the steady state is larger than the value expected

from thermalized states at the initial temperature. The subsequent slow decrease of the interference contrast is due to the effect of temperature in the initial state coming from the small difference of the two quasi-condensates. Such development of the plateau at larger value of interference contrast than the one for equilibrium state of the initial temperature indicates the phenomenon of prethermalization.

Here we proposed the occurrence of such prethermalization within Tomonaga-Luttinger theory. We emphasize that within Tomonaga-Luttinger theory of low energy excitations, different modes are decoupled and therefore no true thermalization can take place. In realistic experimental situations, such integrability can be broken and relaxation and thermalization process are expected to occur after a long time dynamics. The requirement to observe the prethermalization phenomena predicted in this theory in experiments depends on the time-scale of other possible thermalization processes we did not consider in this model such as the effective three-body collisions[108, 109], relaxation of high energy quasi-particles[154], or interactions among the collective modes through anharmonic terms we neglected in Tomonaga-Luttinger theory[24]. When all these processes occur at much slower time scale than the prethermalization time-scale, which is roughly given by the integration length divided by the spin sound velocity $\sim l/c_s$ for decoupling case, the observation of prethermalization should be possible. In one dimension, the dynamics is strongly constrained due to the conservation of energy and momentum, and therefore it is likely that the dynamics is dominated by the modes described by Tomonaga-Luttinger theory for long time for quasi-condensates with low initial temperatures.

Such prethermalizations are expected to occur even in higher dimensional systems[54, 56, 68, 107]. We note that the conditions for the experimental observations of the phenomena might be more stringent because true thermalization processes are expected to take

place much more quickly in two and three dimensional systems.

3.8 Conclusion

In this work, we have shown how noise captured by full distribution functions can be used to study the dynamics of strongly correlated, many-body system in one dimension. The analytical results of joint distribution functions obtained in Sec 3.4.2 allow not only the simple understanding of distribution functions from spin-wave picture, but also an intuitive visualization of the correlation in one dimensional system. Using this picture, we have also shown the phenomena of prethermalization in one dimensional dynamics for the full distribution functions that contain information about the correlation functions of the arbitrary order.

The approach developed in this chapter can be extended to other types of dynamics. While we focused on Ramsey type dynamics or dynamics of interference patterns for a split quasi-condensate, we can also change different physical parameters to induce the dynamics. For example, it is straightforward to apply our study to the sudden change (quench) of interaction strength[70, 71].

In this chapter, we focused on distribution functions obtained from Tomonaga-Luttinger Hamiltonian (3.4). It is of interest to extend our analysis to higher spins[10], and analyze them, for example, in the presence of magnetic field[160]. Since there are more degrees of freedom in these systems, distributions might capture the tendency towards various phases such as ferromagnetic ordering. These questions will be analyzed in the future works.

3.9 Appendices

3.9.1 Distribution function of the z component of spin

In this appendix, we calculate the distribution function of $\hat{S}_l^z$ in the absence of the coupling between charge and spin. The extension to the case in which the charge and spin degrees of freedom mix is straightforward.

It is convenient to evaluate the generating function $\left\langle e^{\lambda \hat{S}_l^z} \right\rangle$, instead of distribution function $P_l^z(a)$. They are related by

$$\left\langle e^{\lambda \hat{S}_l^z} \right\rangle = \int_{-\infty}^{\infty} e^{\lambda a} P_l^z(a) da. \tag{3.53}$$

This equality can be checked by differentiating both sides by λ and evaluating them at $\lambda = 0$. This reproduces the implicit definition of P_l^z in Eq. (3.2).

Analogous to the calculation of mth moment of $\hat{S}_l^\theta$, we first express $\hat{S}_l^z$ in terms of $\gamma_{s,k}$ operators defined in Eq. (3.15)

$$\begin{aligned}
\hat{S}_l^z(r) =& \int_{-l/2}^{l/2} dr \left(\sum_{k \neq 0} (d_{s,k} \gamma_{s,k}^\dagger + d_{s,k}^* \gamma_{s,-k}) e^{ikr} + \frac{n_{s,0}}{\sqrt{L}} \right), \\
d_{s,k} =& \sqrt{\frac{|k| K_s}{2\pi L}} \frac{e^{i c_s |k| t} + 2 W_k e^{-i c_s |k| t}}{\sqrt{1 - 4|W_k|^2}}.
\end{aligned}$$

Then, we can apply the trick introduced in Section 3.4.2 to obtain

$$\begin{aligned}
\left\langle e^{\lambda \hat{S}_l^z} \right\rangle &= e^{\lambda^2 \int_{-l/2}^{l/2} dr_1 dr_2 \left(\sum_{k \neq 0} |d_{s,k}|^2 e^{ik(r_1 - r_2)} + \frac{\left\langle n_{s,0}^2 \right\rangle}{\sqrt{L}} \right)}. \\
&= \exp\left\{ \lambda^2 \left(\frac{\rho \eta l^2}{4L} + \sum_{k \neq 0} \frac{4 |d_{s,k}|^2}{k^2} \sin^2(lk/2) \right) \right\}
\end{aligned}$$

Then the following expression gives the distribution of $\hat{S}_l^z$

$$P_l^z(a) = \frac{1}{2\sqrt{\pi \left\langle \left(\hat{S}_l^z\right)^2 \right\rangle}} \exp\left(-\frac{a^2}{4\left\langle \left(\hat{S}_l^z\right)^2 \right\rangle}\right), \tag{3.54}$$

where

$$\left\langle \left(\hat{S}_l^z\right)^2 \right\rangle = \frac{\rho\eta l^2}{4L} + \sum_{k\neq 0} \frac{4|d_{s,k}|^2}{k^2} \sin^2(lk/2).$$

3.9.2 Expression for $C_{a,k}$ in the presence of mixing between charge and spin

In this section, we derive the expression of $C_{a,k}, a = s, c$ in Eq. (3.36). We first find the transformation from $b_{s,k}, b_{c\uparrow,k}$ to $b_{1,k}, b_{2,k}$. Then we relate $b_{1,k}, b_{2,k}$ and $\gamma_{s,k}(t), \gamma_{c,k}(t)$. Combining these two transformations, we obtain $b_{s,k}$ in terms of $\gamma_{s,k}(t), \gamma_{c,k}(t)$, leading to the expression of $\hat{\phi}_{s,k}$ in terms of $\gamma_{s,k}(t), \gamma_{c,k}(t)$.

From the relations,

$$\begin{aligned}
\phi_{i,k} &= -i\sqrt{\frac{\pi}{2|k|K_i}}(b_{i,k}^\dagger - b_{i,-k}), \\
n_{i,k} &= \sqrt{\frac{|k|K_i}{2\pi}}(b_{i,k}^\dagger + b_{i,-k}), \\
b_{i,k}^\dagger &= i\phi_{i,k}\sqrt{\frac{|k|K_i}{2\pi}} + n_{i,k}\sqrt{\frac{\pi}{2|k|K_i}},
\end{aligned}$$

along with Eq. (3.29), it is straightforward to obtain

$$\begin{pmatrix} b_{c\uparrow,-k}^\dagger \\ b_{c\uparrow,k} \\ b_{s,-k}^\dagger \\ b_{s,k} \end{pmatrix} = D \begin{pmatrix} b_{1,-k}^\dagger \\ b_{1,k} \\ b_{2,-k}^\dagger \\ b_{2,k} \end{pmatrix},$$

where

$$D = \frac{1}{2}\times$$
$$\begin{pmatrix} \cos\kappa\left(\sqrt{\frac{\tilde{K}_{c\uparrow}}{K_1}}+\sqrt{\frac{K_1}{\tilde{K}_{c\uparrow}}}\right) & \cos\kappa\left(-\sqrt{\frac{\tilde{K}_{c\uparrow}}{K_1}}+\sqrt{\frac{K_1}{\tilde{K}_{c\uparrow}}}\right) & -\sin\kappa\left(\sqrt{\frac{\tilde{K}_{c\uparrow}}{K_2}}+\sqrt{\frac{K_2}{\tilde{K}_{c\uparrow}}}\right) & -\sin\kappa\left(-\sqrt{\frac{\tilde{K}_{c\uparrow}}{K_2}}+\sqrt{\frac{K_2}{\tilde{K}_{c\uparrow}}}\right) \\ \cos\kappa\left(-\sqrt{\frac{\tilde{K}_{c\uparrow}}{K_1}}+\sqrt{\frac{K_1}{\tilde{K}_{c\uparrow}}}\right) & \cos\kappa\left(\sqrt{\frac{\tilde{K}_{c\uparrow}}{K_1}}+\sqrt{\frac{K_1}{\tilde{K}_{c\uparrow}}}\right) & -\sin\kappa\left(-\sqrt{\frac{\tilde{K}_{c\uparrow}}{K_2}}+\sqrt{\frac{K_2}{\tilde{K}_{c\uparrow}}}\right) & -\sin\kappa\left(\sqrt{\frac{\tilde{K}_{c\uparrow}}{K_2}}+\sqrt{\frac{K_2}{\tilde{K}_{c\uparrow}}}\right) \\ \sin\kappa\left(\sqrt{\frac{K_s}{K_1}}+\sqrt{\frac{K_1}{K_s}}\right) & \sin\kappa\left(-\sqrt{\frac{K_s}{K_1}}+\sqrt{\frac{K_1}{K_s}}\right) & \cos\kappa\left(\sqrt{\frac{K_s}{K_2}}+\sqrt{\frac{K_2}{K_s}}\right) & \cos\kappa\left(-\sqrt{\frac{K_s}{K_2}}+\sqrt{\frac{K_2}{K_s}}\right) \\ \sin\kappa\left(-\sqrt{\frac{K_s}{K_1}}+\sqrt{\frac{K_1}{K_s}}\right) & \sin\kappa\left(\sqrt{\frac{K_s}{K_1}}+\sqrt{\frac{K_1}{K_s}}\right) & \cos\kappa\left(-\sqrt{\frac{K_s}{K_2}}+\sqrt{\frac{K_2}{K_s}}\right) & \cos\kappa\left(\sqrt{\frac{K_s}{K_2}}+\sqrt{\frac{K_2}{K_s}}\right) \end{pmatrix}, \tag{3.55}$$

where $\tilde{K}_{c\uparrow} = K_{c\uparrow}/\sqrt{s_c}$.

Next, we relate $\gamma_{a,k}(t), a = c, s$ operators to b_1, b_2. At $t = 0$, we have the relation between $\gamma_{a,k}(0), a = c, s$ and $b_{c\uparrow,k}$ and $b_{s,k}$ as described in Sec. 3.5. Since operators $b_{c\uparrow,k}$ and $b_{s,k}$ are related to $b_{1,k}$ and $b_{2,k}$ through the matrix D in Eq.(3.55), we can express $\gamma_{a,k}(0)$ as a linear combinations of $b_{1,k}$ and $b_{2,k}$. The time evolution of $\gamma_{a,k}(0)$ is quite simple now because Hamiltonians are diagonal in the basis $b_{1,k}$ and $b_{2,k}$. These considerations lead to the relations

$$\begin{pmatrix} \gamma^\dagger_{c,-k}(t) \\ \gamma_{c,k}(t) \\ \gamma^\dagger_{s,-k}(t) \\ \gamma_{s,k}(t) \end{pmatrix} = E_k \begin{pmatrix} e^{-ic_1|k|t} b^\dagger_{1,-k} \\ e^{ic_1|k|t} b_{1,k} \\ e^{-ic_2|k|t} b^\dagger_{2,-k} \\ e^{ic_2|k|t} b_{2,k} \end{pmatrix},$$

$$E_k = F_k D,$$

$$F_k = \begin{pmatrix} 1 & 0 & 0 & 0 \\ 0 & 1 & 0 & 0 \\ 0 & 0 & \frac{1}{\sqrt{1-4|W_k|^2}} & \frac{-2W_k}{\sqrt{1-4|W_k|^2}} \\ 0 & 0 & \frac{-2W_k}{\sqrt{1-4|W_k|^2}} & \frac{1}{\sqrt{1-4|W_k|^2}} \end{pmatrix}.$$

Now define a matrix $G(k) = DE_k^{-1}$ so that

$$\begin{pmatrix} b^\dagger_{c,-k} \\ b_{c,k} \\ b^\dagger_{s,-k} \\ b_{s,k} \end{pmatrix} = G(k) \begin{pmatrix} \gamma^\dagger_{c,-k} \\ \gamma_{c,k} \\ \gamma^\dagger_{s,-k} \\ \gamma_{s,k} \end{pmatrix}$$

Then finally $C_{i,k}$ are given by

$$\begin{aligned} C_{s,k} &= -i\sqrt{\frac{\pi}{2L|k|K_s}}(G_{34}(k) - G_{44}(k)), \\ C_{c,k} &= -i\sqrt{\frac{\pi}{2L|k|K_s}}(G_{32}(k) - G_{42}(k)), \end{aligned} \tag{3.56}$$

where $G_{ij}(k)$ are the matrix elements of $G(k)$.

3.9.3 $k = 0$ CONTRIBUTION IN THE PRESENCE OF MIXING BETWEEN CHARGE AND SPIN

In this appendix, we evaluate $\mathrm{Tr}\left\{e^{i(\sum_i s_i)\phi_{s,0}/\sqrt{L}}\rho(t)\right\}$. We first obtain the operator $e^{i\left(\sum_i s_i\right)\phi_{s,0}}$ after time evolution as

$$\begin{aligned} &e^{iHt}e^{i\left(\sum_i s_i\right)\phi_{s,0}}e^{-iHt} = \\ &\exp\left(i\frac{\sum_i s_i}{\sqrt{L}}(A\phi_{s,0} + A'n_{s,0} + \frac{B}{\sqrt{s_c}}\phi_{c,0} + \frac{B'}{\sqrt{s_c}}n_{c,0})\right). \end{aligned} \tag{3.57}$$

Coefficients A, A', B, B' can be found as follows. $k = 0$ part of the Hamiltonian is given by $H_0 = \frac{\pi c_1}{2K_1}n^2_{1,0} + \frac{\pi c_2}{2K_2}n^2_{2,0}$ (see Eq.(3.11)). Using the commutation relation $[n_{i,0}, \phi_{i,0}] = -i$, we have $e^{iHt}\phi_{i,0}e^{-iHt} = \phi_{i,0} + \frac{\pi c_i}{K_i}n_{i,0}t$. With the relation, $\phi_{s,0} = \sin\kappa\phi_{1,0} + \cos\kappa\phi_{2,0}$,

we obtain

$$e^{iHt}e^{\left(\sum_i s_i\right)\phi_{s,0}}e^{-iHt} =$$
$$e^{i\frac{\sum_i s_i}{\sqrt{L}}\left\{\sin\kappa(\phi_{1,0}+\frac{\pi c_1}{K_1}n_{1,0}t)+\cos\kappa(\phi_{2,0}+\frac{\pi c_2}{K_2}n_{2,0}t)\right\}}.$$

Now by transforming back to c, s basis through Eq.(3.29), we find

$$\begin{aligned} A &= 1, \\ A' &= \sin^2\kappa\frac{\pi c_1}{K_1}t + \cos^2\kappa\frac{\pi c_2}{K_2}t, \\ B &= 0, \\ B' &= \sin\kappa\cos\kappa\left(\frac{\pi c_1}{K_1} - \frac{\pi c_2}{K_2}\right)t. \end{aligned}$$

Now that we know the operator after time-evolution Eq. (3.57), we evaluate it in the initial state.

Initial state of the spin sector is $|\psi_{s,k=0}\rangle$ in Eq. (3.12). Since this state is Gaussian, we have the simple result as follows,

$$\begin{aligned} &\langle\psi_{s,k=0}|\exp\left(\left(\sum_i s_i\right)(A\phi_{s,0}+A'n_{s,0})/\sqrt{L}\right)|\psi_{s,k=0}\rangle. \\ &= \exp\left(-\left(\sum_i s_i\right)^2\left(\frac{1}{4\rho\eta L}+(A')^2\frac{\rho\eta}{4L}\right)\right) \end{aligned}$$

For charge sector, $k=0$ part of the initial density matrix is $\frac{1}{\mathcal{N}_{c0}}\exp\left(-\beta\frac{\pi c_{c\uparrow}}{2K_{c\uparrow}}n_{c,0}^2\right)$, where $\mathcal{N}_{c0}$ is the normalization $\mathcal{N}_{c0}$ $=\mathrm{Tr}\left(\exp\left(-\beta\frac{\pi c_{c\uparrow}}{2K_{c\uparrow}}n_{c,0}^2\right)\right)$. The evaluation of the charge sector yields

$$\begin{aligned} &\frac{1}{\mathcal{N}_{c0}}\mathrm{Tr}\left\{\exp\left(i\left(\sum_i s_i\right)B'\frac{n_{c,0}}{\sqrt{s_c L}}\right)\exp\left(-\beta\frac{\pi c_{c\uparrow}}{2K_{c\uparrow}}n_{c,0}^2\right)\right\} \\ &= \exp\left(-\left(\sum_i s_i\right)^2(B')^2\frac{\tilde{K}_{c\uparrow}}{2\pi c_{c\uparrow}\beta L}\right). \end{aligned}$$

Collecting the results above, we conclude

$$\begin{aligned}
&\left\langle e^{i(\sum_i s_i)\phi_{s,0}/\sqrt{L}} \right\rangle \\
&= \exp\left(-\frac{(\sum_i s_i)^2}{4L} \left\{ \frac{1}{\rho\eta} + \rho\eta (A')^2 + (B')^2 \frac{2\tilde{K}_{c\uparrow}}{\pi c_{c\uparrow} \beta} \right\} \right).
\end{aligned}$$

4

Conclusion and future perspective

In this thesis, we have presented the progress of the study for non-equilibrium quantum physics. As we explained in details through numerous experiments in the first chapter, artificial systems provide rich platforms and testing beds for investigating questions in non-equilibrium quantum physics, which has been challenging in the context of condensed matter materials. The importance of such artificial systems lies not only in the possibility to experiment novel and exotic ideas but also in freeing and opening physicists' mind for new ways of thinking about physics. In my works, I have tried to take up this opportunity to propose unique ideas with concrete experimental settings. Some of the detailed theories that have been confirmed in experiments are presented in the second and third chapters. I have tried to construct and describe the theories in a

fashion that the ideas can be easily generalized to condensed matter systems.

One of the main themes of my thesis is the study of topological phenomena in non-equilibrium systems. On one hand, this demonstrates the possibility to realize and study interesting physical phenomena that are already known in equilibrium settings in non-equilibrium systems as well. Some physical phenomena are quite difficult to realize in equilibrium and require fine-tunings and engineering of materials.Non-equilibrium realizations of those phenomena provide a novel approach to them and might prove to be advantageous in the future technologies. While the proposals of realizing IQHE or topologically protected localized states presented in this thesis are far from being useful in everyday-life, they are realistic enough to be studied in experiments in laboratories. In the future, I believe other phenomena such as superconductivities and ferro- & antiferro- magnetism will find non-equilibrium realizations and manipulations which could lead to new ideas for technological usage.

On the other hand, this thesis also demonstrates the possibility to find unique phenomena in non-equilibrium systems that could never be found in equilibriums. 0 and π energy topologically protected bound states have not yet found implications in technology, but maybe some other such unique phenomena could lead to breakthroughs in developing quantum technologies. This venture requires thinking beyond the paradigm of equilibrium systems and therefore tends to be very difficult, but this field has not been investigated much by physicists yet and thus there is large room for improvements and new discoveries.

One possible place to look for such new phenomena is the steady states created by the balance between the periodical drives and dissipation/equilibration process. Such a state is a well-defined, stable state, and thus has the chance of being realized in a robust fashion.

Just in the case of superconductors and topological insulators, such states could possess unique response properties. In the case of atomic systems, periodical drives could be achieved through lattice modulations, laser applications that drive atomic transitions, or modulations of confinement potentials. Dissipations can also be engineered by controlling environments such as placing the systems in a cavity. A ubiquitous notion such as the competitions/corporations of orders might be an interesting viewpoint to investigate this system; maybe it is possible to study the competitions and corporations by driving the systems in such a way to enhance certain order. These ideas can also be combined with the insights that periodic drives effectively increase the dimensionality of the systems by one through the addition of energy ladders. Most orders are sensitive to the underlying dimensionality and thus could be an interesting entry point to study the ordered systems in non-equilibrium systems.

The field of non-equilibrium quantum systems is still young and has potentials for contributing to fundamental understanding of physics as well as to future technologies. I hope some of the works I have done help this trend even by a little bit.

References

[1] T. Kitagawa, Wolfram Demonstration project, http://demonstrations.wolfram.com/TopologicalPhasesWithQuantumWalks/.

[2] Y. Aharonov, L. Davidovich, and N. Zagury. Quantum random walks. *Phys. Rev. A*, 48:1687–1690, Aug 1993. doi: 10.1103/PhysRevA.48.1687. URL http://link.aps.org/doi/10.1103/PhysRevA.48.1687.

[3] A. Aspect, D. Boiron, and C. Westbrook. Quantum atom optics with bosons and fermions. *Europhysics News*, 39(1):25–29, 2008. ISSN 0531-7479. doi: 10.1051/epn. URL http://arxiv.org/pdf/0803.2828.

[4] Alain Aspect, Philippe Grangier, and Gérard Roger. Experimental Realization of Einstein-Podolsky-Rosen-Bohm Gedankenexperiment: A New Violation of Bell's Inequalities. *Physical Review Letters*, 49(2):91–94, July 1982. ISSN 0031-9007. doi: 10.1103/PhysRevLett.49.91. URL http://prl.aps.org/abstract/PRL/v49/i2/p91_1.

[5] M. Atala, M. Aidelsburger, J. T. Barreiro, D. Abanin, T. Kitagawa, E. Demler, and I. Bloch. Direct Measurement of the Zak phase in Topological Bloch Bands. *ArXiv e-prints*, December 2012.

[6] W. S. Bakr, A. Peng, M. E. Tai, R. Ma, J. Simon, J. I. Gillen, S. Fölling, L. Pollet, and M. Greiner. Probing the superfluid–to–mott insulator transition at the single-atom level. *Science*, 329(5991):547–550, 2010. doi: 10.1126/science.1192368.

URL
http://www.sciencemag.org/content/329/5991/547.abstract.

[7] Waseem S. Bakr, Jonathon I. Gillen, Amy Peng, Simon Folling, and Markus Greiner. A quantum gas microscope for detecting single atoms in a hubbard-regime optical lattice. *Nature*, 462 (7269):74–77, Nov 2009. ISSN 0028-0836. doi: 10.1038/nature08482. URL http://dx.doi.org/10.1038/nature08482.

[8] Leon Balents. Spin liquids in frustrated magnets. *Nature*, 464 (7286):199–208, Mar 2010. ISSN 0028-0836. doi: 10.1038/nature08917. URL http://dx.doi.org/10.1038/nature08917.

[9] Peter Barmettler, Matthias Punk, Vladimir Gritsev, Eugene Demler, and Ehud Altman. Relaxation of Antiferromagnetic Order in Spin-1/2 Chains Following a Quantum Quench. *Physical Review Letters*, 102(13), April 2009. ISSN 0031-9007. doi: 10.1103/PhysRevLett.102.130603. URL http://prl.aps.org/abstract/PRL/v102/i13/e130603.

[10] Ryan Barnett, Daniel Podolsky, and Gil Refael. Geometrical approach to hydrodynamics and low-energy excitations of spinor condensates. *Physical Review B*, 80(2), July 2009. ISSN 1098-0121. doi: 10.1103/PhysRevB.80.024420. URL http://prb.aps.org/abstract/PRB/v80/i2/e024420.

[11] Ryan Barnett, Anatoli Polkovnikov, and Mukund Vengalattore. Do Quenched Spinor Condensates Thermalize? page 4, September 2010. URL http://arxiv.org/abs/1009.1646.

[12] M. T. Batchelor, M. Bortz, X. W. Guan, and N. Oelkers. Exact results for the one-dimensional mixed boson-fermion interacting gas. *Physical Review A*, 72(6), December 2005. ISSN 1050-2947. doi: 10.1103/PhysRevA.72.061603. URL http://pra.aps.org/abstract/PRA/v72/i6/e061603.

[13] Benjamin Bederson. *Advances in atomic, molecular, and optical physics, Volume 48*. Gulf Professional Publishing, 2002. ISBN

012003848X. URL http://books.google.com/books?id=74hBmEjf5DMC&pgis=1.

[14] Maxime Ben Dahan, Ekkehard Peik, Jakob Reichel, Yvan Castin, and Christophe Salomon. Bloch oscillations of atoms in an optical potential. *Phys. Rev. Lett.*, 76:4508–4511, Jun 1996. doi: 10.1103/PhysRevLett.76.4508. URL http://link.aps.org/doi/10.1103/PhysRevLett.76.4508.

[15] J. Berges, Sz. Borsányi, and C. Wetterich. Prethermalization. *Phys. Rev. Lett.*, 93:142002, Sep 2004. doi: 10.1103/PhysRevLett.93.142002. URL http://link.aps.org/doi/10.1103/PhysRevLett.93.142002.

[16] B. Andrei Bernevig, Taylor L. Hughes, and Shou-Cheng Zhang. Quantum spin hall effect and topological phase transition in hgte quantum wells. *Science*, 314(5806):1757–1761, 2006. doi: 10.1126/science.1133734. URL http://www.sciencemag.org/content/314/5806/1757.abstract.

[17] T. Betz, S. Manz, R. Bücker, T. Berrada, Ch. Koller, G. Kazakov, I. Mazets, H.-P. Stimming, A. Perrin, T. Schumm, and J. Schmiedmayer. Two-Point Phase Correlations of a One-Dimensional Bosonic Josephson Junction. *Physical Review Letters*, 106(2), January 2011. ISSN 0031-9007. doi: 10.1103/PhysRevLett.106.020407. URL http://prl.aps.org/abstract/PRL/v106/i2/e020407.

[18] Philippe Biane, Luc Bouten, Fabio Cipriani, Norio Konno, Nicolas Privault, Quanhua Xu, and Norie Konno. Quantum walks. In *Quantum Potential Theory*, volume 1954 of *Lecture Notes in Mathematics*, pages 309–452. Springer Berlin / Heidelberg, 2008. ISBN 978-3-540-69364-2. URL http://dx.doi.org/10.1007/978-3-540-69365-9_7. 10.1007.

[19] Juliette Billy, Vincent Josse, Zhanchun Zuo, Alain Bernard, Ben Hambrecht, Pierre Lugan, David Clement, Laurent Sanchez-Palencia, Philippe Bouyer, and Alain Aspect. Direct observation of anderson localization of matter waves in a controlled disorder. *Nature*, 453(7197):891–894, Jun 2008. ISSN

0028-0836. doi: 10.1038/nature07000. URL http://dx.doi.org/10.1038/nature07000.

[20] R Bistritzer and E Altman. Intrinsic dephasing in one-dimensional ultracold atom interferometers. *Proceedings of the National Academy of Sciences of the United States of America*, 104(24):9955–9, June 2007. ISSN 0027-8424. doi: 10.1073/pnas.0608910104. URL http://www.pnas.org/cgi/content/abstract/104/24/9955.

[21] Immanuel Bloch, Jean Dalibard, and Wilhelm Zwerger. Many-body physics with ultracold gases. *Rev. Mod. Phys.*, 80: 885–964, Jul 2008. doi: 10.1103/RevModPhys.80.885. URL http://link.aps.org/doi/10.1103/RevModPhys.80.885.

[22] T. Bourdel, L. Khaykovich, J. Cubizolles, J. Zhang, F. Chevy, M. Teichmann, L. Tarruell, S. J. J. M. F. Kokkelmans, and C. Salomon. Experimental study of the bec-bcs crossover region in lithium 6. *Phys. Rev. Lett.*, 93:050401, Jul 2004. doi: 10.1103/PhysRevLett.93.050401. URL http://link.aps.org/doi/10.1103/PhysRevLett.93.050401.

[23] M. A. Broome, A. Fedrizzi, B. P. Lanyon, I. Kassal, A. Aspuru-Guzik, and A. G. White. Discrete single-photon quantum walks with tunable decoherence. *Phys. Rev. Lett.*, 104: 153602, Apr 2010. doi: 10.1103/PhysRevLett.104.153602. URL http://link.aps.org/doi/10.1103/PhysRevLett.104.153602.

[24] A. Burkov, M. Lukin, and Eugene Demler. Decoherence Dynamics in Low-Dimensional Cold Atom Interferometers. *Physical Review Letters*, 98(20), May 2007. ISSN 0031-9007. doi: 10.1103/PhysRevLett.98.200404. URL http://prl.aps.org/abstract/PRL/v98/i20/e200404.

[25] Amy Cassidy, Douglas Mason, Vanja Dunjko, and Maxim Olshanii. Threshold for Chaos and Thermalization in the One-Dimensional Mean-Field Bose-Hubbard Model. *Physical Review Letters*, 102(2), January 2009. ISSN 0031-9007. doi: 10.1103/PhysRevLett.102.025302. URL http://prl.aps.org/abstract/PRL/v102/i2/e025302.

[26] Jean-Sébastien Caux and Pasquale Calabrese. Dynamical density-density correlations in the one-dimensional Bose gas. *Physical Review A*, 74(3), September 2006. ISSN 1050-2947. doi: 10.1103/PhysRevA.74.031605. URL http://pra.aps.org/abstract/PRA/v74/i3/e031605.

[27] V. Chabanov and B. Zakhariev. Resonance Absolute Quantum Reflection at Selected Energies. *Physical Review Letters*, 87(16), October 2001. ISSN 0031-9007. doi: 10.1103/PhysRevLett.87.160408. URL http://prl.aps.org/abstract/PRL/v87/i16/e160408.

[28] David Chen, Matthew White, Cecilia Borries, and Brian DeMarco. Quantum quench of an atomic mott insulator. *Phys. Rev. Lett.*, 106:235304, Jun 2011. doi: 10.1103/PhysRevLett.106.235304. URL http://link.aps.org/doi/10.1103/PhysRevLett.106.235304.

[29] Y. L. Chen, J. G. Analytis, J.-H. Chu, Z. K. Liu, S.-K. Mo, X. L. Qi, H. J. Zhang, D. H. Lu, X. Dai, Z. Fang, S. C. Zhang, I. R. Fisher, Z. Hussain, and Z.-X. Shen. Experimental realization of a three-dimensional topological insulator, bi2te3. *Science*, 325 (5937):178–181, 2009. doi: 10.1126/science.1173034. URL http://www.sciencemag.org/content/325/5937/178.abstract.

[30] Yu-Ao Chen, Sylvain Nascimbène, Monika Aidelsburger, Marcos Atala, Stefan Trotzky, and Immanuel Bloch. Controlling correlated tunneling and superexchange interactions with ac-driven optical lattices. *Phys. Rev. Lett.*, 107:210405, Nov 2011. doi: 10.1103/PhysRevLett.107.210405. URL http://link.aps.org/doi/10.1103/PhysRevLett.107.210405.

[31] Marc Cheneau, Peter Barmettler, Dario Poletti, Manuel Endres, Peter Schausz, Takeshi Fukuhara, Christian Gross, Immanuel Bloch, Corinna Kollath, and Stefan Kuhr. Light-cone-like spreading of correlations in a quantum many-body system. *Nature*, 481(7382):484–487, Jan 2012. ISSN 0028-0836. doi: 10.1038/nature10748. URL http://dx.doi.org/10.1038/nature10748.

[32] C. De Grandi, R. Barankov, and A. Polkovnikov. Adiabatic Nonlinear Probes of One-Dimensional Bose Gases. *Physical Review Letters*, 101(23), December 2008. ISSN 0031-9007. doi: 10.1103/PhysRevLett.101.230402. URL http://prl.aps.org/abstract/PRL/v101/i23/e230402.

[33] R. De-Picciotto, M. Reznikov, M. Heiblum, V. Umansky, G. Bunin, and D. Mahalu. Direct observation of a fractional charge. 389(6647):162–164, September 1997. ISSN 0028-0836. doi: 10.1038/38241. URL http://dx.doi.org/10.1038/38241.

[34] Sebastian Diehl, Enrique Rico, Mikhail A. Baranov, and Peter Zoller. Topology by dissipation in atomic quantum wires. *Nat Phys*, 7(12):971–977, Dec 2011. ISSN 1745-2473. doi: 10.1038/nphys2106. URL http://dx.doi.org/10.1038/nphys2106.

[35] M Dolev, M Heiblum, V Umansky, Ady Stern, and D Mahalu. Observation of a quarter of an electron charge at the nu = 5/2 quantum Hall state. *Nature*, 452(7189):829–34, April 2008. ISSN 1476-4687. doi: 10.1038/nature06855. URL http://dx.doi.org/10.1038/nature06855.

[36] André Eckardt, Martin Holthaus, Hans Lignier, Alessandro Zenesini, Donatella Ciampini, Oliver Morsch, and Ennio Arimondo. Exploring dynamic localization with a bose-einstein condensate. *Phys. Rev. A*, 79:013611, Jan 2009. doi: 10.1103/PhysRevA.79.013611. URL http://link.aps.org/doi/10.1103/PhysRevA.79.013611.

[37] Edward Farhi and Sam Gutmann. Quantum computation and decision trees. *Phys. Rev. A*, 58:915–928, Aug 1998. doi: 10.1103/PhysRevA.58.915. URL http://link.aps.org/doi/10.1103/PhysRevA.58.915.

[38] Simon Fölling, Fabrice Gerbier, Artur Widera, Olaf Mandel, Tatjana Gericke, and Immanuel Bloch. Spatial quantum noise interferometry in expanding ultracold atom clouds. *Nature*, 434 (7032):481–4, March 2005. ISSN 1476-4687. doi: 10.1038/nature03500. URL http://dx.doi.org/10.1038/nature03500.

[39] Ron Folman, Peter Krüger, Donatella Cassettari, Björn Hessmo, Thomas Maier, and Jörg Schmiedmayer. Controlling Cold Atoms using Nanofabricated Surfaces: Atom Chips. *Physical Review Letters*, 84(20):4749–4752, May 2000. ISSN 0031-9007. doi: 10.1103/PhysRevLett.84.4749. URL http://prl.aps.org/abstract/PRL/v84/i20/p4749_1.

[40] Holger Frahm and Guillaume Palacios. Correlation functions of one-dimensional Bose-Fermi mixtures. *Physical Review A*, 72(6), December 2005. ISSN 1050-2947. doi: 10.1103/PhysRevA.72.061604. URL http://pra.aps.org/abstract/PRA/v72/i6/e061604.

[41] Liang Fu and C. L. Kane. Topological insulators with inversion symmetry. *Phys. Rev. B*, 76:045302, Jul 2007. doi: 10.1103/PhysRevB.76.045302. URL http://link.aps.org/doi/10.1103/PhysRevB.76.045302.

[42] Liang Fu, C. L. Kane, and E. J. Mele. Topological insulators in three dimensions. *Phys. Rev. Lett.*, 98:106803, Mar 2007. doi: 10.1103/PhysRevLett.98.106803. URL http://link.aps.org/doi/10.1103/PhysRevLett.98.106803.

[43] J. N. Fuchs, A. Recati, and W. Zwerger. Exactly Solvable Model of the BCS-BEC Crossover. *Physical Review Letters*, 93 (9), August 2004. ISSN 0031-9007. doi: 10.1103/PhysRevLett.93.090408. URL http://prl.aps.org/abstract/PRL/v93/i9/e090408.

[44] T. Fukuhara, A. Kantian, M. Endres, M. Cheneau, P. Schauß, S. Hild, D. Bellem, U. Schollwöck, T. Giamarchi, C. Gross, I. Bloch, and S. Kuhr. Quantum dynamics of a single, mobile spin impurity. *ArXiv e-prints*, September 2012.

[45] D. Gangardt and G. Shlyapnikov. Stability and Phase Coherence of Trapped 1D Bose Gases. *Physical Review Letters*, 90(1), January 2003. ISSN 0031-9007. doi: 10.1103/PhysRevLett.90.010401. URL http://prl.aps.org/abstract/PRL/v90/i1/e010401.

[46] Thierry Giamarchi. *Quantum Physics in One Dimension (The International Series of Monographs on Physics)*. Oxford University Press, USA, 2004. ISBN 0198525001. URL http://www.amazon.com/Quantum-Physics-Dimension-International-Monographs/dp/0198525001.

[47] M. Greiner, C. A. Regal, J. T. Stewart, and D. S. Jin. Probing Pair-Correlated Fermionic Atoms through Correlations in Atom Shot Noise. *Physical Review Letters*, 94(11), March 2005. ISSN 0031-9007. doi: 10.1103/PhysRevLett.94.110401. URL http://prl.aps.org/abstract/PRL/v94/i11/e110401.

[48] Markus Greiner, Olaf Mandel, Theodor W. Hansch, and Immanuel Bloch. Collapse and revival of the matter wave field of a bose-einstein condensate. *Nature*, 419(6902):51–54, Sep 2002. ISSN 0028-0836. doi: 10.1038/nature00968. URL http://dx.doi.org/10.1038/nature00968.

[49] Geoffrey Grimmett, Svante Janson, and Petra F. Scudo. Weak limits for quantum random walks. *Phys. Rev. E*, 69:026119, Feb 2004. doi: 10.1103/PhysRevE.69.026119. URL http://link.aps.org/doi/10.1103/PhysRevE.69.026119.

[50] M. Gring, M. Kuhnert, T. Langen, T. Kitagawa, B. Rauer, M. Schreitl, I. Mazets, D. Adu Smith, E. Demler, and J. Schmiedmayer. Relaxation and prethermalization in an isolated quantum system. *Science*, 337(6100):1318–1322, 2012. doi: 10.1126/science.1224953. URL http://www.sciencemag.org/content/337/6100/1318.abstract.

[51] Vladimir Gritsev, Ehud Altman, Eugene Demler, and Anatoli Polkovnikov. Full quantum distribution of contrast in interference experiments between interacting one-dimensional Bose liquids. *Nature Physics*, 2(10):705–709, September 2006. ISSN 1745-2473. doi: 10.1038/nphys410. URL http://www.nature.com.ezp-prod1.hul.harvard.edu/nphys/journal/v2/n10/full/nphys410.html.

[52] Vladimir Gritsev, Eugene Demler, Mikhail Lukin, and Anatoli Polkovnikov. Spectroscopy of Collective Excitations in

Interacting Low-Dimensional Many-Body Systems Using Quench Dynamics. *Physical Review Letters*, 99(20), November 2007. ISSN 0031-9007. doi: 10.1103/PhysRevLett.99.200404. URL http://prl.aps.org/abstract/PRL/v99/i20/e200404.

[53] V. Guarrera, N. Fabbri, L. Fallani, C. Fort, K. van der Stam, and M. Inguscio. Noise Correlation Spectroscopy of the Broken Order of a Mott Insulating Phase. *Physical Review Letters*, 100 (25), June 2008. ISSN 0031-9007. doi: 10.1103/PhysRevLett.100.250403. URL http://prl.aps.org/abstract/PRL/v100/i25/e250403.

[54] Zoran Hadzibabic and Jean Dalibard. Two-dimensional Bose fluids: An atomic physics perspective. page 51, December 2009. URL http://arxiv.org/abs/0912.1490.

[55] Zoran Hadzibabic, Sabine Stock, Baptiste Battelier, Vincent Bretin, and Jean Dalibard. Interference of an Array of Independent Bose-Einstein Condensates. *Physical Review Letters*, 93(18), October 2004. ISSN 0031-9007. doi: 10.1103/PhysRevLett.93.180403. URL http://prl.aps.org/abstract/PRL/v93/i18/e180403.

[56] Zoran Hadzibabic, Peter Krüger, Marc Cheneau, Baptiste Battelier, and Jean Dalibard. Berezinskii-Kosterlitz-Thouless crossover in a trapped atomic gas. *Nature*, 441(7097):1118–21, June 2006. ISSN 1476-4687. doi: 10.1038/nature04851. URL http://dx.doi.org/10.1038/nature04851.

[57] F. D. M. Haldane. Model for a quantum hall effect without landau levels: Condensed-matter realization of the "parity anomaly". *Phys. Rev. Lett.*, 61:2015–2018, Oct 1988. doi: 10.1103/PhysRevLett.61.2015. URL http://link.aps.org/doi/10.1103/PhysRevLett.61.2015.

[58] B. I. Halperin. Quantized hall conductance, current-carrying edge states, and the existence of extended states in a two-dimensional disordered potential. *Phys. Rev. B*, 25: 2185–2190, Feb 1982. doi: 10.1103/PhysRevB.25.2185. URL http://link.aps.org/doi/10.1103/PhysRevB.25.2185.

[59] M. Z. Hasan and C. L. Kane. *Colloquium* : Topological insulators. *Rev. Mod. Phys.*, 82:3045–3067, Nov 2010. doi: 10.1103/RevModPhys.82.3045. URL http://link.aps.org/doi/10.1103/RevModPhys.82.3045.

[60] S. Hofferberth, I. Lesanovsky, B. Fischer, T. Schumm, and J. Schmiedmayer. Non-equilibrium coherence dynamics in one-dimensional bose gases. *Nature*, 449(7160):324–327, Sep 2007. ISSN 0028-0836. doi: 10.1038/nature06149. URL http://dx.doi.org/10.1038/nature06149.

[61] S. Hofferberth, I. Lesanovsky, T. Schumm, A. Imambekov, V. Gritsev, E. Demler, and J. Schmiedmayer. Probing quantum and thermal noise in an interacting many-body system. *Nat Phys*, 4(6):489–495, Jun 2008. ISSN 1745-2473. doi: 10.1038/nphys941. URL http://dx.doi.org/10.1038/nphys941.

[62] D. Hsieh, D. Qian, L. Wray, Y. Xia, Y. S. Hor, R. J. Cava, and M. Z. Hasan. A topological dirac insulator in a quantum spin hall phase. *Nature*, 452(7190):970–974, Apr 2008. ISSN 0028-0836. doi: 10.1038/nature06843. URL http://dx.doi.org/10.1038/nature06843.

[63] Chen-Lung Hung, Xibo Zhang, Nathan Gemelke, and Cheng Chin. Slow mass transport and statistical evolution of an atomic gas across the superfluid mott-insulator transition. *Phys. Rev. Lett.*, 104:160403, Apr 2010. doi: 10.1103/PhysRevLett.104.160403. URL http://link.aps.org/doi/10.1103/PhysRevLett.104.160403.

[64] A IMAMBEKOV and E DEMLER. Applications of exact solution for strongly interacting one-dimensional Bose–Fermi mixture: Low-temperature correlation functions, density profiles, and collective modes. *Annals of Physics*, 321(10): 2390–2437, October 2006. ISSN 00034916. doi: 10.1016/j.aop.2005.11.017. URL http://dx.doi.org/10.1016/j.aop.2005.11.017.

[65] A. Imambekov, I. Mazets, D. Petrov, V. Gritsev, S. Manz, S. Hofferberth, T. Schumm, E. Demler, and J. Schmiedmayer.

Density ripples in expanding low-dimensional gases as a probe of correlations. *Physical Review A*, 80(3), September 2009. ISSN 1050-2947. doi: 10.1103/PhysRevA.80.033604. URL http://pra.aps.org/abstract/PRA/v80/i3/e033604.

[66] Adilet Imambekov and Eugene Demler. Exactly solvable case of a one-dimensional Bose–Fermi mixture. *Physical Review A*, 73 (2), February 2006. ISSN 1050-2947. doi: 10.1103/PhysRevA.73.021602. URL http://pra.aps.org/abstract/PRA/v73/i2/e021602.

[67] Adilet Imambekov and Leonid I. Glazman. Exact Exponents of Edge Singularities in Dynamic Correlation Functions of 1D Bose Gas. *Physical Review Letters*, 100(20), May 2008. ISSN 0031-9007. doi: 10.1103/PhysRevLett.100.206805. URL http://prl.aps.org/abstract/PRL/v100/i20/e206805.

[68] Adilet Imambekov, Vladmir Gritsev, and Eugene Demler. *Proceedings of the Enrico Fermi Summer School on Ultracold Fermi Gases 2006*. IOS Press, Amsterdam, 2007.

[69] Adilet Imambekov, Vladimir Gritsev, and Eugene Demler. Mapping of coulomb gases and sine-gordon models to statistics of random surfaces. *Phys. Rev. A*, 77:063606, Jun 2008. doi: 10.1103/PhysRevA.77.063606. URL http://link.aps.org/doi/10.1103/PhysRevA.77.063606.

[70] A Iucci and M A Cazalilla. Quantum quench dynamics of the sine-Gordon model in some solvable limits. *New Journal of Physics*, 12(5):055019, May 2010. ISSN 1367-2630. doi: 10.1088/1367-2630/12/5/055019. URL http://stacks.iop.org/1367-2630/12/i=5/a=055019.

[71] A Iucci and M A Cazalilla. Quantum quench dynamics of the sine-gordon model in some solvable limits. *New Journal of Physics*, 12(5):055019, 2010. URL http://stacks.iop.org/1367-2630/12/i=5/a=055019.

[72] R. Jackiw and C. Rebbi. Solitons with fermion number ½. *Phys. Rev. D*, 13:3398–3409, Jun 1976. doi: 10.1103/PhysRevD.13.3398. URL http://link.aps.org/doi/10.1103/PhysRevD.13.3398.

[73] R. Jackiw and J.R. Schrieffer. Solitons with fermion number 12 in condensed matter and relativistic field theories. *Nuclear Physics B*, 190(2):253 – 265, 1981. ISSN 0550-3213. doi: 10.1016/0550-3213(81)90557-5. URL http://www.sciencedirect.com/science/article/pii/0550321381905575.

[74] D Jaksch and P Zoller. Creation of effective magnetic fields in optical lattices: the hofstadter butterfly for cold neutral atoms. *New Journal of Physics*, 5(1):56, 2003. URL http://stacks.iop.org/1367-2630/5/i=1/a=356.

[75] Antti-Pekka Jauho, Ned S. Wingreen, and Yigal Meir. Time-dependent transport in interacting and noninteracting resonant-tunneling systems. *Phys. Rev. B*, 50:5528–5544, Aug 1994. doi: 10.1103/PhysRevB.50.5528. URL http://link.aps.org/doi/10.1103/PhysRevB.50.5528.

[76] F. Jendrzejewski, A. Bernard, K. Muller, P. Cheinet, V. Josse, M. Piraud, L. Pezze, L. Sanchez-Palencia, A. Aspect, and P. Bouyer. Three-dimensional localization of ultracold atoms in an optical disordered potential. *Nat Phys*, 8(5):398–403, May 2012. ISSN 1745-2473. doi: 10.1038/nphys2256. URL http://dx.doi.org/10.1038/nphys2256.

[77] Liang Jiang, Takuya Kitagawa, Jason Alicea, A. R. Akhmerov, David Pekker, Gil Refael, J. Ignacio Cirac, Eugene Demler, Mikhail D. Lukin, and Peter Zoller. Majorana fermions in equilibrium and in driven cold-atom quantum wires. *Phys. Rev. Lett.*, 106:220402, Jun 2011. doi: 10.1103/PhysRevLett.106.220402. URL http://link.aps.org/doi/10.1103/PhysRevLett.106.220402.

[78] C. L. Kane and E. J. Mele. Quantum spin hall effect in graphene. *Phys. Rev. Lett.*, 95:226801, Nov 2005. doi: 10.1103/PhysRevLett.95.226801. URL http://link.aps.org/doi/10.1103/PhysRevLett.95.226801.

[79] C. L. Kane and E. J. Mele. Z_2 topological order and the quantum spin hall effect. *Phys. Rev. Lett.*, 95:146802, Sep 2005. doi: 10.1103/PhysRevLett.95.146802. URL http://link.aps.org/doi/10.1103/PhysRevLett.95.146802.

[80] Michal Karski, Leonid Förster, Jai-Min Choi, Andreas Steffen, Wolfgang Alt, Dieter Meschede, and Artur Widera. Quantum walk in position space with single optically trapped atoms. *Science*, 325(5937):174–177, 2009. doi: 10.1126/science.1174436. URL http://www.sciencemag.org/content/325/5937/174.abstract.

[81] J Kempe. Quantum random walks: An introductory overview. *Contemporary Physics*, 44(4):307–327, 2003. doi: 10.1080/0010715103100011077 6.

[82] Markus Kindermann. Quantum mechanics: interference in the matter. *Nature*, 448(7151):262–3, July 2007. ISSN 1476-4687. doi: 10.1038/448262a. URL http://dx.doi.org/10.1038/448262a.

[83] Toshiya Kinoshita, Trevor Wenger, and David S. Weiss. A quantum newton's cradle. *Nature*, 440(7086):900–903, Apr 2006. ISSN 0028-0836. doi: 10.1038/nature04693. URL http://dx.doi.org/10.1038/nature04693.

[84] A. Kitaev. Periodic table for topological insulators and superconductors. In V. Lebedev and M. Feigel'Man, editors, *American Institute of Physics Conference Series*, volume 1134 of *American Institute of Physics Conference Series*, pages 22–30, May 2009. doi: 10.1063/1.3149495.

[85] Takuya Kitagawa. Topological phenomena in quantum walks: elementary introduction to the physics of topological phases. *Quantum Information Processing*, 11:1107–1148, 2012. ISSN 1570-0755. doi: 10.1007/s11128-012-0425-4. URL http://dx.doi.org/10.1007/s11128-012-0425-4.

[86] Takuya Kitagawa, Erez Berg, Mark Rudner, and Eugene Demler. Topological characterization of periodically driven quantum systems. *Phys. Rev. B*, 82:235114, Dec 2010. doi: 10.1103/PhysRevB.82.235114. URL http://link.aps.org/doi/10.1103/PhysRevB.82.235114.

[87] Takuya Kitagawa, Susanne Pielawa, Adilet Imambekov, Jörg Schmiedmayer, Vladimir Gritsev, and Eugene Demler. Ramsey Interference in One-Dimensional Systems: The Full Distribution

Function of Fringe Contrast as a Probe of Many-Body Dynamics. *Physical Review Letters*, 104(25), June 2010. ISSN 0031-9007. doi: 10.1103/PhysRevLett.104.255302. URL http://prl.aps.org/abstract/PRL/v104/i25/e255302.

[88] Takuya Kitagawa, Susanne Pielawa, Adilet Imambekov, Jörg Schmiedmayer, Vladimir Gritsev, and Eugene Demler. Ramsey interference in one-dimensional systems: The full distribution function of fringe contrast as a probe of many-body dynamics. *Phys. Rev. Lett.*, 104:255302, Jun 2010. doi: 10.1103/PhysRevLett.104.255302. URL http://link.aps.org/doi/10.1103/PhysRevLett.104.255302.

[89] Takuya Kitagawa, Mark S. Rudner, Erez Berg, and Eugene Demler. Exploring topological phases with quantum walks. *Phys. Rev. A*, 82:033429, Sep 2010. doi: 10.1103/PhysRevA.82.033429. URL http://link.aps.org/doi/10.1103/PhysRevA.82.033429.

[90] Takuya Kitagawa, Adilet Imambekov, Jörg Schmiedmayer, and Eugene Demler. The dynamics and prethermalization of one-dimensional quantum systems probed through the full distributions of quantum noise. *New Journal of Physics*, 13(7): 073018, 2011. URL http://stacks.iop.org/1367-2630/13/i=7/a=073018.

[91] Takuya Kitagawa, Takashi Oka, Arne Brataas, Liang Fu, and Eugene Demler. Transport properties of nonequilibrium systems under the application of light: Photoinduced quantum hall insulators without landau levels. *Phys. Rev. B*, 84:235108, Dec 2011. doi: 10.1103/PhysRevB.84.235108. URL http://link.aps.org/doi/10.1103/PhysRevB.84.235108.

[92] Takuya Kitagawa, Matthew A. Broome, Alessandro Fedrizzi, Mark S. Rudner, Erez Berg, Ivan Kassal, Alan Aspuru-Guzik, Eugene Demler, and Andrew G. White. Observation of topologically protected bound states in photonic quantum walks. *Nat Commun*, 3:882, Jun 2012. doi: 10.1038/ncomms1872. URL http://dx.doi.org/10.1038/ncomms1872.

[93] Takuya Kitagawa, Takashi Oka, and Eugene Demler. Photo control of transport properties in a disordered wire: Average conductance, conductance statistics, and time-reversal symmetry. *Annals of Physics*, 327(7):1868 – 1889, 2012. ISSN 0003-4916. doi: 10.1016/j.aop.2012.02.012. URL http://www.sciencedirect.com/science/article/pii/S0003491612000309. <ce:title>July 2012 Special Issue</ce:title>.

[94] K. v. Klitzing, G. Dorda, and M. Pepper. New method for high-accuracy determination of the fine-structure constant based on quantized hall resistance. *Phys. Rev. Lett.*, 45:494–497, Aug 1980. doi: 10.1103/PhysRevLett.45.494. URL http://link.aps.org/doi/10.1103/PhysRevLett.45.494.

[95] Sigmund Kohler, JÃ¶rg Lehmann, and Peter HÃ¤nggi. Driven quantum transport on the nanoscale. *Physics Reports*, 406(6): 379 – 443, 2005. ISSN 0370-1573. doi: 10.1016/j.physrep.2004.11.002. URL http://www.sciencedirect.com/science/article/pii/S0370157304005071.

[96] S. S. Kondov, W. R. McGehee, J. J. Zirbel, and B. DeMarco. Three-dimensional anderson localization of ultracold matter. *Science*, 334(6052):66–68, 2011. doi: 10.1126/science.1209019. URL http://www.sciencemag.org/content/334/6052/66.abstract.

[97] M. Kuhnert, R. Geiger, T. Langen, M. Gring, B. Rauer, T. Kitagawa, E. Demler, D. Adu Smith, and J. Schmiedmayer. Multimode dynamics and emergence of a characteristic length-scale in a one-dimensional quantum system. *ArXiv e-prints*, November 2012.

[98] Markus König, Steffen Wiedmann, Christoph Brüne, Andreas Roth, Hartmut Buhmann, Laurens W. Molenkamp, Xiao-Liang Qi, and Shou-Cheng Zhang. Quantum spin hall insulator state in hgte quantum wells. *Science*, 318(5851):766–770, 2007. doi: 10.1126/science.1148047. URL http://www.sciencemag.org/content/318/5851/766.abstract.

[99] Austen Lamacraft and Paul Fendley. Order Parameter Statistics in the Critical Quantum Ising Chain. *Physical Review Letters*,

100(16), April 2008. ISSN 0031-9007. doi: 10.1103/PhysRevLett.100.165706. URL http://prl.aps.org/abstract/PRL/v100/i16/e165706.

[100] R. B. Laughlin. Quantized hall conductivity in two dimensions. *Phys. Rev. B*, 23:5632–5633, May 1981. doi: 10.1103/PhysRevB.23.5632. URL http://link.aps.org/doi/10.1103/PhysRevB.23.5632.

[101] Elliott H. Lieb. Exact Analysis of an Interacting Bose Gas. II. The Excitation Spectrum. *Physical Review*, 130(4):1616–1624, May 1963. ISSN 0031-899X. doi: 10.1103/PhysRev.130.1616. URL http://prola.aps.org/abstract/PR/v130/i4/p1616_1.

[102] Elliott H. Lieb and Werner Liniger. Exact Analysis of an Interacting Bose Gas. I. The General Solution and the Ground State. *Physical Review*, 130(4):1605–1616, May 1963. ISSN 0031-899X. doi: 10.1103/PhysRev.130.1605. URL http://prola.aps.org/abstract/PR/v130/i4/p1605_1.

[103] H. Lignier, C. Sias, D. Ciampini, Y. Singh, A. Zenesini, O. Morsch, and E. Arimondo. Dynamical control of matter-wave tunneling in periodic potentials. *Phys. Rev. Lett.*, 99:220403, Nov 2007. doi: 10.1103/PhysRevLett.99.220403. URL http://link.aps.org/doi/10.1103/PhysRevLett.99.220403.

[104] Roman M. Lutchyn, Jay D. Sau, and S. Das Sarma. Majorana fermions and a topological phase transition in semiconductor-superconductor heterostructures. *Phys. Rev. Lett.*, 105:077001, Aug 2010. doi: 10.1103/PhysRevLett.105.077001. URL http://link.aps.org/doi/10.1103/PhysRevLett.105.077001.

[105] A. H. MacDonald. Introduction to the Physics of the Quantum Hall Regime. *eprint arXiv:cond-mat/9410047*, October 1994.

[106] S. Manz, R. Bücker, T. Betz, Ch. Koller, S. Hofferberth, I. E. Mazets, A. Imambekov, E. Demler, A. Perrin, J. Schmiedmayer, and T. Schumm. Two-point density correlations of quasicondensates in free expansion. *Physical Review A*, 81(3),

March 2010. ISSN 1050-2947. doi: 10.1103/PhysRevA.81.031610. URL http://pra.aps.org/abstract/PRA/v81/i3/e031610.

[107] L. Mathey and A. Polkovnikov. Light cone dynamics and reverse Kibble-Zurek mechanism in two-dimensional superfluids following a quantum quench. *Physical Review A*, 81(3), March 2010. ISSN 1050-2947. doi: 10.1103/PhysRevA.81.033605. URL http://pra.aps.org/abstract/PRA/v81/i3/e033605.

[108] I. Mazets, T. Schumm, and J. Schmiedmayer. Breakdown of Integrability in a Quasi-1D Ultracold Bosonic Gas. *Physical Review Letters*, 100(21), May 2008. ISSN 0031-9007. doi: 10.1103/PhysRevLett.100.210403. URL http://prl.aps.org/abstract/PRL/v100/i21/e210403.

[109] I E Mazets and J Schmiedmayer. Thermalization in a quasi-one-dimensional ultracold bosonic gas. *New Journal of Physics*, 12(5):055023, May 2010. ISSN 1367-2630. doi: 10.1088/1367-2630/12/5/055023. URL http://stacks.iop.org/1367-2630/12/i=5/a=055023.

[110] R. Moessner and S. L. Sondhi. Resonating valence bond phase in the triangular lattice quantum dimer model. *Phys. Rev. Lett.*, 86:1881–1884, Feb 2001. doi: 10.1103/PhysRevLett.86.1881. URL http://link.aps.org/doi/10.1103/PhysRevLett.86.1881.

[111] Joel E. Moore, Ying Ran, and Xiao-Gang Wen. Topological surface states in three-dimensional magnetic insulators. *Phys. Rev. Lett.*, 101:186805, Oct 2008. doi: 10.1103/PhysRevLett.101.186805. URL http://link.aps.org/doi/10.1103/PhysRevLett.101.186805.

[112] M. Moskalets and M. Büttiker. Floquet scattering theory of quantum pumps. *Phys. Rev. B*, 66:205320, Nov 2002. doi: 10.1103/PhysRevB.66.205320. URL http://link.aps.org/doi/10.1103/PhysRevB.66.205320.

[113] Hideaki Obuse and Norio Kawakami. Topological phases and delocalization of quantum walks in random environments. *Phys. Rev. B*, 84:195139, Nov 2011. doi: 10.1103/PhysRevB.84.195139. URL http://link.aps.org/doi/10.1103/PhysRevB.84.195139.

[114] Teemu Ojanen and Takuya Kitagawa. Photoinduced helical metal and magnetization in two-dimensional electron systems with spin-orbit coupling. *Phys. Rev. B*, 85:161202, Apr 2012. doi: 10.1103/PhysRevB.85.161202. URL http://link.aps.org/doi/10.1103/PhysRevB.85.161202.

[115] Takashi Oka and Hideo Aoki. Photovoltaic hall effect in graphene. *Phys. Rev. B*, 79:081406, Feb 2009. doi: 10.1103/PhysRevB.79.081406. URL http://link.aps.org/doi/10.1103/PhysRevB.79.081406.

[116] Takashi Oka, Norio Konno, Ryotaro Arita, and Hideo Aoki. Breakdown of an electric-field driven system: A mapping to a quantum walk. *Phys. Rev. Lett.*, 94:100602, Mar 2005. doi: 10.1103/PhysRevLett.94.100602. URL http://link.aps.org/doi/10.1103/PhysRevLett.94.100602.

[117] M. Olshanii. Atomic Scattering in the Presence of an External Confinement and a Gas of Impenetrable Bosons. *Physical Review Letters*, 81(5):938–941, August 1998. ISSN 0031-9007. doi: 10.1103/PhysRevLett.81.938. URL http://prl.aps.org/abstract/PRL/v81/i5/p938_1.

[118] Yuval Oreg, Gil Refael, and Felix von Oppen. Helical liquids and majorana bound states in quantum wires. *Phys. Rev. Lett.*, 105:177002, Oct 2010. doi: 10.1103/PhysRevLett.105.177002. URL http://link.aps.org/doi/10.1103/PhysRevLett.105.177002.

[119] G. Orso. Attractive Fermi Gases with Unequal Spin Populations in Highly Elongated Traps. *Physical Review Letters*, 98(7), February 2007. ISSN 0031-9007. doi: 10.1103/PhysRevLett.98.070402. URL http://prl.aps.org/abstract/PRL/v98/i7/e070402.

[120] K. Osterloh, M. Baig, L. Santos, P. Zoller, and M. Lewenstein. Cold atoms in non-abelian gauge potentials: From the hofstadter "moth" to lattice gauge theory. *Phys. Rev. Lett.*, 95 (1):010403, Jun 2005. doi: 10.1103/PhysRevLett.95.010403.

[121] Anton Öttl, Stephan Ritter, Michael Köhl, and Tilman Esslinger. Correlations and Counting Statistics of an Atom

Laser. *Physical Review Letters*, 95(9), August 2005. ISSN 0031-9007. doi: 10.1103/PhysRevLett.95.090404. URL http://prl.aps.org/abstract/PRL/v95/i9/e090404.

[122] D. Pekker, B. Wunsch, T. Kitagawa, E. Manousakis, A. S. Sørensen, and E. Demler. Signatures of the superfluid to mott insulator transition in equilibrium and in dynamical ramps. *Phys. Rev. B*, 86:144527, Oct 2012. doi: 10.1103/PhysRevB.86.144527. URL http://link.aps.org/doi/10.1103/PhysRevB.86.144527.

[123] Susanne Pielawa, Takuya Kitagawa, Erez Berg, and Subir Sachdev. Correlated phases of bosons in tilted frustrated lattices. *Phys. Rev. B*, 83:205135, May 2011. doi: 10.1103/PhysRevB.83.205135. URL http://link.aps.org/doi/10.1103/PhysRevB.83.205135.

[124] Anatoli Polkovnikov, Ehud Altman, and Eugene Demler. Interference between independent fluctuating condensates. *Proceedings of the National Academy of Sciences*, 103(16): 6125–6129, 2006. doi: 10.1073/pnas.0510276103. URL http://www.pnas.org/content/103/16/6125.abstract.

[125] Xiao-Liang Qi and Shou-Cheng Zhang. Topological insulators and superconductors. *Rev. Mod. Phys.*, 83:1057–1110, Oct 2011. doi: 10.1103/RevModPhys.83.1057. URL http://link.aps.org/doi/10.1103/RevModPhys.83.1057.

[126] Xiao-Liang Qi, Taylor L. Hughes, and Shou-Cheng Zhang. Topological field theory of time-reversal invariant insulators. *Phys. Rev. B*, 78:195424, Nov 2008. doi: 10.1103/PhysRevB.78.195424. URL http://link.aps.org/doi/10.1103/PhysRevB.78.195424.

[127] A. Rahmani, T. Kitagawa, E. Demler, and C. Chamon. Cooling through optimal control of quantum evolution. *ArXiv e-prints*, October 2012.

[128] Jakob Reichel and Vladan Vuletic, editors. *Atom Chips*. Wiley-VCH, 2011. ISBN 3527407553. URL http://www.amazon.com/Atom-Chips-Jakob-Reichel/dp/3527407553.

[129] S. Richard, F. Gerbier, J. Thywissen, M. Hugbart, P. Bouyer, and A. Aspect. Momentum Spectroscopy of 1D Phase Fluctuations in Bose-Einstein Condensates. *Physical Review Letters*, 91(1), July 2003. ISSN 0031-9007. doi: 10.1103/PhysRevLett.91.010405. URL http://prl.aps.org/abstract/PRL/v91/i1/e010405.

[130] Marcos Rigol, Vanja Dunjko, and Maxim Olshanii. Thermalization and its mechanism for generic isolated quantum systems. *Nature*, 452(7189):854–858, Apr 2008. ISSN 0028-0836. doi: 10.1038/nature06838. URL http://dx.doi.org/10.1038/nature06838.

[131] Stephan Ritter, Anton Öttl, Tobias Donner, Thomas Bourdel, Michael Köhl, and Tilman Esslinger. Observing the formation of long-range order during bose-einstein condensation. *Phys. Rev. Lett.*, 98:090402, Mar 2007. doi: 10.1103/PhysRevLett.98.090402. URL http://link.aps.org/doi/10.1103/PhysRevLett.98.090402.

[132] Giacomo Roati, Chiara D/'Errico, Leonardo Fallani, Marco Fattori, Chiara Fort, Matteo Zaccanti, Giovanni Modugno, Michele Modugno, and Massimo Inguscio. Anderson localization of a non-interacting bose-einstein condensate. *Nature*, 453 (7197):895–898, Jun 2008. ISSN 0028-0836. doi: 10.1038/nature07071. URL http://dx.doi.org/10.1038/nature07071.

[133] Daniel S. Rokhsar and Steven A. Kivelson. Superconductivity and the quantum hard-core dimer gas. *Phys. Rev. Lett.*, 61: 2376–2379, Nov 1988. doi: 10.1103/PhysRevLett.61.2376. URL http://link.aps.org/doi/10.1103/PhysRevLett.61.2376.

[134] T Rom, Th Best, D van Oosten, U Schneider, S Fölling, B Paredes, and I Bloch. Free fermion antibunching in a degenerate atomic Fermi gas released from an optical lattice. *Nature*, 444(7120):733–6, December 2006. ISSN 1476-4687. doi: 10.1038/nature05319. URL http://dx.doi.org/10.1038/nature05319.

[135] M. S. Rudner and L. S. Levitov. Topological transition in a non-hermitian quantum walk. *Phys. Rev. Lett.*, 102:065703, Feb 2009. doi: 10.1103/PhysRevLett.102.065703. URL http://link.aps.org/doi/10.1103/PhysRevLett.102.065703.

[136] Shinsei Ryu and Yasuhiro Hatsugai. Topological origin of zero-energy edge states in particle-hole symmetric systems. *Phys. Rev. Lett.*, 89:077002, Jul 2002. doi: 10.1103/PhysRevLett.89.077002. URL http://link.aps.org/doi/10.1103/PhysRevLett.89.077002.

[137] Subir Sachdev, K. Sengupta, and S. M. Girvin. Mott insulators in strong electric fields. *Phys. Rev. B*, 66:075128, Aug 2002. doi: 10.1103/PhysRevB.66.075128. URL http://link.aps.org/doi/10.1103/PhysRevB.66.075128.

[138] L. E. Sadler, J. M. Higbie, S. R. Leslie, M. Vengalattore, and D. M. Stamper-Kurn. Spontaneous symmetry breaking in a quenched ferromagnetic spinor bose-einstein condensate. *Nature*, 443(7109):312–315, Sep 2006. ISSN 0028-0836. doi: 10.1038/nature05094. URL http://dx.doi.org/10.1038/nature05094.

[139] L. Saminadayar, D. Glattli, Y. Jin, and B. Etienne. Observation of the e/3 Fractionally Charged Laughlin Quasiparticle. *Physical Review Letters*, 79(13):2526–2529, September 1997. ISSN 0031-9007. doi: 10.1103/PhysRevLett.79.2526. URL http://prl.aps.org/abstract/PRL/v79/i13/p2526_1.

[140] Jay D. Sau, Takuya Kitagawa, and Bertrand I. Halperin. Conductance beyond the landauer limit and charge pumping in quantum wires. *Phys. Rev. B*, 85:155425, Apr 2012. doi: 10.1103/PhysRevB.85.155425. URL http://link.aps.org/doi/10.1103/PhysRevB.85.155425.

[141] Ulrich Schneider, Lucia Hackermuller, Jens Philipp Ronzheimer, Sebastian Will, Simon Braun, Thorsten Best, Immanuel Bloch, Eugene Demler, Stephan Mandt, David Rasch, and Achim Rosch. Fermionic transport and out-of-equilibrium dynamics in a homogeneous hubbard model with ultracold atoms. *Nat Phys*,

8(3):213–218, Mar 2012. ISSN 1745-2473. doi: 10.1038/nphys2205. URL http://dx.doi.org/10.1038/nphys2205.

[142] Andreas P. Schnyder, Shinsei Ryu, Akira Furusaki, and Andreas W. W. Ludwig. Classification of topological insulators and superconductors in three spatial dimensions. *Phys. Rev. B*, 78: 195125, Nov 2008. doi: 10.1103/PhysRevB.78.195125. URL http://link.aps.org/doi/10.1103/PhysRevB.78.195125.

[143] U. Schollwöck. The density-matrix renormalization group. *Reviews of Modern Physics*, 77(1):259–315, April 2005. ISSN 0034-6861. doi: 10.1103/RevModPhys.77.259. URL http://rmp.aps.org/abstract/RMP/v77/i1/p259_1.

[144] Christian Schori, Thilo Stöferle, Henning Moritz, Michael Köhl, and Tilman Esslinger. Excitations of a superfluid in a three-dimensional optical lattice. *Phys. Rev. Lett.*, 93:240402, Dec 2004. doi: 10.1103/PhysRevLett.93.240402. URL http://link.aps.org/doi/10.1103/PhysRevLett.93.240402.

[145] A. Schreiber, K. N. Cassemiro, V. Potoček, A. Gábris, P. J. Mosley, E. Andersson, I. Jex, and Ch. Silberhorn. Photons walking the line: A quantum walk with adjustable coin operations. *Phys. Rev. Lett.*, 104:050502, Feb 2010. doi: 10.1103/PhysRevLett.104.050502. URL http://link.aps.org/doi/10.1103/PhysRevLett.104.050502.

[146] T. Schumm, S. Hofferberth, L. M. Andersson, S. Wildermuth, S. Groth, I. Bar-Joseph, J. Schmiedmayer, and P. Krüger. Matter-wave interferometry in a double well on an atom chip. *Nature Physics*, 1(1):57–62, September 2005. ISSN 1745-2473. doi: 10.1038/nphys125. URL http://dx.doi.org/10.1038/nphys125.

[147] A Sø rensen, L M Duan, J I Cirac, and P Zoller. Many-particle entanglement with Bose-Einstein condensates. *Nature*, 409 (6816):63–6, January 2001. ISSN 0028-0836. doi: 10.1038/35051038. URL http://dx.doi.org/10.1038/35051038.

[148] Anders S. Sørensen, Eugene Demler, and Mikhail D. Lukin. Fractional quantum hall states of atoms in optical lattices.

Phys. Rev. Lett., 94(8):086803, Mar 2005. doi: 10.1103/PhysRevLett.94.086803.

[149] I. Spielman, W. Phillips, and J. Porto. Mott-Insulator Transition in a Two-Dimensional Atomic Bose Gas. *Physical Review Letters*, 98(8), February 2007. ISSN 0031-9007. doi: 10.1103/PhysRevLett.98.080404. URL http://prl.aps.org/abstract/PRL/v98/i8/e080404.

[150] H.-P. Stimming, N. Mauser, J. Schmiedmayer, and I. Mazets. Fluctuations and Stochastic Processes in One-Dimensional Many-Body Quantum Systems. *Physical Review Letters*, 105(1), July 2010. ISSN 0031-9007. doi: 10.1103/PhysRevLett.105.015301. URL http://prl.aps.org/abstract/PRL/v105/i1/e015301.

[151] Niels Strohmaier, Daniel Greif, Robert Jördens, Leticia Tarruell, Henning Moritz, Tilman Esslinger, Rajdeep Sensarma, David Pekker, Ehud Altman, and Eugene Demler. Observation of elastic doublon decay in the fermi-hubbard model. *Phys. Rev. Lett.*, 104:080401, Feb 2010. doi: 10.1103/PhysRevLett.104.080401. URL http://link.aps.org/doi/10.1103/PhysRevLett.104.080401.

[152] J. Struck, C. lschl ger, R. Le Targat, P. Soltan-Panahi, A. Eckardt, M. Lewenstein, P. Windpassinger, and K. Sengstock. Quantum simulation of frustrated classical magnetism in triangular optical lattices. *Science*, 333(6045): 996–999, 2011. doi: 10.1126/science.1207239. URL http://www.sciencemag.org/content/333/6045/996.abstract.

[153] W. P. Su, J. R. Schrieffer, and A. J. Heeger. Solitons in polyacetylene. *Phys. Rev. Lett.*, 42:1698–1701, Jun 1979. doi: 10.1103/PhysRevLett.42.1698. URL http://link.aps.org/doi/10.1103/PhysRevLett.42.1698.

[154] Shina Tan, Michael Pustilnik, and Leonid I. Glazman. Relaxation of a high-energy quasiparticle in a one-dimensional bose gas. *Phys. Rev. Lett.*, 105:090404, Aug 2010. doi: 10.1103/PhysRevLett.105.090404. URL http://link.aps.org/doi/10.1103/PhysRevLett.105.090404.

[155] D. J. Thouless. Quantization of particle transport. *Phys. Rev. B*, 27:6083–6087, May 1983. doi: 10.1103/PhysRevB.27.6083. URL http://link.aps.org/doi/10.1103/PhysRevB.27.6083.

[156] D. J. Thouless, M. Kohmoto, M. P. Nightingale, and M. den Nijs. Quantized hall conductance in a two-dimensional periodic potential. *Phys. Rev. Lett.*, 49:405–408, Aug 1982. doi: 10.1103/PhysRevLett.49.405. URL http://link.aps.org/doi/10.1103/PhysRevLett.49.405.

[157] I. V. Tokatly. Dilute Fermi Gas in Quasi-One-Dimensional Traps: From Weakly Interacting Fermions via Hard Core Bosons to a Weakly Interacting Bose Gas. *Physical Review Letters*, 93(9), August 2004. ISSN 0031-9007. doi: 10.1103/PhysRevLett.93.090405. URL http://prl.aps.org/abstract/PRL/v93/i9/e090405.

[158] S. Trotzky, Y.-A. Chen, A. Flesch, I. P. McCulloch, U. Schollwock, J. Eisert, and I. Bloch. Probing the relaxation towards equilibrium in an isolated strongly correlated one-dimensional bose gas. *Nat Phys*, advance online publication, Feb 2012. ISSN 1745-2481. doi: 10.1038/nphys2232. URL http://dx.doi.org/10.1038/nphys2232.

[159] A. K. Tuchman, C. Orzel, A. Polkovnikov, and M. A. Kasevich. Nonequilibrium coherence dynamics of a soft boson lattice. *Phys. Rev. A*, 74:051601, Nov 2006. doi: 10.1103/PhysRevA.74.051601. URL http://link.aps.org/doi/10.1103/PhysRevA.74.051601.

[160] M. Vengalattore, S. R. Leslie, J. Guzman, and D. M. Stamper-Kurn. Spontaneously Modulated Spin Textures in a Dipolar Spinor Bose-Einstein Condensate. *Physical Review Letters*, 100(17), May 2008. ISSN 0031-9007. doi: 10.1103/PhysRevLett.100.170403. URL http://prl.aps.org/abstract/PRL/v100/i17/e170403.

[161] Zheng Wang, Yidong Chong, J. D. Joannopoulos, and Marin Soljacic. Observation of unidirectional backscattering-immune topological electromagnetic states. *Nature*, 461(7265):772–775,

Oct 2009. ISSN 0028-0836. doi: 10.1038/nature08293. URL http://dx.doi.org/10.1038/nature08293.

[162] Christof Weitenberg, Manuel Endres, Jacob F. Sherson, Marc Cheneau, Peter Schausz, Takeshi Fukuhara, Immanuel Bloch, and Stefan Kuhr. Single-spin addressing in an atomic mott insulator. *Nature*, 471(7338):319–324, Mar 2011. ISSN 0028-0836. doi: 10.1038/nature09827. URL http://dx.doi.org/10.1038/nature09827.

[163] P. Wicke, S. Whitlock, and N. J. van Druten. Controlling spin motion and interactions in a one-dimensional Bose gas. page 15, October 2010. URL http://arxiv.org/abs/1010.4545.

[164] Artur Widera, Stefan Trotzky, Patrick Cheinet, Simon Fölling, Fabrice Gerbier, Immanuel Bloch, Vladimir Gritsev, Mikhail Lukin, and Eugene Demler. Quantum Spin Dynamics of Mode-Squeezed Luttinger Liquids in Two-Component Atomic Gases. *Physical Review Letters*, 100(14), April 2008. ISSN 0031-9007. doi: 10.1103/PhysRevLett.100.140401. URL http://prl.aps.org/abstract/PRL/v100/i14/e140401.

[165] Artur Widera, Stefan Trotzky, Patrick Cheinet, Simon Fölling, Fabrice Gerbier, Immanuel Bloch, Vladimir Gritsev, Mikhail D. Lukin, and Eugene Demler. Quantum spin dynamics of mode-squeezed luttinger liquids in two-component atomic gases. *Phys. Rev. Lett.*, 100:140401, Apr 2008. doi: 10.1103/PhysRevLett.100.140401. URL http://link.aps.org/doi/10.1103/PhysRevLett.100.140401.

[166] Sebastian Will, Thorsten Best, Ulrich Schneider, Lucia Hackermuller, Dirk-Soren Luhmann, and Immanuel Bloch. Time-resolved observation of coherent multi-body interactions in quantum phase revivals. *Nature*, 465(7295):197–201, May 2010. ISSN 0028-0836. doi: 10.1038/nature09036. URL http://dx.doi.org/10.1038/nature09036.

[167] D. Wineland, J. Bollinger, W. Itano, and D. Heinzen. Squeezed atomic states and projection noise in spectroscopy. *Physical Review A*, 50(1):67–88, July 1994. ISSN 1050-2947. doi:

10.1103/PhysRevA.50.67. URL http://pra.aps.org/abstract/PRA/v50/i1/p67_1.

[168] K. Winkler, G. Thalhammer, F. Lang, R. Grimm, J. Hecker Denschlag, A. J. Daley, A. Kantian, H. P. BÃŒchler, and P. Zoller. Repulsively bound atom pairs in an optical lattice. *Nature*, 441(7095):853–856, Jun 2006. ISSN 0028-0836. doi: 10.1038/nature04918. URL http://dx.doi.org/10.1038/nature04918.

[169] Y. Xia, D. Qian, D. Hsieh, L. Wray, A. Pal, H. Lin, A. Bansil, D. Grauer, Y. S. Hor, R. J. Cava, and M. Z. Hasan. Observation of a large-gap topological-insulator class with a single dirac cone on the surface. *Nat Phys*, 5(6):398–402, Jun 2009. ISSN 1745-2473. doi: 10.1038/nphys1274. URL http://dx.doi.org/10.1038/nphys1274.

[170] F. Zähringer, G. Kirchmair, R. Gerritsma, E. Solano, R. Blatt, and C. F. Roos. Realization of a quantum walk with one and two trapped ions. *Phys. Rev. Lett.*, 104:100503, Mar 2010. doi: 10.1103/PhysRevLett.104.100503. URL http://link.aps.org/doi/10.1103/PhysRevLett.104.100503.

[171] Alessandro Zenesini, Hans Lignier, Donatella Ciampini, Oliver Morsch, and Ennio Arimondo. Coherent control of dressed matter waves. *Phys. Rev. Lett.*, 102:100403, Mar 2009. doi: 10.1103/PhysRevLett.102.100403. URL http://link.aps.org/doi/10.1103/PhysRevLett.102.100403.

[172] Shi-Liang Zhu, Hao Fu, C.-J. Wu, S.-C. Zhang, and L.-M. Duan. Spin hall effects for cold atoms in a light-induced gauge potential. *Phys. Rev. Lett.*, 97(24):240401, Dec 2006. doi: 10.1103/PhysRevLett.97.240401.

Colophon

This thesis was typeset using LaTeX, originally developed by Leslie Lamport and based on Donald Knuth's TeX. The body text is set in 11 point Arno Pro, designed by Robert Slimbach in the style of book types from the Aldine Press in Venice, and issued by Adobe in 2007. A template, which can be used to format a PhD thesis with this look and feel, has been released under the permissive MIT (X11) license, and can be found online at github.com/suchow/ or from the author at suchow@post.harvard.edu.